FACULTY OF ENGINEERING AND BUILT ENVIRONMENT

DEPARTMENT OF CIVIL ENGINEERING

DYNAMIC MODELLING OF ARCH DAMS IN THE AMBIENT STATE

Prepared by: **Mfundo Vezi**

Supervisor: **Prof. P. Moyo**

THIS THESIS HAS BEEN SUBMITTED TO THE DEPARTMENT OF CIVIL ENGINEERING, FACULTY OF ENGINEERING AND BUILT ENVIRONMENT, UNIVERSITY OF CAPE TOWN, IN PARTIAL FULLFILLMENT OF THE REQUIREMENTS FOR AN MSc DEGREE IN CIVIL ENGINEERING.

PLAGIARISM DECLARATION

THESIS SUPERVISOR: PROF P. MOYO

1. I know the meaning of plagiarism and declare that all the work in the document, save for that which properly acknowledged, is my own.
2. I have used the Harvard Convention for citation and referencing. Each significant contribution to and quotation in this research forms the work or works of other people that has been attributed and has been cited and referenced.
3. I have not allowed and will not allow anyone to copy my work with the intension of passing it as his or her own work.

Name: Mfundo Vezi Student No.: VZXMFU001

Date: Signature: _____

DEDICATION

To my family and friends and the one and only God

ABSTRACT

To date, dam failures have resulted in significant losses in the commercial economy and in human life. Raising awareness in the field of structural health monitoring is neccesary to develop contemporary structural analysis and monitoring methods to ensure the integrity of these structures. Hence, the research aims at developing an analytical formulation that can be used in the dynamic modelling of arch dams, for structural health monitoring purposes.

A hypothetical arch dam model was created to investigate the influence of a reservoir's orientation and geometry on the dam's dynamic properties, and the discrepancies between the Westergaard and Fluid Structure Interaction (FSI) analysis methods. The two analysis methods were then utilized to develop an updatable finite element model, in a case study pertaining to the 72m high Roode Elsberg concrete-arch dam. Thereafter, ambient vibration tests were conducted on the Roode Elsberg dam to measure its dynamic properties and validate the finite element models. The excitation on the dam was provided by the wind and the reservoir flowing over the spillway. Vibrations of the dam were measured and recorded by accelerometers placed on the cantilevered arch blocks. Finally, the Frequency Domain Decomposition (FDD) algorithm was used to analyse the acquired data and identify the natural frequencies of the dam.

The parametric study indicated that the dam's dynamic properties are insensitive to changes in the reservoir orientation and geometry in the ambient state. The comparative study results obtained from the Westergaard and FSI model illustrated that for the lower modes an average discrepancy of 23 % existed between the natural frequencies of the two methods. The two finite element models of Roode Elsberg exhibited an average difference of 20%, which is similar to that obtained above in the comparative study. The FDD modal analysis of the field test measurements, yielded the first six modal parameters of vibration for the dam. These compared quite well with those obtained from the FSI Model, however a poor estimation was obtained from the Westergaard formulation. Based on the results of the analysis, a conclusion can be made that Acoustic finite elements provide a good representation of the impounded water body, and hence, the dynamic properties in the ambient sate. Contrary, the Westergaard method does not give a good representation, and underestimates the natural frequencies in the ambient state.

ACKNOWLEDGEMENT

Firstly, I would like to thank my supervisor Prof. P. Moyo for his guidance in the compilation and completion of this work. Secondly, the Water Research Commission (WRC) and the Council of Science and Industrial Research (CSIR) for their financial and professional support over the past two years, it has gone a long way in the pursuit of completing my master's studies. The Department of Water Affairs provided access to their dams and for this I am grateful.

I would also like to acknowledge the Concrete Materials and Structural Integrity Research Unit (CoMSIRU) from the University of Cape Town for their support and feedback throughout the compilation of this thesis. A special thanks to Patrick Bukenya, a PhD student for his assistance in the field testing component of this research. Furthermore, I'd like to thank Mbogeni Nzuza and Romananta Makha senior MSc students, for assisting me with essential modelling material required to carry out my research. A special thanks also goes to Ms. Elly Yelverton for her assistance all the time.

Finally, I'd like to acknowledge everyone in the department of Civil Engineering, at the University of Cape Town for always striving towards providing a conducive environment to produce relevant and effective research, addressing current engineering problems.

TABLE OF CONTENTS

LIST OF FIGURES

LIST OF TABLES

NOMENCLATURE

Latin Upper Case

A	tributary area
B	Strain displacement matrix
C	Damping matrix
$\overline{D}$	Stress-strain matrix
E_f	Foundation material elastic modulus
E_c	Concrete material elastic modulus
$\vec{f}$	Vector of nodal force
F_p	Ambient hydrodynamic forces
F_g	Forces induced by ground motion
G	Lame's constant
G_{xx}	Value of cross spectrum between signal and frequency
H	Depth of reservoir
K	Bulk Modulus
K_s	Stiffness matrix
L	Dam reservoir length
M_s	Mass of Solid
M_f	Mass of fluid
N	Array of shape functions
P	Hydrodynamic pressure
Q	Transformation matrix of hydrodynamic pressures into forces
R	residual of Galerkin FEM
R_f	Foundation radius
S_{fs}	Coupling of the solid and acoustic motion
U	The unitary matrix holding singular values
X^L	Matrix of left eigenvector
X^R	Matrix of right eigenvector

Z	Distance from the base of the dam
C_{ijkl}	Rank four material stiffness tensor

Latin Lower Case

c_s	Propagation velocity of p-wave and s-wave
e	Surface emissivity
f	External loads
m	Meters
m_{ai}	Added mass matrix
n	Maximum number of time steps
n_s	Outward normal direction from reservoir surface
p	Hydrodynamic pressure in the fluid
r_h	Relative humidity
s	Seconds
t	Time
$\ddot{u}$	Acceleration
$\ddot{u}_g$	Horizontal ground acceleration
$\dot{u}$	Velocity
u	Displacement
w	Test / weighting function
x, y, z	Cartesian coordinate system
y	Reservoir depth
z	Foundation depth

Greek Upper Case

∂	Partial differential
Γ_{α}^{l}	Left acoustic participation factor
Γ_{α}^{R}	Right acoustic participation factor
∇^2	Laplacian operator
Δt	Time step length
Ω	Finite element domain

Greek lower Case

α	Westergaard pressure distribution
β	Sloping angle of dam surface
δ	Variational field
ρ	Unit mass of water
θ_p	Angle of parabolic section of the dam wall
θ_R	Angle of radial section of the dam wall
λ	Normal direction cosines
$\emptyset$	Matrix of mode shapes
φ	Latitude of location
ω	Angular frequency
ε_{kl}^{e}	Strain tensor
$\bar{\sigma}$	Average stress values
γ_{xy}	Coherence function

CHAPTER 1

1 INTRODUCTION

1.1 Background

Dam structures serve as important water storage facilities as water is a valuable resource to the population at large. The failure to assess the safety of these structures has resulted in numerous catastrophic incidents around the world. Such events not only include billions of dollars being spent rehabilitating and reconstructing damaged property, but also fatalities globally. It is for these reasons that national government has had to exercise good structural health monitoring practices to ensure that dams are continually assessed and evaluated for safety.

Over the years, analytical and field testing methods have been developed and improved to ensure that all structural properties are taken into consideration during the design and monitoring of dams. Static and dynamic properties are the fundamental elements considered when analysing concrete arch dams. Traditionally, static properties of the dam took preference in the design and post-construction monitoring and surveillance phase. However, the importance of dynamic characteristics has become prevalent with contemporary research, especially in the dynamic structural monitoring of dams in seismic zones. Research has been conducted in this area using field testing and computational analyses techniques, with the objective of understanding the dynamic behaviour of concrete dams under seismic loading and continuous long term structural health performance (Fenves, Mojtahedi, & Reimer, 1992).

Dynamic monitoring constitutes of two aspects, computational analyses and field dynamic testing. The computational analyses of arch dams has been positively impacted by the development of the Finite Element Method of Analysis (FEA). The FEA method of analysis provides for a better understanding of the parameters which govern the static and dynamic behaviour of dams. Allowing for the analyses of various load combinations which are not measurable through surveillance and monitoring techniques (Moyo & Oosthuizen, 2013). The point of interest in dynamic analysis, is in seismic evaluation and the extraction of dynamic modal properties such as natural frequencies, mode shapes and damping ratios.

The challenges in modal analysis, are developing a finite element model that can accurately predict the as built operational modal parameters and use these for long term structural monitoring. The problem is attributed to the uncertainties that exist in defining the: (i) operational material parameters, (ii) dam and foundation geometries, (iii) representation of the impounded reservoir, and (iv) boundary conditions which represent the as built dam conditions. This has been the challenge in the verification of the Shaahid-Rajaee arch dam model developed by Mivehchi, et al (2003). Also, in developing the dynamic model of the Roode Elsberg arch dam. This study will attempt to overcome the challenges experienced in developing the dynamic finite element model of the Roode Elsberg arch dam.

Operational dynamic characteristics of concrete dam structures are extracted through dynamic field testing techniques. These techniques can be used to obtain important modal parameters of the dam that can be used in structural health monitoring. This was previously not used in dam safety due to the absence of adequate field testing technologies. However, improvements in this field has resulted in highly accurate field testing methods which are used to obtain as built dynamic characteristics (Moyo & Oosthuizen, 2013). Forced vibration and ambient vibration testing are the most common field tests used in the industry, and the latter is found to be a useful method in determining the primary modes of an arch dam wall (Mivehchi et al., 2003). In force vibration testing mechanical forces are applied to the structure to excite it, while ambient vibration testing relies on mainly environmental forces e.g. wind and impounded reservoir. In areas where seismic activity is minimal, it is economical to conduct long term ambient vibration testing of the structure, as it does not require expensive mechanical exciters. These results can be used to verify and update dynamic finite element models. This allows for a better understanding of the dynamic properties and how the structure is performing under ambient conditions (Darbre & Proulx, 2002).

1.2 Objectives

The aim of this research is to develop an updatable dynamic finite element model of the Roode Elsberg arch dam based on ambient vibration testing. This forms a sub-section of continuing research that is currently being carried out in the structural health monitoring of arch dams by the Department of Civil Engineering, University of Cape Town, funded by the Water Research Commission.

The objectives of this research are outlined as follows:

1. To investigate the effect of a reservoir's orientation and geometry on the dynamic properties of the dam.
2. To analyse and assess the discrepancies in modal parameters produced by the Modified Westergaard and Fluid Structure Interaction (FSI) analysis methods.
3. To develop a dynamic updatable finite element model (FEM) of the Roode Elsberg concrete arch dam.
4. To conduct ambient vibration tests on the Roode Elsberg dam, measuring the operational dynamic properties, and hence, validate the dynamic updatable finite element model of the dam

1.3 Limitations and Scope of Research

The scope of the research is limited to the Roode Elsberg dam located in Worcester, Western Cape, South Africa. Research work conducted in this thesis is aimed towards developing a Finite Element Model (FEM), which will be used to monitor and assess the safety of the dam. An existing static finite element model of the Roode Elsberg dam has been verified and will form basis of the dynamic model. The research was limited to the following:

1. The study focuses only on the approach of modelling the hydrodynamic loading acting on the dam. Development of sedimentation and existing crack defects on the dam are not included in this work. The previously stated could have a significant influence on the final model.
2. There is inadequate data for the elastic properties of the foundation for Roode Elsberg Dam. The left and right abutments of the valley including the bedrock beneath the dam have dissimilar elastic properties.
3. The operational dynamic properties obtained for the dam were extracted from ambient vibration measurements carried out on the dam.

1.4 Plan and Structure of Thesis

The thesis constitutes 5 chapters which comprehensively outline the work conducted in the compilation of this dissertation. The document begins with literature that covers parameters and methods used in the dynamic modelling of arch dams. A summary of the methodical steps used in Abaqus to develop a dynamic finite element model of the Roode Elsberg dam are then provided. Followed by results obtained from the finite element model and field testing conducted on the Roode Elsberg dam are discussed. Lastly, conclusions and recommendations related to the developed finite element model are drawn.

Chapter 1 – Introduction

This chapter provides an introduction into the dynamic modelling of arch dams in the context of structural health monitoring. It highlights the objectives of the research, which mainly focuses on developing a dynamic updateable finite element model for the Roode Elsberg dam.

Chapter 2 – Review on Dynamic Analysis of Arch dams

This chapter provides literature which is relevant to fulfil the proposed objectives. It constitutes the main aspects and methods used to develop a dynamic finite element model of an arch dam. It also contains literature on the field testing techniques used to obtain operational modal parameters.

Chapter 3 – Methodology

This chapter provides a detailed outline on the procedure followed in the development of the finite element models in Abaqus. Furthermore, it contains the details and process followed in the ambient vibration testing of the Roode Elsberg dam.

Chapter 4 – Results and Discussion

This chapter contains the results obtained in the following studies: The parametric and comparative study conducted on a hypothetical arch dam, The development of the finite element model of the Roode Elsberg dam, and verification of the dynamic model of the Roode Elsberg dam using ambient vibration testing.

Chapter 5 – Conclusion and Recommendations

Concludes on the results obtained in this study and makes recommendations for future works related to this topic.

Bibliography

Contains a list of literature used in this research and also references work related to this topic.

Appendices

This section contains the theory of procedures and techniques used in Abaqus to develop a dynamic finite element model. It also contains dam data used in the geometric development of the hypothetical arch dam. Furthermore, it contains dynamic modelling results obtained from Abaqus,

CHAPTER 2

2 Review on Dynamic Analysis Methods and Parameters of Arch Dams

2.1 Introduction

The review focuses on illustrating past literature produced in analysing the dynamic behaviour of arch dams. Firstly, a review on static and dynamic analysis loading of arch dams will be analysed to obtain an understanding of the aspects that must be taken into consideration in the analysis phase. Secondly, a review of existing dynamic analysis methods which are currently used to analyse the impounded water body is provided. Also, a review of eigenvalue solving techniques that are applicable to solving and extracting modal parameters of fluid structures such as dams. Finally, a review of field testing techniques used in structural surveillance and health monitoring of arch dams.

2.2 Analysis of Loading on Arch Dams

Arch dams are constructed as a uniform sequence of monolithic blocks separated by vertical joints that are later grouted under high pressure to form a complete monolithic structure (USBRR, 1977). The joints are designed to purely take on compressive loading during the operation stage. However, they may open and close in between seasons, due to sever temperatures and changes in reservoir level. Linear elastic analysis approaches model arch dam as a monolithic, and do not consider joint openings and slippage of contraction joints.

Understanding the structural behaviour of arch dams is essential in developing refined design and health monitoring analysis techniques. A thorough understanding on the form and function must be established in order to develop analysis techniques that account for the loading and the influence it has on the structure. This section reviews existing general static and dynamic loading acting on arch dams. It will simply highlight the static loading considerations, as it does not fall in the scope of the research topic.

2.2.1 Analysis of Static Loads

- Gravity Loading

The self -weight of a concrete structure can be considered as a non-varying load that is always present in operation. The self-weight of an arch dam constitutes of the weight of

concrete and the weight of appurtenances such as gates, and bridges. The dead weight of the structure can be calculated using the uniform weight density throughout each element (Ghanaat, 1993). The unit weight of concrete can be determined using laboratory testing or assuming a typical value. The weight of appurtenances is sufficiently less in magnitude when compared to the weight of the dam and is normally considered as being negligible in structural analysis models (Ghanaat, 1993).

- Hydrostatic Loads

The hydrostatic load is considered as the linearly distributed hydro pressure acting on the wetted upstream surface of the dam wall. Hydrostatic loading causes an increase in the compressive stresses in the grouted contraction joints of the arches, resulting in the structure acting as a monolithic body. The static analysis of hydro static forces should include the complete dam foundation interaction where the water load is applied as an external hydrostatic surface load acting on the dam and foundation rock. Theses foundation effects should not be ignored as they have an influence on the deformation behaviour of the dam. The weight of the water acting on the valley rocks causes deformation on the foundation rock, abutments and valley floor, which results in the stresses and deformations in the dam (Ghanaat, 1993).

- Temperature Loads

Temperature loads are important in the safety evaluation of arch dams. Operating temperatures are applied to the arch structure after the contraction joints are grouted. Generally, the temperature distributions within a dam vary in a nonlinear manner but are usually approximated by a combination of uniform and linear equations (Ghanaat, 1993).

The variation of temperature in arch dams, results in thermal stresses if volumetric changes are not permitted by the supporting foundation rock. The magnitude of the closing temperature is dependent on the difference between the closure temperature of the contraction joints, and the concrete temperature expected during operation. The closure temperature is the mean concrete temperature at the time the contraction joints are closed to form a monolithic arch. This temperature is very important as it has the largest influence on the thermal stresses, and may be controlled to minimize the effects by grouting the cantilever blocks at an appropriate closure temperature (Ghanaat, 1993) .

The effects of concrete temperatures in arch dams may be analysed by determining the operational ambient air temperatures, reservoir water temperatures, and solar radiation. These variables can be used in conjunction with the material thermal properties to investigate the influence of temperature on the arch dam.

- Silt Loads

Silt loads are analysed in a similar manner as hydrostatic loads. A hydrostatic load is applied as an external surface load with the appropriate density of the ground material.

- Uplift Pressures

Uplift pressures develop when the water enters interstitial spaces within the arch, foundation joints and cracks. The uplift pressures commonly result in a reduction of compressive stress on horizontal sections within the concrete and an increase in corresponding tensile stresses. Uplift pressures are found to have negligible stresses in thin arch dams but have a significant influence on gravity arch dams and should therefore be included in the analysis (Ghanaat, 1993).

The effects of uplift within the concrete are generally not considered in a static finite element analysis of thin arch dams, as they have an insignificant influence on the stresses. Uplift pressure distribution within the foundation rock and interface of the foundation and dam depend on the depth and size of drains, grout curtain, rock porosity, jointing, faulting, and geological features which may influence the flow of water through the system (Ghanaat, 1993). The effects of pore pressure may be analysed by using Terzaghi's effective stress concept.

2.2.2 Analysis of Dynamic Loading

The consideration of dynamic loads, which develop in dam structures during earthquakes and ambient conditions is essential when designing and monitoring water retaining structures. The seismic behaviour of concrete dams has been the main focus of research over the past decade, owing to major safety concerns of dams located in earthquake prone regions. These concerns arise as the uncertainties which exist in these adverse conditions can have unprecedented outcomes on the structural integrity of the dam (Ghaemian & Ghobarah, 1999).

An arch dam undergoing seismic and ambient dynamic loading can be analysed using the multi degree of freedom, equation of motion (2.1) below:

$$M_s\ddot{u} + C_s\dot{u} + K_s u = [F_g(t) + F_P(t)] \quad (2.1)$$

Where, M_s, C_s and K_s refer to the mass, damping and stiffness matrices of the dam wall and foundation respectively, u is the displacement vector of the structure. One must note, that, if the foundation model is considered to be massless it only contributes to the stiffness of the model and not the mass. The time dependent forces F_g and F_p represent loading induced by ground acceleration and ambient loading on the structure. Q in equation (2.3) represents a transformation matrix which converts hydrodynamic pressures into forces. The forces are defined below:

$$F_g = -M_s\ddot{u}_g \quad (2.2)$$

$$F_p = QP \quad (2.3)$$

As previously mentioned, the majority of the work conducted in dynamic analysis is heavily inclined towards seismic loading, hence the ground acceleration term in equation (2.1). Since the focus of the study considers ambient conditions, thus, we can ignore the ground acceleration term as it is assumed to be zero resulting in equation (2.4) below:

$$M_s\ddot{u} + C_s\dot{u} + K_s u = [F_P(t)] \quad (2.4)$$

- Eigenvalue Extraction

They are two main important areas of structural analysis which it is essential to extract and obtain the eigenvalues of equation (2.1), and hence, its natural frequencies of vibration. The most common area is the structural evaluation for seismic events considered in the design and seismic monitoring phase. This is based on a linear analysis using the structures modes up to limiting frequency usually 33Hz (Simulia, 2010). The other new area is in the context of structural health monitoring, which the research forms a part of, this is a recent form of

structural analysis which focuses on evaluating the safety of aging concrete dam structures. The method of structural analysis involves updating the finite element model based on ambient vibration test results, which gives insight on the dams current health status (Moyo & Oosthuizen, 2013). Modal analysis methods which evaluate eigenvalues of dynamic models will be further discussed in *Section 2.3.2*.

- Foundation Rock and Boundary Conditions

Ideally a complete dynamic model must include the foundation rock, as it has a significant influence on the dynamic behaviour of the arch dam. Selecting and assigning the boundary and material parameters becomes difficult as not much geological data is available about the foundation support and rocky canyon environment. Material and boundary parameters such as: (i) the foundation modulus (dynamic modulus), (ii) the wave absorption in the foundation bottom and flanks, and (iii) the dissipation of energy in the foundation (material and radiation damping) depends on the extent of geological information available of the site (Proulx, Darbre, & Kamileris, 2004). The components considered to idealise the foundation rock have been further outlined in *Section 2.3.3*.

- Impounded water body

The impounded water body and the concrete dam wall are known to interact dynamically with each other, where the two cannot be decoupled and analysed independently (Zienkiewics and Taylor, 2000). The continuous dynamic interactive loading process results in hydrodynamic loads being exerted on the upstream dam wall surface. Hydrodynamic loading is the most important and complex aspect to measure, and has a significant influence on the dynamic characteristics of the structure (Leung et al, 2008). This interaction is influenced by the reservoir geometry and energy absorption in the reservoir bottom. The reservoir geometry is usually a complicated shape which depends on the topography of the site. The energy absorption is heavily influenced by the bottom geology, and as previously stated, measurement data is usually not available.

Currently, two procedures are available for modelling the impounded water body. The most preferred being the added mass formulation, as it provides an efficient and simplistic idealisation of the reservoir. Alternatively, the fluid structure interaction is considered a more realistic formulation, but due to its complexity, it has not gained popularity as the preferred method of use.

2.3 Dynamic Analyses

2.3.1 Hydrodynamic Analysis Methods

This section provides a detailed review of methods used to analyse the impounded water body and its influence on concrete dam wall. The different formulations of the added mass techniques and the fluid structure interaction methods have been detailed and contrasted against each other.

The 'added mass' technique is considered the most efficient and economical technique accepted by practicing engineers (Rodríguez, Crespo, Lacoma, & Martínez, 2012). The main assumptions include: (i) incompressible fluid, (ii) infinite rigidity in the boundaries provided by the dam-wall and (iii) surrounding environment. This method has been employed by academics such as Westergaard (1933) and Housner (1954) on hydro-structures located in earthquake regions, and has proven to yield acceptable results (Rodríguez et al., 2012)

Currently, the 'added mass technique' has been overlooked due to its conservative nature. More complex methods have been employed to consider important effects such as dam deformability, water compressibility, non-linear effects (cracks) and dam-foundation interaction (Du, Zhang, & Zhang, 2006).The new formulations such as FEA, have been complemented with the innovation of high speed computing, which has made the analysis of these structures much more efficient and realistic. Furthermore, they have brought across complex interaction modules, making modelling this effect more laborious and complex than the added mass theory (Gersdorff, 2009). Nonetheless, they result in improved approximations as important considerations (parameters and boundary conditions) are taken into account.

2.3.1.1 Westergaard (1933)

Westergaard (1933) analysed the hydrodynamic effects on gravity dams during earthquakes. The formulated approach analysed the acceleration of the dam and the changes of water pressures. The formulation considers that for small displacements, simple equations which apply to sound in liquids can be used to track down the movement of the water particles causing increases in the pressures on the dam. These equations can be interpreted in terms of the theory of elasticity without shear stresses (Westergaard, 1933). A final solution was

formulated by taking a numerical approach yielding the hydrodynamic pressures as a series of sines and is illustrated in equation (2.5).

$$P = \frac{8\omega h}{\pi^2} \sum_{1,3,5}^{n} \frac{1}{n^2 c_n} \sin \frac{n\pi y}{2h} \tag{2.5}$$

Where:

p = maximum pressure of the water on the dam, due to the dynamic action

ω = weight of water per unit of volume

h= depth of reservoir

value defined by n , ,

The following assumptions were made by Westergaard in his formulation:

- Dam and water body are idealised as a two dimensional rigid monolith with vertical upstream face.
- The reservoir extends to infinity in the upstream direction.
- Displacements of fluid particles are small
- Surface waves are ignored
- Only horizontal ground motion in the upstream-downstream direction is considered.

Westergaard proposed that this series be represented by a simpler method, where the hydrodynamic pressure distribution is approximated by a parabolic (equation (2.6) & figure 1) or elliptic shape with simplified factors, the former being argued to provide a better approximation of equation (2.5).

Provided below as equation (2.6) is the parabolic approximation:

$$P_Z = \frac{7}{8} \ddot{u}_o \rho \sqrt{H(H-Z)}$$

(2.6)

Where:

P_Z = Hydrodynamic pressure at height Z from the base of the dam, applied horizontally to the dam face

ρ = unit mass of water

$\ddot{u}_g$ = horizontal ground acceleration

H = depth of reservoir above the base of the dam

Z = distance from the base of the dam

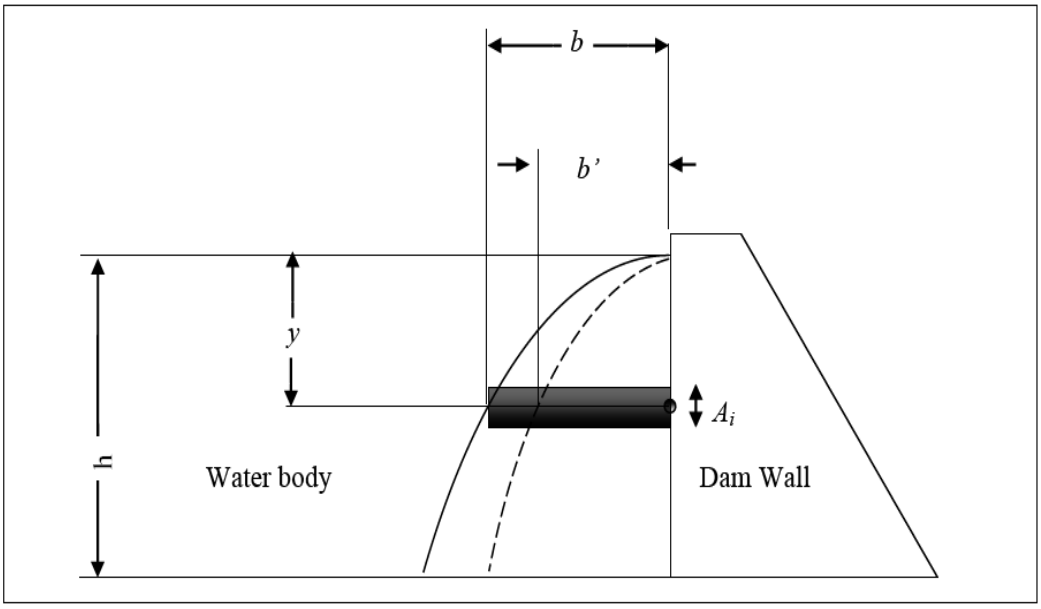

Figure 1: Parabolic (solid) body of water considered to move with the dam wall. The dotted parabolic curve shows equivalent body of concrete. source (Makha, 2012)

As previously mentioned, the Westergard method is restricted to the above mentioned assumptions, thus making it applicable to dams with vertical upstream surfaces. In the first assumption it is assumed that the dam and reservoir are considered to be two-dimensional in a vertical plane. Arch-dams are completely three-dimensional and it is impossible to use a two dimensional model to analyse them. It is also noted that the dam upstream surface is considered vertical and completely rigid, the dam in this study has a curvature and is flexible. Finally, the last assumption whereby the ground motion is considered to be horizontal in the upstream-downstream direction is impractical as ground acceleration is associated in all three planes.

With the above limitations mentioned about the Westergaard method, there was a need to modify the basic assumptions and make it applicable to flexible curvilinear arch dams. Consequently, this resulted in a modified method which was introduced by Kuo (1982).

2.3.1.2 Modified Westergaard Method (Kuo, 1982)

Kuo (1982), reproduced a modification of the Original Westergaard method. Reconsidering the generalised prismatic body of water which is of unit width by applying it normal to the upstream surface of the dam. Figure 2, illustrates the normal prismatic body of water.

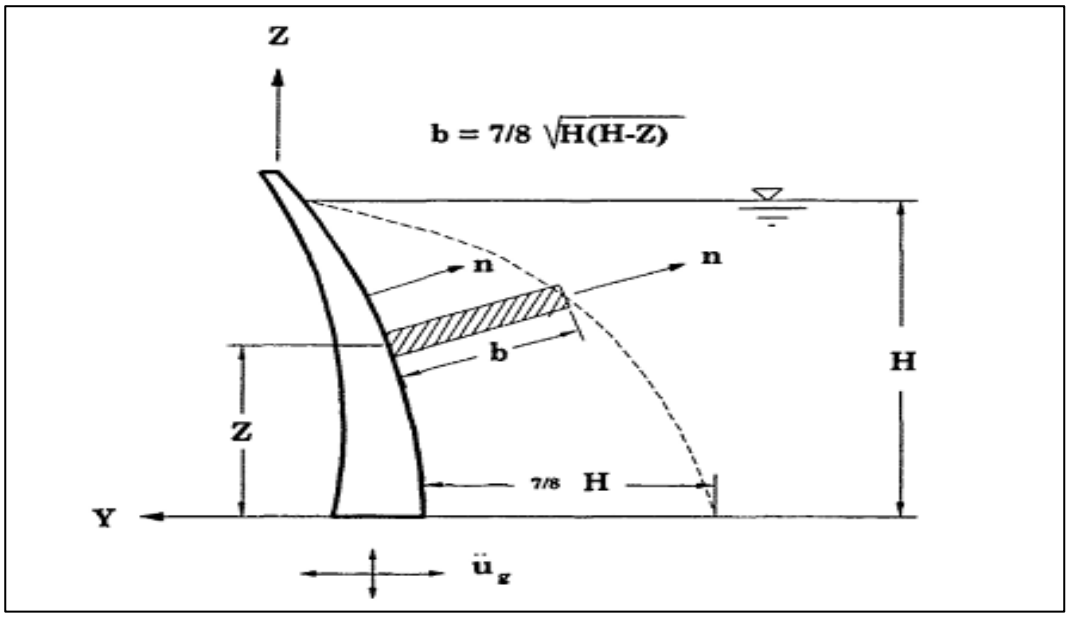

Figure 2: Body of water acting normally to the dam surface. (Kuo, 1982)

The parabolic shape is the same as that defined in equation (2.6). The distinction between the original and generalised method is the normal *n* vector which is introduced into the Westergaard method. Provided below is equation (2.7), which illustrates the hydrodynamic pressure acting normal on the dam surface.

$$p_i = \alpha \ddot{u}_{ni} \tag{2.7}$$

Where:

p_i = hydrodynamic pressure at node *i*

$\ddot{u}_{ni}$ = total normal acceleration at node *i*

$\alpha = \frac{7}{8}\ddot{u}_o \rho\sqrt{H(H-Z)}$ (parameters as defined in equation 2.6)

The normal acceleration vector can be represented in the Cartesian co-ordinate components as a summation of the ground acceleration $\ddot{u}_g$ and that relative to the base of the dam $\ddot{u}_i$. Hereafter, the directional cosines are applied in the direction of the normal, resulting in equation (2.8), which defines the normal nodal hydrodynamic pressures exerted on the upstream dam surface. In finite elements implementing this formulation requires the external pressures to be integrated over the appropriate surface and applied as a nodal hydrodynamic forces.

$$p_i = \alpha\lambda_i(\ddot{u}_i + \beta_i\ddot{u}_g) \tag{2.8}$$

Where:

p_i = hydrodynamic pressure at node *i*

$\alpha = \frac{7}{8}\ddot{u}_o \rho\sqrt{H(H-Z)}$

$\ddot{u}_i$ = acceleration relative to base of dam at node i

$\ddot{u}_g$ = ground acceleration Cartesian components node i

λ_i = normal direction cosines

- Hydrodynamic Forces Acting on the Dam

A simple method employed to obtain nodal loads, is to lump the hydrodynamic pressures by multiplying by the tributary area associated with that node. The hydrodynamic pressure is assumed to be constant over the tributary area and has the same value as node *i*, and is defined to act normal to the surface of the dam at that point. Since the pressures act normal on the surface the same could be said about the nodal forces defined in equation (2.9).

$$F_{ni} = -p_i A_i \tag{2.9}$$

Where

F_{ni} = Equivalent normal hydrodynamic nodal force, outward normal from the dam face as positive

p_i = Hydrodynamic pressure at node *i*, compression as positive

A_i = tributary area associated with node *i*

The normal force should be resolved into its Cartesian components which are given by equation (2.10).

$$F_i = F_{ni}\lambda_i^T \tag{2.10}$$

Where

$$F_i = [F_{x,} F_{Y,} F_Z]$$

$$\lambda_i = [\lambda_{x,} \lambda_{Y,} \lambda_Z]$$

Combining equations (2.8) and (2.9) with (2.10) leads to equation (2.11).

$$F_i = -m_{ai}(\ddot{u}_i + \beta_i \ddot{u}_g) \tag{2.11}$$

Where:

$$m_{ai} = \alpha A_i \lambda_i^T \lambda_i \tag{2.12}$$

Here $m_{\mathbf{ai}}$ is the added mass matrix as a result of the hydrodynamic forces acting on the upstream surface of the dam wall. The added mass matrix is a 3x3 sub-matrix associated with each node, which is not coupled with the neighbouring node. The added mass sub-matrices are substituted into the equation (2.13) of motion to include the hydrodynamic effects of the reservoir (Ghanaat, 1993).

$$(m + m_a)\ddot{u} + c\dot{u} + ku = -(m + m_a)\, r\ddot{u}_g \tag{2.13}$$

The right hand side of equation (2.13) is the effective earthquake loads which are dependent on the added mass of the reservoir and the as well as the mass of the dam structure. The added mass of the reservoir needs to be combined directly with the mass matrix of the upstream dam wall surface when implementing the Westergaard added mass. For each node the mass of the concrete associated with that element is combined with added mass of the impounded water.

Ghanaat (1993) suggests that the Generalised Westergaard method does not properly represent the pressures acting on an arch dam. This is due to the assumptions of an incompressible fluid under seismic action being implausible, hence, resulting in inaccurate results. The limitations of the method have been justified by Kuo (1982) as he evaluated the accuracy of the generalized Westergaard method by conducting a parametric study, and a case study of Techi arch dam. His findings on the seismic parametric study revealed that the method overestimated the hydrodynamic pressures and can be considered to be too conservative for seismic analyses. The case study of the Techi arch dam showed that the Generalised Westergaard method overestimated the natural frequencies when compared to those obtained by ambient and forced vibration testing. Goldgruber et al., (2013) goes on to suggest that added mass technique should be used for estimation purposes and dams not higher than 100 meters. This is after the dynamic stress levels were overestimated by more than 100% when compared to acoustic elements.

2.3.1.3 Housner (1954)

G.W Housner (1954) developed an approximate method which presented physical meaning and avoided laborious differential equations and series formulations (Housner, 1954).In doing so developed a method to estimate the simple type of flow which is similar to the actual flow in fluid containing structures. The method not only allowed for the computation of hydrodynamic pressures but it was also similar to the analogy which was brought forward by the Rayleigh-Ritz method.

Housner (1954) considered the impulsive forces acting on tanks with various geometries and orientations. The study will only consider the derivation of the hydrodynamic pressures exerted on rectangular tanks, as the Housner method will be used to validate hydrodynamic loading of a rectangular tank model (figure 3). The following considerations where taken into account upon deriving the closed form solution:

- The tank is considered to have a horizontal foundation (base), and the wall subjected to a horizontal acceleration $\ddot{u}$ in the x-direction.
- Let the fluid have a depth of *h*, a length of *2l* and unit thickness.
- The fluid is considered to be incompressible

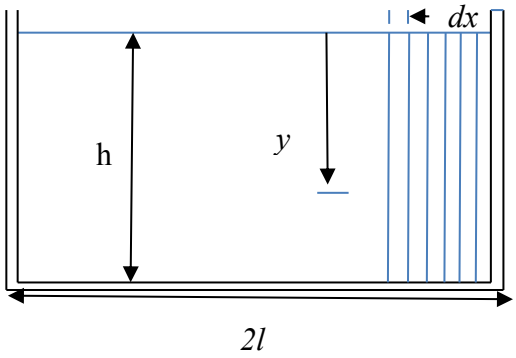

Figure 3: Rectangular tank proposed by Housner and illustrating the membrane slices which govern the theory.

The horizontal velocity of the fluid was considered to be independent of the vertical position. In other words, the fluid could be considered being constrained by massless membranes of dx (*see figure 3*), which are free to translate in the x-direction. Thus, when the tank is accelerated in the *x*-direction, the fluid will be accelerated with the membrane and squeezed vertically between the adjacent membranes. The vertical velocity is dependent on the horizontal velocity and is as defined in equation (2.13). The standard hydrodynamic pressure between the two membranes are be given by equation (2.14).

$$v = (h - y)\frac{du}{dx} \tag{2.14}$$

$$\frac{\partial p}{\partial y} = -\rho\ddot{v}` \tag{2.15}$$

Substituting equation (2.14) into (2.15) and integrating with respect to **y**, we can obtain the expression of the hydrodynamic pressures (equation 2.16) in terms of the horizontal acceleration. Equation (2.16*)* represents the horizontal pressure acting on the membrane wall at a height of ***y***, and equation (2.17) the total hydrodynamic pressure on the membrane.

$$p = -\rho h^2 \left(\frac{y}{h} - \frac{1}{2} \left(\frac{y}{h} \right)^2 \right) \frac{d\ddot{u}}{dx} \tag{2.16}$$

$$P = -\rho \frac{h^3}{3} \frac{d\ddot{u}}{dx} \tag{2.17}$$

The equation of motion (*2.17*) for a slice is governed by the differential pressures existing on the two adjacent membranes. Where P represents the total pressure exerted on the membrane which can be obtained from equation (2.17), and substituted into equation (2.18), yielding the differential equation (2.18).

$$\frac{dP}{dx} dx = -\rho h dx \ddot{u} \tag{2.18}$$

$$\frac{d^2\ddot{u}}{dx^2} - \frac{3}{h^2} \ddot{u} = 0 \tag{2.19}$$

The solution to the differential equation (2.19) is obtained, with the following boundary conditions applied to the problem.

$$\ddot{u} = C_1 \cosh\left(\sqrt{3} \tfrac{x}{h}\right) + C_2 \sinh\left(\sqrt{3} \tfrac{x}{h}\right) \tag{2.20}$$

Where

$$\ddot{u} = \ddot{u}_0 \text{ at } x = \pm l$$

The initial acceleration produces an increase of pressure on the wall given by:

$$P_w = \rho \ddot{u}_0 h \left(\frac{y}{h} - \frac{1}{2} \left(\frac{y}{h} \right)^2 \right) \sqrt{3} \tanh\left(\sqrt{3} \frac{l}{h}\right) \tag{2.21}$$

2.3.1.4 Galerkin Finite Element Analysis of Incompressible Water

The Westergaard and Housner method are computationally efficient and simplistic to employ, but do not provide a good representation of the hydrodynamic forces exerted on an arch dam wall surface. A better idealisation is to represent the impounded water using the Galerkin Finite Element Method.

The Galerkin weak form relates the fluid pressures to the dam accelerations on the upstream face. The domain is discretized by the Finite Element Method where the fluid domain is defined as a 3-D volume and the dam-reservoir interface defined by a 2-D surface. It may be noted that the bottom and sides of the reservoir are assumed to be rigid. The elemental hydrodynamic pressures acting on the dam-reservoir interface are determined by incompressible discretised elements and the dam using compressible Langragian elements. The following step is to lump the pressure values into equivalent hydrodynamic nodal forces. Once the nodal forces are obtained the following step is to obtain the added-mass coefficient matrix. This can then be added to the mass of the dam and the dynamic characteristics determined.

In the Galerkin formulation the hydrodynamic pressures are assumed to be governed by the pressure wave equation defined in equation (2.22) (Kuo, 1982). A boundary value problem needs to be established and solved in order to determine the hydrodynamic pressures acting on the dam wall surface.

$$\bar{V}^2 p(x,y,z,t) = \frac{1}{c^2} p(x,y,z,t) \qquad (2.22)$$

Where

p (x,y,z,t) = pressure distribution in reservoir

$c = \sqrt{\frac{k}{\rho}}$ celerity wave equation

K =bulk Modulus

ρ = unit mass of water

In order to determine the hydrodynamic pressures the boundary conditions defined below (See figure 4) must be assigned to the reservoir surfaces:

(1) At dam reservoir interface $\frac{\partial p}{\partial n_s} = -p\ddot{v}^t_{n_s}$

(2) At floor or reservoir the normal acceleration is zero. $\frac{\partial p}{\partial n_s}$ or $p\ddot{v}^t_{n_s} = 0$

(3) At the upstream end of the reservoir $\frac{\partial p}{\partial n_s}$ or $p\ddot{v}_{n_s}^t = 0$

(4) At free surface of reservoir: the surface pressure is assigned p= 0 or surface waves are neglected

(5) At canyon walls: $\frac{\partial p}{\partial n_s}$ or $p\ddot{v}_{n_s}^t = 0$

(6) L = The dam reservoir which should extend upstream three times the dam height

Where

n_s is defined as the outward normal direction from the reservoir surface

$\ddot{v}_{n_s}^t$ is the total normal acceleration of the fluid at the boundaries of the reservoir

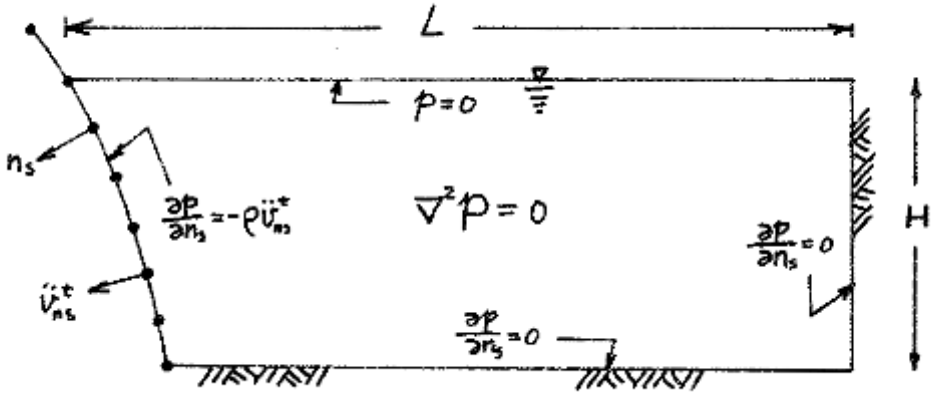

Figure 4: boundary conditions applied in the Galerkin Finite Element model to the three dimensional water body (Kuo, 1982).

The next step would be to determine the hydrodynamic pressures exerted on the dam water interface, but due to the complex geometry of the reservoir boundary, a closed integral solution of the form leads to a complex solution. Therefore the problem is approximated using a numerical solution based on the Galerkin Finite Element Method.

The Galerkin method is a weighted residual method which has an associated residual caused by the error of the numerical solution. Defining the numerical solution of the pressure wave equation (2.22) requires that the hydrodynamic pressures be approximated by a variable $\overline{p}$.

By defining the approximate solution to be approximated by $\overline{p}$, the residual of small magnitude and the strong form of equation (2.22) is defined by equation (2.23) and (2.24) respectively.

$$\overline{V}^2 \overline{p} - \frac{1}{c^2} \ddot{\overline{p}} = R \tag{2.23}$$

$$\iiint_V \underline{N}^T (\overline{V}^2 \overline{p} - \frac{1}{c^2} \ddot{\overline{p}}) dV = \underline{0} \tag{2.24}$$

Where:

N = A row vector of weighting functions

R = A residual of very small magnitude

We then apply greens theorem to equation (2.24) leading to equation (2.25), where the first term only exists along the boundaries of the reservoir.

$$\iint_S \underline{N}_S^T \frac{\partial p}{\partial n_s} dA - \frac{1}{c^2} \iiint_V \underline{N}^T \ddot{\overline{p}} dV - \iiint_V \underline{\overline{V} N}^T \cdot \overline{V} \ddot{\overline{p}} dV = 0 \tag{2.25}$$

After applying the boundary conditions previously listed to equation (2.25), equation (2.26) is produced:

$$\iint_S \underline{N}_S^T \frac{\partial p}{\partial n_s} dA = -\rho \iint_S \underline{N}_S^T \ddot{v}_{n_s}^t \, dA \tag{2.26}$$

It is noted that with the applied assumptions that $\ddot{v}_{n_s}^t$ vanishes along other boundaries and exists only at the dam-reservoir interface. The acceleration of the fluid at the interface can be related and expressed as the acceleration of the dam $\ddot{r}_{n_s}^t$. It must be noted that the dam acceleration and fluid accelerations are positive in the opposite directions.

$$\ddot{v}_{n_s}^t = - \ddot{r}_{n_s}^t \tag{2.27}$$

The normal acceleration of the dam can be expressed in terms of normal direction cosines using the three RCC components:

$$\ddot{r}_{n_s}^t = \underline{\lambda}\ddot{U}^t \tag{2.28}$$

Where

$\underline{\lambda} = [\lambda_X, \lambda_y, \lambda_z]$ the direction cosines at the points where $\ddot{r}_{n_s}^t$.

$\underline{\ddot{U}}^t = [\ddot{U}_x^t, \ddot{U}_y^t, \ddot{U}_x^t]$ total acceleration of the dam face in RCC components

Substituting equations (2.26), (2.27) and (2.28) into equation (2.29) simplifies to the weak form of the Galerkin expression equation (2.28). As for compressible water C = 4720ft/sec and for incompressible water C= ∞ which result in the second term vanishing.

$$\rho \iint_S \underline{N}_S^T \underline{\lambda} \underline{\ddot{U}}^t dA - \frac{1}{c^2} \iiint_V \underline{N}^T \ddot{\bar{p}} dV + \iiint_V \underline{\bar{V}N}^T \cdot \bar{V}\ddot{\bar{p}} dV = 0$$

(2.29)

After determining the Galerkin form of the differential equation, the domain is discretized by the finite element method, where the hydrodynamic pressures acting on the dam-reservoir interface are determined. After determining the hydrodynamic pressures, the interest of the formulation is to find the added mass representation of the hydrodynamic effects. This requires converting the hydrodynamic pressures acting on the face of the dam into lumped equivalent nodal forces, and thus the added-mass coefficient matrix.

Kuo (1982) and Ghanaat (1993) recommend the Glaerkin Finite Element method as it has the capabilities of accounting for the reservoir geometry, hence provides a better representation of the problem However, the complexity of defining the boundary value problem makes the method unattractive as it requires the representation of the site geometry very accurately. It is a cumbersome process which requires advance understanding of finite element modelling. In contrast to the previously mention added mass formulations, Kuo (1982) yielded satisfactory results when he used the Galerkin finite element approach.

2.3.1.5 Compressible Fluid Structure Interaction Method

All approaches discussed above ignore the compressibility of the water and the energy loss due to radiation of the pressure waves in the upstream direction, and also due to reflection and refraction at the reservoir bottom and canyons (US Army Corps of Engineers, 1994). A preferred approach method is to setup a coupled problem, which represents the impounded

water body and arch dam using compressible finite elements (See figure (5)). This provides a realistic representation as a compressible complex impounded water body can be taken into consideration. The fluid - structure interaction of the dam wall and impounded water body are represented by an asymmetric coupled system which is generally defined by a mixed formulation defined in equation (2.30) (Tillioune & Seghir, 1998).

$$\begin{bmatrix} M_s & 0 \\ \rho_W Q^T & M_F \end{bmatrix}\begin{bmatrix} \ddot{u} \\ \ddot{p} \end{bmatrix}+\begin{bmatrix} C_s & 0 \\ 0 & C_F \end{bmatrix}\begin{bmatrix} \dot{u} \\ \dot{p} \end{bmatrix}+\begin{bmatrix} K_s & -Q \\ 0 & K_F \end{bmatrix}\begin{bmatrix} u \\ p \end{bmatrix}=\begin{bmatrix} F_G \\ 0 \end{bmatrix} \tag{2.30}$$

Where

M_s & M_F = Dam wall-foundation system and impounded fluid mass matrices

C_s & C_F = The damping factors of the dam wall and impounded fluid

K_S & K_F = Stiffness of dam-foundation system and bulk modulus of the fluid

ρ_w = The density of the impounded water body

Q = Transformation matrix that converts nodal pressures into hydrodynamic forces

The displacement of the dam wall *u* and pressures *p* of the fluid are the arguments of the system.

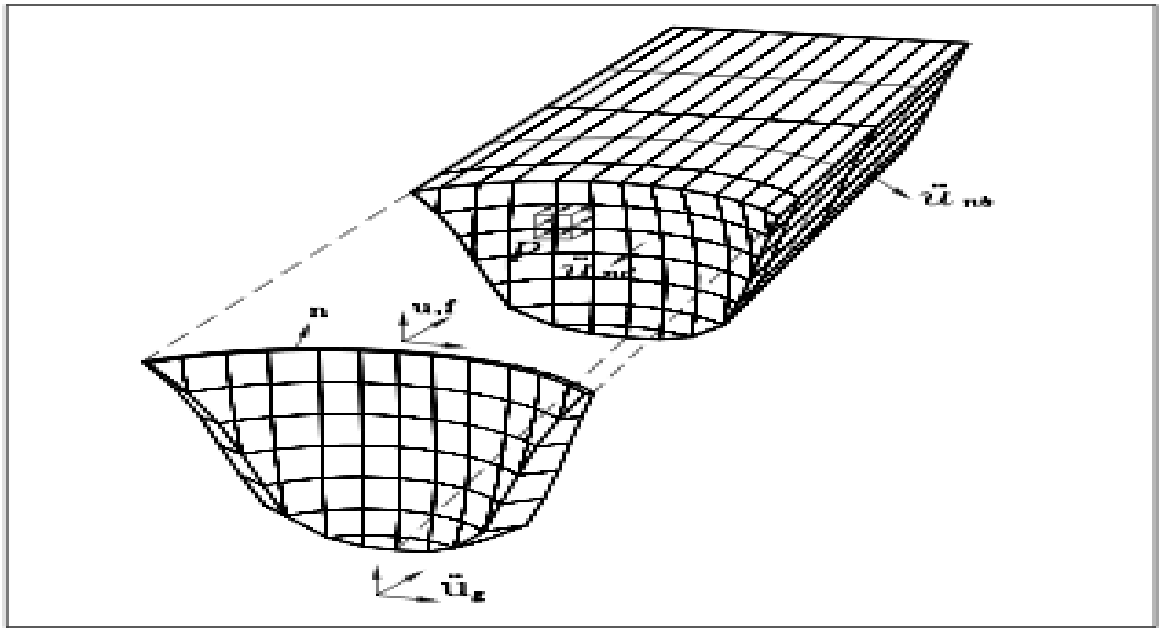

Figure 5: discretisation of dam wall and compressible impounded water body (Ghanaat, 1993)

The idea of water compressibilty in the analysis of seismic loading induced hydrodynamic effects was first introduced by Fok and Chopra (1985). They introduced frequency-dependent hydrodynamic terms in the equation of motion which could be interpreted as an added mass, added damping and and added force. The added damping term is as a result of the refraction of hydrodyanmic pressure waves into the absorptive reservoir bottom and propergation of pressure waves in the upstream direction (See figure (6)). The energy loss is approximated by the wave reflective coefficient α, defined as the ratio of reflected-to-incident wave amplitude of a pressure wave striking the reservoir bottom (US Army Corps of Engineers,1994). The value of α can be varied from 1 for a rigid nonabsorptive boundary and α =0 for a fully absorptive boundary.

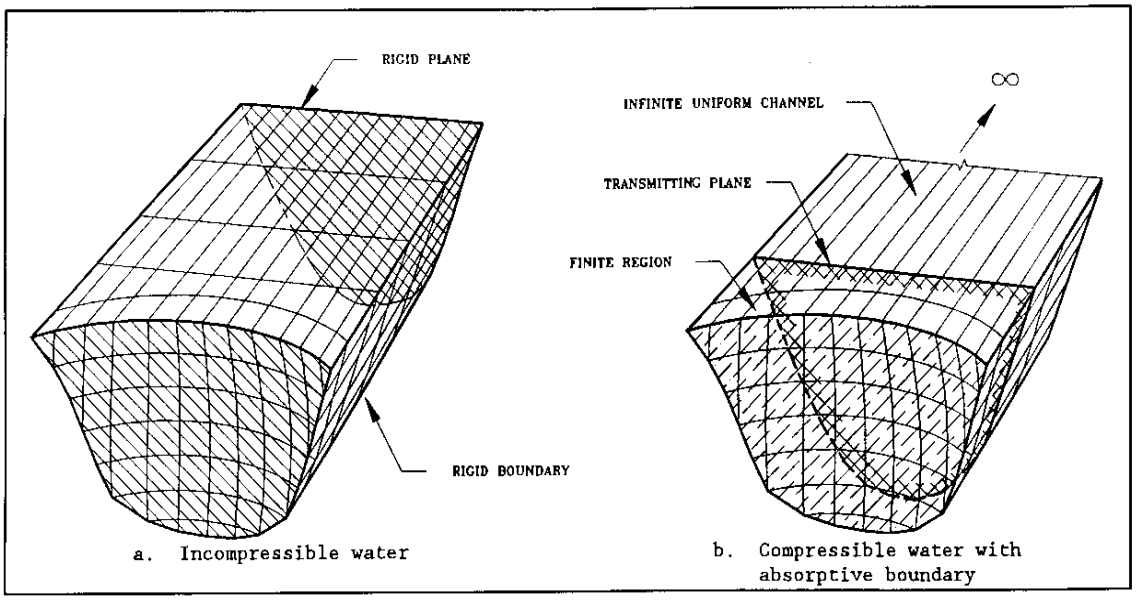

Figure 6: incompressible water body with rigid boundaries and compressible water body with absorptive boundary conditions (Ghanaat, 1993).

Mivehchi et al. (2003) carried out the compressible fluid structure interaction formulation when developing the computational model of two Iranian arch dams, the Saveh arch dam and Shahid-Rajaee arch dam. Features of the model included a dam-reservoir-foundation system where the reservoir was discretized using compressible acoustic elements with an acoustic velocity of $v \approx 1440$ m/s. The models were verified by experimental measurement of ambient response of the two dams. The models gave a good representation of the impounded water body and yielded satisfactory results for both the dams. The Saveh arch dam model was found to give correlating results when compared to the as-built dynamic properties obtained from ambient vibration tests. The Shahid-Rajaee dam gave results with slight discrepancies that could be minimized by applying an appropriate massive foundation and actual material properties (Mivehchi et al., 2003). This method has also been used successfully to calibrate the Berke arch dam located in Turkey, using ambient vibration testing results. The Berke arch dam was calibrated by changing the material parameters of the foundation and arch dam. In the calibration of the finite element model the dam-reservoir-foundation were represented by the Lagrangian approach were both the reservoir and dam variables are displacements. This avoided any compatibility matrices which are required on the dam-reservoir interface (Sevim, Bayraktar & Altunisik, 2011).

2.3.2 Modal Analysis

Eigenvalue extraction

Modal parameters (Mode shapes and natural frequencies) of the dam-reservoir system are computed by solving the eigen problem generally represented by equation (2.30). One must note, that the added mass which is the equivalent of the hydrodynamic pressures is included in the equation by the added mass matrix defined by m_a **.** It is stated that for the undamped free vibration structure, ϕ and ω represent the mode shapes and natural frequencies respectively. The modal parameters obtained from equation (2.30) are for the coupled dam-water-foundation system. The foundation flexibility is accounted for by including the stiffness of the foundation rock, and the compressibility of the reservoir water is incorporated into equation (2.31) by the added mass matrix.

$$k\phi = \omega^2 (m + m_a)\phi \tag{2.31}$$

The eigenvalue problem is solved by using an iterative procedure based on a variation of Stodola 's method (Ghanaat, 1993). The method assumes an initial mode shape and is adjusted accordingly until an appropriate adequate solution of the true mode shape is obtained. This will be followed by attaining the corresponding frequency form the equation of motion (Ghanaat, 1993). A popular used method which implements this algorithm is the Subspace Iteration Method, (Bathe & Wilson, 1976) which is found in most general purpose structural analysis programs.

- Subspace Iteration Method

The subspace iteration method is based on the simple idea of a simultaneous inverse power iteration. A small set of base vectors defining a 'subspace' are created. The subspace is transformed by an iteration into the space containing the lower few eigenvectors of the overall system (2.32).

$$k\phi = (m + m_a)\Omega^2\phi \tag{2.32}$$

Where

Ω^2 = The diagonal of ω^2

ϕ = The matrix of mode shapes [ϕ_1 , ϕ_2 , ….ϕ_p]

Assume that, at the *i*th iteration, a set of *m* vectors, V_i^n n=*1*,…, *m* , exist, where *m* is less than the number of degrees of freedom. These can be considered as the base vectors that define *m* dimensional subspace out of *n* dimensions in the model. The matrix $[V]_{(i)}$ is arranged such that subspace vectors are the columns, and the rows are the complete number degrees of freedom in the finite model.

The first step is to define a new set of base vectors by solving the equation:

$$[K][V]_{(i+1)} = [M][V]_{(i)} \tag{2.33}$$

This is the generalised inverse power sweep operation with *m* vectors which involves the solution of a complete set of linear stiffness equations for several right hand side vectors. The stiffness and mass matrices of these structure are then projected onto the subspace by equation (2.34) and (2.35), thus defining a mass matrix and stiffness matrix (*m x m matrices*) in the subspace.

$$[K^*] = [\hat{V}]_{(i+1)}^T [K][\hat{V}]_{(i+1)} \tag{2.34}$$

$$[M^*] = [\hat{V}]_{(i+1)}^T [M][\hat{V}]_{(i+1)} \tag{2.35}$$

The below eigen problem equation (2.36) is now solved using the Householder method. The method is used to reduce a general matrix to a symmetric diagonal, upper or lower triangle matrix. This is done by using a cholesky decomposition of $[M^*]$ and pre-multiplying and post-multiplying $[K^*]$ by the inverse of the lower and upper triangular matrices. Thus, equation (2.36) is defined into a tri-diagonal form equation (2.37) where the eigenvectors can be determined.

$$([K^*] - \omega^2[M^* + M_a^*])\{\phi\} = 0 \tag{2.36}$$

$$([A] - \omega^2[I])\{\phi\} = 0 \tag{2.37}$$

Where [*A*] is symmetric tridiagonal matrix, and [*I*] is the identity matrix. The eigenvectors defined in the reduced space can be transformed back to the full space of the structural

problem to define [V] for the next iteration. The entire iterative cycle is repeated many times until the process converges to the true mode shapes and natural frequencies.

$$[V]_{(i+1)} = [\hat{V}]_{(i+1)}[\phi] \tag{2.38}$$

The advantages of the subspace method is that it extracts the eigenvalues in a reduce space, which leads to a rapid convergence of the eigenvectors in full space. The number of base vectors carried in the iterations and the choice of initial base vectors are important for an economical solution. The disadvantage of the Subspace iteration method, is that, it's a conventional method limited to symmetric problems. This is suitable for solving uncoupled eigen-modes for the added mass methods, but is inadequate for coupled dam-water problems as they result in asymmetric governing equations (Simulia, 2010).

Decoupled and Coupled Modes

The dynamic analysis of a fluid structure interaction problem is a demanding procedure because of its complexity. The governing matrices of the coupled system are asymmetric (see equation 2.29) and it gets computationally cumbersome to solve such an eigen problem. The modal approach is the recommended method, as the modal parameters (mode shapes and natural frequencies) are calculated based on the eigen problem. This makes it more efficient than the direct method (e.g., Subspace method) which computes dynamic properties based on the number of unknowns.

When analysing the dynamic characteristics of the fluid structure interaction approach a coupled dam-reservoir system must be considered (Poursartip & Lotfi, 2008).The eigen problem of this system can be analysed in one of two ways: The first being a decoupled modes, which can be obtained very efficiently by using standard eigen – solution routines, such as the subspace iteration method previously discussed, which determines the mode shapes of the dam alone and the mode shapes of the reservoir with rigid walls at the boundaries. Secondly, coupled modal analysis is also utilised which uses coupled mode shapes of the dam-reservoir system (Poursartip & Lotfi, 2008) . A specific technique is utilised to solve the asymmetric eigen problem.

This technique uses the advantage of orthogonallity conditions, where two sets of eigenvectors need to be calculated by the following eigen-problem

$$\overline{K}X^R = \overline{M}X^R\overline{\Lambda} \tag{2.39}$$

$$\overline{K}^T X^L = \overline{M}^T X^L \overline{\Lambda} \tag{2.40}$$

In the above equation X^R and X^L are denoted as matrices of the right and left eigenvector for the coupled system. Since the coefficient matrices of equation (2.39) and (2.40) are the transposes of each other, the eigenvalues of a specific mode are the same but the corresponding eigenvectors are different. Equation (2.39) and (2.40) are solved using the inverse iteration method, which is capable of solving asymmetric eigen problems. The convergence rate is improved by using the shifting technique, which always converges to the eigenvector corresponding to the smallest eigenvalue. It is recommended that the inverse iteration technique be used to attain an approximation due to that convergences can be associated with a deviation between the smallest eigenvector and its corresponding eigenvalue. This can be overcome by using the Rayleigh quotient shift to reach the desired accuracy.

2.3.3 Foundation Rock Analysis

Arch dams are designed to transfer all of the compressive loads onto the abutment canyon walls. This results in the foundation rock having a significant influence in the response of an arch dam, and hence, they must be included in the dynamic analysis. An idealistic foundation is one that includes all geological features and extends to a distance whereby boundary effects have no influence on the stresses and dynamic characteristics. This becomes practically impossible as finite element techniques are not yet sufficiently developed to account for such analytical procedures, and models would become computationally intensive.

For the limitations stated above a simplified idealisation of the deformable foundation is considered in practice (Clough, 1980). Only a significant portion of the foundation is include as part of the arch dam model. The US Army Corps of Engineers (1994) specifies that an elliptical shaped flexible foundation rock system must be considered, that requires the deformation modulus of the supporting rocks, which accounts for faults and joints in the foundation rock, and the Poisson's ratio to be defined for the material properties. The inertial and damping effects of the foundation rock should be ignored in the dynamic analysis (Ghanaat, 1993).

The foundation mesh is constructed using solid mesh elements constructed on semicircular planes that cut into the canyon walls and are oriented normal to the rock-concrete interface as illustrated in figure 7. Each semi-circle is rotated about a diameter always oriented in the upstream-downstream direction. The foundation model should be assembled out of eight-node finite elements, where the elements have anisotropic material properties and are smaller near the dam-foundation interface and increase in size as you move to the boundary of the foundation (US Army Corps of Engineers, 1994).

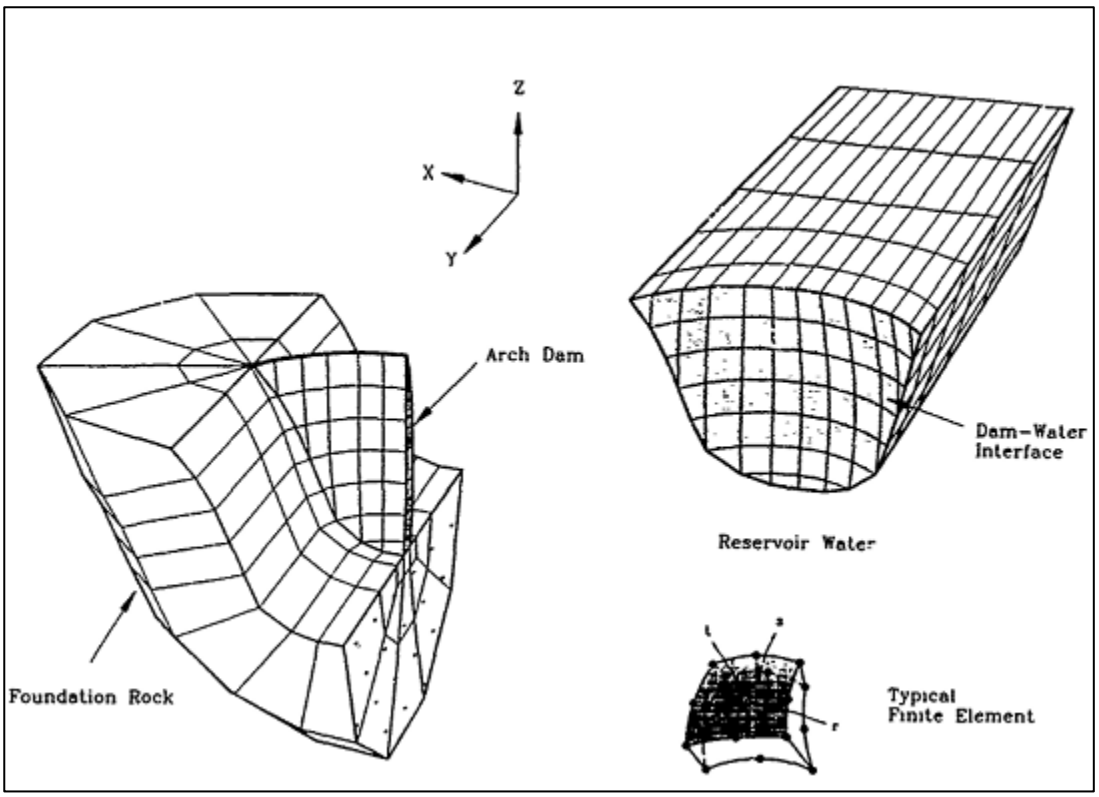

Figure 7: Foundation Rock model using semicircle planes cut into the canyon walls (Ghanaat, 1993).

2.3.3.1 Deformability of Foundation

The US Army of Engineers (1994) point out the importance of having a deformable foundation by analysing its influence on the static properties. The result of a parametric study conducted on the Morrow Point dam, illustrated that the foundation flexibility has an influence on the response of the dam. Three values of the foundation modulus were considered: firstly a rigid foundation, with the same modulus of concrete, and secondly one-fifth the modulus of concrete. The analyses were conducted for hydrostatic loading and loading acting on the foundation flanks and bed. The results showed that stresses and deflection of the dam are considerably affected by foundation flexibility. The same can be

said about the effect on the dynamic properties by the foundation stiffness. This was investigated by Nzuza (2013) on a case study of the Roode Elsbeg dam, where the natural frequencies illustrated a rapid increase for a soft foundation type, with the Youngs modulus of the foundation E_f less than that of the dam ($E_f < E_c$), and a gradual increase for hard foundation $E_f > E_c$ (see figure 8). Therefore, this study concluded that the dynamic properties are sensitive to stiffness variation of the considered foundation.

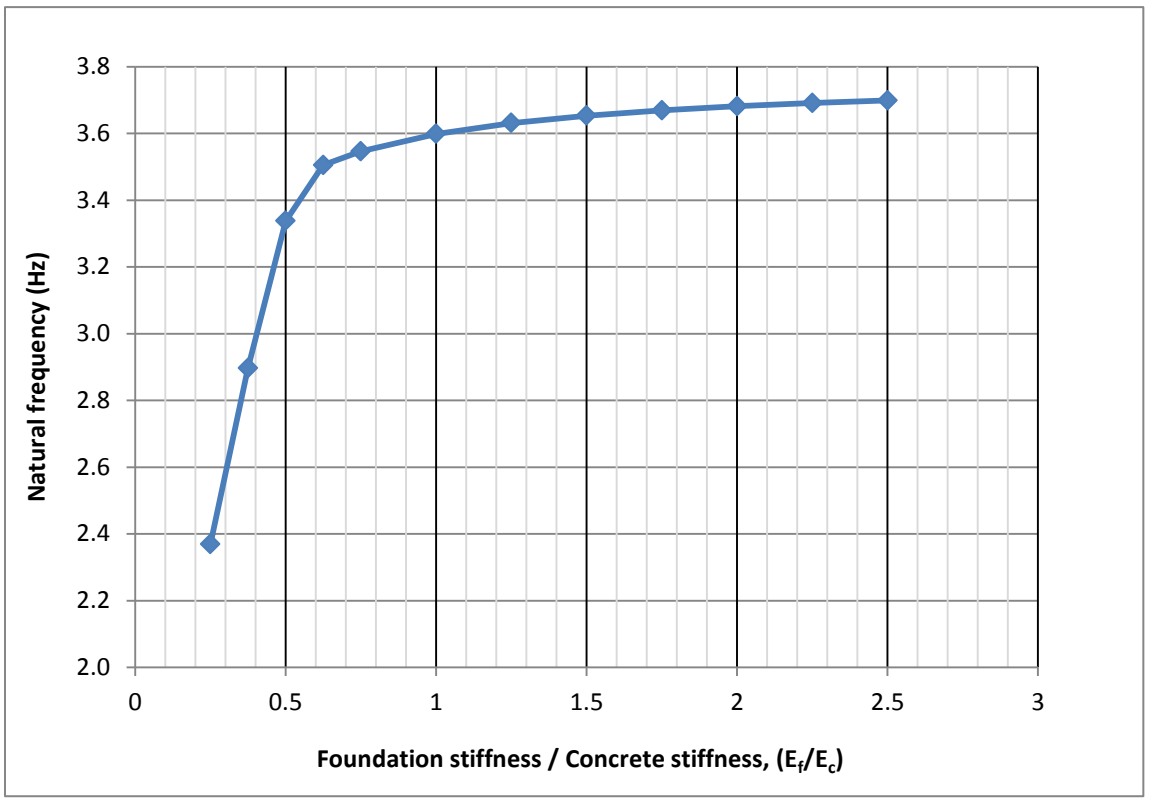

Figure 8: Dynamic properties with change in foundation stiffness (Nzuza, 2013)

2.3.3.2 Size of Foundation

In a dynamic analysis the natural frequencies and mode shapes control the foundation size. The size of the foundation model should be selected such that it has no influence on the natural frequencies and mode shapes of vibration. The natural frequencies are known to decrease with an increase in foundation size, but for massless foundation the size has a negligible influence when the foundation size R_f (radius foundation) greater the one dam height, except for foundation rocks which have low modulus of elasticity. The guidelines provided by the US Army Corps of Engineers (1994) recommend that for a massless foundation, a R_f equal to one dam height is generally accepted. However, when the

stiffness of the foundation rock is less than half the modulus of the concrete, a model with a R_f of two times the dam height is acceptable.

Makha (2012) conducted a parametric study which investigated the influence of foundation size on the natural frequencies. A standard foundation equal to one height of the dam wall was chosen as the reference height. This was increased by increments until a height of 50m above the reference. The increase in R_f resulted in a slight decrease of 0.2% in the lower natural frequencies, and 10% for modes higher than 13. For arch dams, the lower modes are of great importance. The above result show that a depth and an upstream-downstream radius equal to a height of the dam wall, recommended by the US Army Corps of Engineers (1994) is acceptable.

2.3.4 Earthquake Foundation Input mechanisms

When evaluating the response of a dam during a seismic event, the free field earthquake acceleration is applied at the foundation base and is allowed to propagate through the foundation by the elastic wave propagation mechanism until it reaches the foundation surface (Sooch & Bagchi, 2007).

This section discusses the different earthquake input mechanisms which are currently being used. It is important to note that the selection of an earthquake input mechanisms is not significant in ambient studies as seismic ground accelerations are not considered. However, it is important to understand the foundation input mechanisms for a completing review of the dynamic modelling aspect.

- Massless foundation

Most dynamic models assume that the rock foundation is massless. Without mass the foundation does not develop vibration waves which modify the properties of the seismic waves travelling throughout the foundation (Zienkiewicks et al. 1984).In this method the ground acceleration as function of time recorded from previous earthquakes is applied uniformly at the truncated foundation base. The wave propagation in massless foundations is allowed to travel at an infinite speed, this allowing the input accelerations to be transferred instantaneously through the foundation to the dam-foundation interface. This makes the method preferable in the analysis of seismic loading as the motions at the interface would be the inputs (Chuhan et al. 2009).

In a study conducted by Proulx (2004), he evaluated the seismic analyses of three arch dams using numerical finite elements. He considered the calibration of three dams using recorded earthquake responses. The foundation input approaches included a massless foundation and an energy dissipating foundation (Mass foundation). The results obtained illustrated that high damping ratios of 8-15% were required to calibrate the dams which is to be not realistic as the values have no physical basis. Chuhan (2009) conducted a linear and nonlinear seismic analyses of the Dagangshan arch dam using two different input models, this included also the massless foundation approach which only considered the flexibility of the dam, hence, no energy dissipating factor. The results he obtained was similar to Proulx (2004) using this approach with damping ratios of 5% and 10% showed that massless foundation approach overestimates the seismic response of the dam both in the linear elastic case and nonlinear analyses.

From the above results it is seen that a massless foundation result in an overestimation of the earthquake response for an arch dam. This is due to that a massless foundation does not consider energy dissipation in the foundation. The inaccuracy mentioned above is problematic in seismic analyses, but can be considered to be negligible in the extraction of modal parameters as vibration waves are non-existence in the foundation. This is due to that no external loads are considered on the boundary of the foundation.

- Deconvolution Input Method

In this case the foundation is considered to be an energy dissipating foundation. The foundation mass of the foundation rock and the foundation material and radiation damping effects are taken into account in the model (Darbre & Proulx, 2002). In this method, the analysis is carried out in the two procedures: (i) Firstly a deconvolution is performed to determine the acceleration time history that can be employed to the base of the foundation produce the specified free field acceleration time history at the base of the da. (ii) The calibrated base foundation is then applied to the base of the foundation to perform the seismic analysis (Sooch & Bagchi, 2007).

The deconvolution analysis allows for the alteration of the amplitude and frequency contents of seismic ground motion defined at the base of the foundation attain the specified ground acceleration at the dam-foundation interface. Initially when commencing the procedure the base foundation acceleration is assumed to be the same as the free field ground acceleration. The acceleration at the dam-foundation interface is estimated using by

solving the wave propagation problem of the dam-foundation system using the finite element procedure. This estimated ground acceleration at benchmark point on the dam-foundation is then compared to the original free field ground acceleration after transforming both the signals into the frequency domain using a Fourier analysis. The Fast Fourier transform (FFT) and inverse Fast Fourier transform (IFFT) are used for transforming time domain signals to a frequency domain signal and vice versa. The free field acceleration is applied at the foundation base and by solving the wave propagation problem, the acceleration signal at an arbitrary point on the dam-foundation interface is determined. The free-field acceleration signal at the dam-foundation is compared in the frequency domain, and a correction factor for each frequency is computed using the ratio of the Fourier amplitudes of the synthesized and free-field ground acceleration signals in a given iteration (Sooch & Bagchi, 2007).

The acceleration signal applied at the base of the foundation is modified using the correction factor for each frequency. The modified acceleration history is then transformed back into time domain using the IFFT and the analysis of the wave propagation analysis for the foundation system is repeated new ground acceleration at the base of the foundation. The procedure is repeated until the original free-field ground motion at the dam-foundation interface closely matches the original free-field ground motion.

- Viscous-spring boundary input model

The viscous boundary model was used by Chuhan et al. (2009) to account for wave transmitting in the foundation boundary. This method is sophisticated as it can be used in the non-linear analysis which includes contraction joints of the arch dam. They consider this method to be very efficient and convenient as it can be incorporated in the finite element code quite easily and has sufficient accuracy without much increase in the computational time of the model. In this method, pairs of dashpots and springs are installed in all of the boundaries. Each node on the boundary contains three pairs of dashpots and springs, one in the normal direction of the boundary plane, and the other two in the tangential directions. The parameter of spring and dashpots of arbitrary node *i* are given by the following equations:

$$K_{in} = \frac{\lambda + 2G}{(1+a)r}, \qquad C_{in} = b\rho c_p \tag{2.41}$$

$$K_{is} = \frac{\lambda + 2G}{(1+a)r}, \qquad C_{is} = b\rho c_s \tag{2.42}$$

Where n and s refer to the normal and tangential directions of the boundary plane. K is the stiffness of the spring and C is the viscous damping. λ and G are the lame's constants, c_p and c_s denote the propagation velocity of p-wave ad s-wave, ρ is the mass density and r is the distance from the wave source to the node i.

Unlike the massless foundation the input of the earthquake motions cannot be defined directly at the truncated bases of the foundation. The wave motion problem is converted into a problem of equivalent force input on the artificial boundaries. The springs and dashpots also act as radiation energy absorbers for scattering waves reflected by the canyon.

As previously mentioned seismic analyses of the Dagangshan arch dam also included the linear and non-linear viscous input model to study the behaviour of the earthquake input mechanism. Results show that the use of the viscous spring boundary input leads to a reduction of about 25-40% of dynamic response of the arch dam, which is regarded to be a better estimate than the massless foundation as it over estimates the response of the dam both in the linear and non-linear analysis.

2.4 Ambient Vibration Testing

Dynamic field testing techniques are important as they provide reliable testing techniques which allow engineers to obtain the as built dynamic properties of a structure. Dynamic monitoring of structures allows us to obtain natural frequencies, mode shapes, and damping ratios which are related to structural properties such as mass, stiffness and damping. Any change in anyone of the dynamic properties can therefore indicate structural damage. Measured dynamic properties can be used to update and fine tune Finite Element Models to replicate as closely as possible the as built behaviour of a dam (Moyo & Oosthuizen, 2010). Finite Element Models play a key role in condition assessment of dams and which is done by comparing the updated models to the design model.

The main aim of dynamic testing is to obtain the modal properties of the structure from vibration measurements. Forced vibration testing (FVT) and ambient vibration testing

(AVT) are the two most popular methods widely being used in industry. They take into account the interdependent reservoir–foundation system (Darbre & Proulx, 2002).

Forced vibration testing is an expensive method which requires mechanical exciters to produce vibrations within the structure. This method is effective but due to its associated costs with excitation equipment, dam owners do not consider the approach. Ambient vibration testing is a technique which has gained popularity amongst dam owners as it provides a cost effective method which does not interfere with the operation of the structure, and is fairly good method when it comes to measuring the dynamic characteristics of a structure (Mivehchi et al., 2003). Ambient vibration testing is based on the structures responsiveness to the natural environment forces (wind, temperature, water and earthquake).This is in contrast to forced vibration testing where a known load is applied to the structure. The environmental forces cannot be computed, and therefore the structures responsiveness is used to compute the natural frequencies and mode shapes (Daniell & Taylor, 1999).

Since the early 990' s more researchers have gained trust in the use of ambient vibration testing as more sensitive equipment have been produced which are able to capture subtle vibration movement. Darbre (2000) showed that it was possible to attain reliable filed results over three year duration of measurements. His research was further followed up by Mivehchi et al. (2003) where two dams in Iran underwent successful testing. The ambient vibration testing results were further used to verify the results obtained from finite element mathematical model by comparing with behaviour of the as-built structures. It was found that model gave good results that correlated with the ambient vibration test results. (Mivehchi et al., 2003).

The main challenges in the development of the AVT has been the extracting of the modal parameters from measured data. To this day many modal parameter techniques have been developed, these include methods based on the time history of the outputted signals which are referred to as time domain methods, and those based on the Fourier transform of signals, referred to as frequency domain based methods. *Figure 9* below illustrates ambient vibration testing conducted on the Roode Elsberg dam in Worcester.

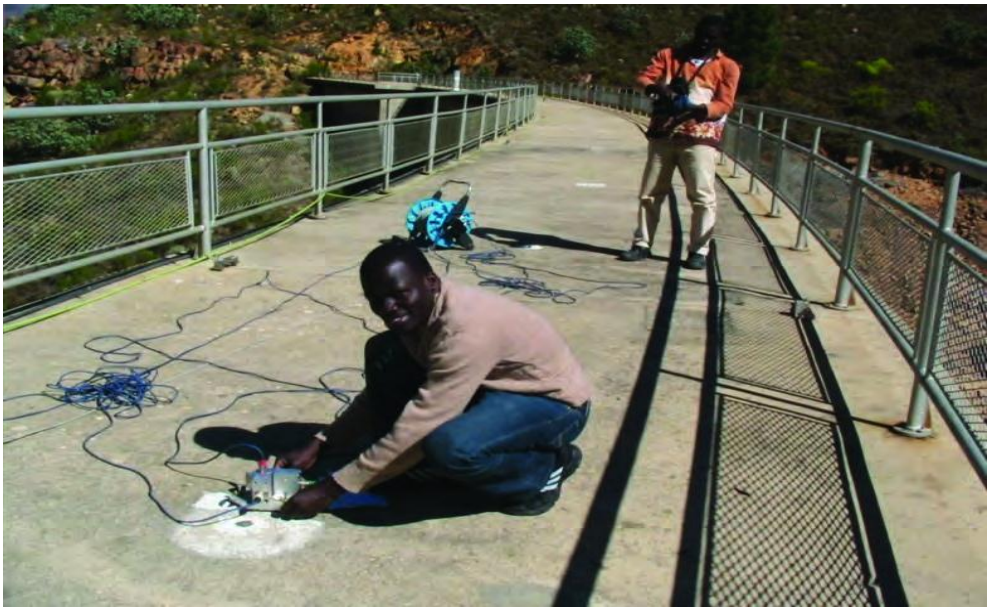

Figure 9: Ambient vibration testing of the Roode Elsberg dam located in Worcester, Western Cape, South Africa (Moyo & Oosthuizen, 2013)

2.5 Modal Parameter Estimation Techniques used in AVT

2.5.1 Frequency domain methods

- Peak Picking

One of the oldest techniques used in modal parameter estimation is the Peak Picking technique. The method is based on an output only and identifies the natural frequencies by the peaks of the frequency response function (FRF) curves. The half power bandwidth method is used to obtain the damping ratios and the FRF amplitude give a good estimation of the mode shape.

The natural frequencies are determined by not only looking at the FRF spectra but also inspecting the coherence function between two signals (Brinker et al. 2000)

$$\gamma_{xy}^2(f) = \frac{\left|G_{xy}(f)\right|^2}{G_{xz}(f)G_{yy}(f)} \tag{2.43}$$

Where

$G_{xy}(f)$ = The value of the cross spectrum between signal x and s at the frequency f

$G_{xx}(f)$ & $G_{yy}(f)$ = the values of the auto spectra of signal *y* and signal *s* at the same frequency

If f is defined as a natural frequency then the coherence function is then close to unit because of the high signal-to-noise ratio at that frequency, this is very useful in determining the correct natural frequency. The method is considered to be the easiest and most popular technique for quick estimation of modal parameters of civil engineering structures (Felber, 1993. Danielle & Taylor, 1999). However, like all methods it has drawbacks as it works well when damping is low and the modes are well spaced out. If the natural frequencies are closely situated then erroneous results can be expected. The second drawback is that the selection of the natural frequency is subjective task if the spectrum peaks are not clear. The last drawback is that a fine frequency resolution is needed to obtain a very good approximation of the natural frequency (Moyo & Oosthuizen, 2013).

- Frequency Domain Decomposition

The Frequency domain decomposition resolves the main drawbacks of the Peak picking method but still keeps the ease of application of the classical approach. The FDD technique is based on the input and output power spectrum density (PSD) relationship (Brincker et al. 2000).

$$G_{yy}(j\omega) = \overline{H}(j\omega)G_{xx}(j\omega)H(J\omega)^{P} \tag{2.44}$$

Where $G_{xx}(j\omega)$ is the *r x r* power spectral density (PSD) matrix of inputs, $G_{yy}(j\omega)$ is an *m x m* matrix of response, m is the number of responses. $\overline{H}(j\omega)$ is a *m x r* Frequency Response function (FRF) matrix which is expressed as partial fractions (see equation (2.45) below) form via poles λ_k and residues R_k which contain information about the mode shapes.

$$H(j\omega) = \sum_{k=1}^{n} \frac{R_k}{j\omega - \lambda_k} + \frac{\overline{R}_k}{j\omega - \overline{\lambda}_k} \tag{2.45}$$

Where

$$R_k = \phi_k \gamma_k^T$$

ϕ_k and γ_k^T are the mode shapes and the modal participation vectors respectively.

If the input is defined as white noise then the PSD becomes a constant square matrix.

$$G_{yy}(j\omega) = \sum_{k=1}^{n}\sum_{s=1}^{n}\left[\frac{R_k}{j\omega-\lambda_k}+\frac{\overline{R}_k}{j\omega-\lambda_k}\right]xC\left[\frac{R_s}{j\omega-\lambda_s}+\frac{\overline{R}_s}{j\omega-\overline{\lambda}_s}\right]^P$$

(2.46)

With the use of the partial fraction theorem, multiplying the two partial fractions, the output PSD can be reduced to a residue form as shown below:

$$G_{yy}(j\omega) = \sum_{k=1}^{n}\frac{A_k}{j\omega-\lambda_k}+\frac{\overline{A}_k}{j\omega-\lambda_k}+\frac{B_k}{j\omega-\lambda_k}+\frac{B_k}{-j\omega-\lambda_k}+\frac{\overline{B}_k}{-j\omega-\lambda_k} \quad (2.47)$$

Where

A_k is the K^{th} residue (m x m) matrix of the output PSD also known as the matrix given by:

$$A_k = R_k C\left(\sum_{k=1}^{n}\frac{R_s^P}{-\lambda_k-\lambda_k}+\frac{\overline{R}_s^P}{-\lambda_k-\lambda_k}\right)$$

(2.48)

Where the contribution of to the residue from the K^{th} mode is given by

$$A_k = \frac{R_k C\overline{R_k^P}}{2\alpha_k} \quad (2.49)$$

Where α_k is the negative of the real part of the pole $\lambda_k = -\alpha_k + j\omega_k$, this term becomes dominating when damping is light, and thus, for case of light damping, the residue becomes proportional to the mode shape vector (Brincker et al. 2000):

$$A_k \alpha R_k CAR_k = \phi_k \gamma_k^p C\gamma_k \phi_k^p = d_k \phi_k \phi_k^p \quad (2.50)$$

Where $d_k = \gamma_k^p G_{xx}\gamma_k$ is a real scalar for white noise excitation. In the vicinity of a natural frequency, PSD can be approximated by modal decomposition (Zhang et al. 2005).

$$G_{yy}(j\omega) = \phi_k \frac{2d_k}{j\omega - \lambda_k} \phi_k^p = \alpha_k \phi_k \phi_k^p \tag{2.51}$$

The FDD method is the backbone of the frequency domain and works on a systematic identification. In the Frequency Domain Decomposition (FDD) identification the first step is to estimate the power spectral density matrix. The estimated output PSD known at discreet frequencies $\omega = \omega_i$ is then decomposed by taking the Singular Value Decomposition (SVD) of the matrix.

$$G_{yy}(j\omega) = U_i S_I U_i^H \tag{2.52}$$

Where

U_i = The unitary matrix holding the singular vectors

S_I = Is a diagonal matrix holding the scalar singular values.

Near a peak corresponding to the K_{th} mode in the spectrum, this mode or a possible close mode will be dominating. If only the K_{th} mode is dominating there will be one term in spectral density. In the above mentioned scenario, the first singular vector is an estimate of the mode shape and the corresponding singular value is the auto power spectral density function of the single degree of freedom system, this spectral density function is identified around the peak by comparing the mode shape estimate ϕ with the singular vectors for the frequency lines around the peak.

From the piece of the SDOF density function obtained around the peak of the PSD, the natural frequency and the damping can be obtained.

The advantage of the FDD is its ability of calculating closely spaced modes but still being user friendly. The main disadvantage in the FDD method is that it can compute damping rations, and relies on the user to analysis techniques to determine the modes and hence approximate the modal parameters of the structure and leakage of the fast Fourier transform. The user needs to have good knowledge in optimisation procedures for parameter estimation as it will be required to obtain the appropriate frequency resolution for FDD,

2.6 Chapter Summary

This chapter reviews all important aspects that must be considered when developing a dynamic model of an arch dam. These included a review of the methods used to model the hydrodynamic behavior of the impounded water body, the algorithms used to extract the modal parameters of a coupled and decoupled dam-reservoir system, the foundation rock and the parameters that must be considered in idealizing the bedrock and canyon supports. Although field testing will only be used for verifying the dynamic model, a minor review of the existing field techniques was discussed to provide a comprehensive review.

The Westergaard method is efficient and easy to apply, using the 'added-mass' matrix to account for the influence of the hydrodynamic pressures on the dynamic behaviour. It must be noted, that all of the 'added mass' methods where derived under the consideration of ground motion induced by earthquakes and defined with the crude assumptions. Researchers who have previously applied the modified Westergaard method, state that the method does not properly represent the pressures acting on the arch dam and results in an overestimation of the dynamic pressures, and hence, the dynamic properties of the arch dam. The Galerkin finite element method and the FSI method provide better representations as the fluid medium is considered in the idealization of the problem. Kuo (1982) showed that the Galerkin method provided a good representation of the dynamic behavior of the Techi arch dam. It is considered that the fluid structure interaction method provides an even better representation as the compressibility effect of the fluid is considered in the idealization.

Eigenvalue extraction techniques such as the Subspace Iterative eigenvalue extraction method are only applicable with the use of the added mass technique, and a decoupled modal analysis of the dam-reservoir system. In the decoupled method, the fluid and dam wall modal parameters are obtained independently of each other, and hence, the interaction at the dam-reservoir surface is not considered. In the instant where the fluid structure interaction method is analysed as a coupled problem (fluid structure interaction method), the governing system equation becomes asymmetric, and calls for a more sophisticated method such as the Coupled Modes methods which can be used to extract the modal parameters of the coupled system. Thus, in the extraction of the modal parameters, the dam-reservoir system is coupled and influences the modal parameters of the system.

The review indicated that defining the foundation rock accurately is very important as it has a significant influence on the dynamic behavior of the dam. As discussed in the review, aspects such as the deformability and foundation size and shape, play a major role in the behavior of the dynamic model. It must also be noted that while earthquake input mechanism are important to be defined properly, it has a major influence in the context of seismic evaluation, as when contrasted to the extraction of the modal parameters in the ambient state. Thus, selecting to define the mass of the foundation has an insignificant influence in the extraction of the dynamic parameters.

Finally, literature shows that ambient vibration testing is a cheap and reliable field testing technique. It is important to verify this, as in the context of the Roode Elsberg dam, ambient vibration testing equipment is currently setup and recording the operational modal parameters of the arch dam. This gives us assurance that if the equipment is setup appropriately on site then the data recorded by the instruments is of high accuracy.

It is important to understand that in the context of the proposed research, the dam will be only considered under the influence of ambient conditions, thus the fluid medium and dam will not be undergoing magnitudes of displacement that it would undergo in seismic conditions. This makes the added mass method questionable in the applicability of the proposed context. Modelling the reservoir will also be important as the current reservoir geometry and orientation is complex and could have an influence on the dynamic properties as discovered by Kuo (1982) in a parametric study of a diverging reservoir in a seismic evaluation context.

CHAPTER 3

3 METHODOLOGY

3.1 Modelling

3.1.1 Validation of Acoustic Elements

The validation procedure considered the use of compressible acoustic finite elements to measure the hydrodynamic pressures acting on a 15m vertical wall surface. Acoustic elements are predefined elements provided to model an impounded fluid medium undergoing small pressure variations and interface conditions to structural models (Simulia, 2010). The Abaqus manual indicates that these elements model stress as being purely elastic, considering hydrostatic pressures only (i.e. no shear stresses), and the pressure being directly proportional to the volumetric strain.

The results obtained from the approach were verified by comparing with known 'added mass' solutions obtained using the Original Westergaard (1933) and Housner (1954) formulations. The validation model constituted of the following sample problem: A vertical wall – fluid system subjected to a horizontal ground acceleration of 1 Hz, with peak amplitude of 1.2g. This section discusses the development of the acoustic finite element solution. The development of the Original Westergaard (1933) and Housner (1954) solutions have not been discussed as they were obtained using equations (2.6) & (2.20) already covered in the *Literature Review* section.

- Geometric Parts

A shell part was used to model the steel container and a deformable solid part considered for the water. The parts were simplified by making them prismatic. Only the front and the side walls were considered as the geometry was symmetric, and the hydrodynamic pressures acting on the front wall were of interest. The geometric parts used in the validation model are shown in figure 10.

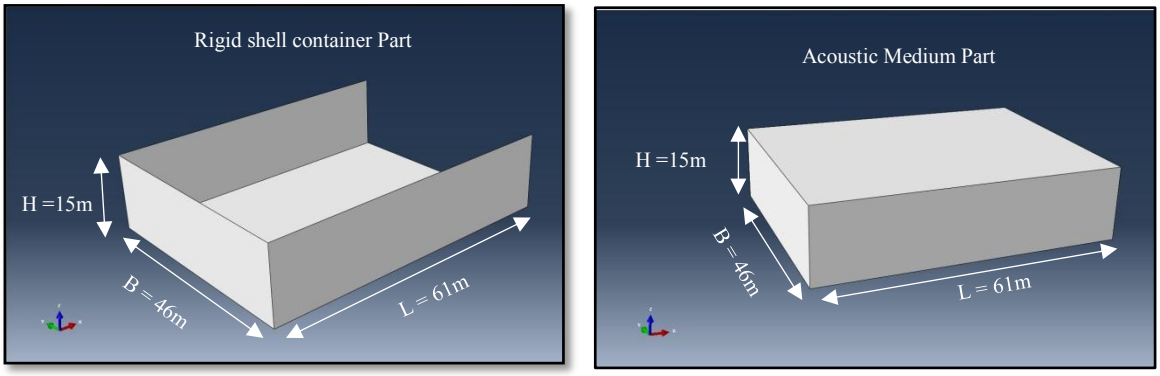

Figure 10: (left) Rigid shell container part and (right) deformable acoustic medium part.

- Material Properties

Typical linear elastic mechanical properties for steel and water were applied to the two parts. The material properties are summarised below in Table1:

Table 1: Elastic material parameters which were are assigned to the shell and acoustic part.

Material Properties	Shell Container	Acoustic Fluid
Elastic & Bulk Modulus (GPa)	200	2,2
Poison Ratio	0.32	-
Density (kg/m^3)	7580	1000

- Assembly, Boundary Conditions, and Interaction of the instance models

Two independent part instances were created in the assembly module. Thereafter, the shell container was meshed using linear quadrilateral 4 node shell elements with reduced integration (S4R). The acoustic medium was meshed with linear acoustic continuum three dimensional 8-node brick elements (AC3D8) (See figure 11).

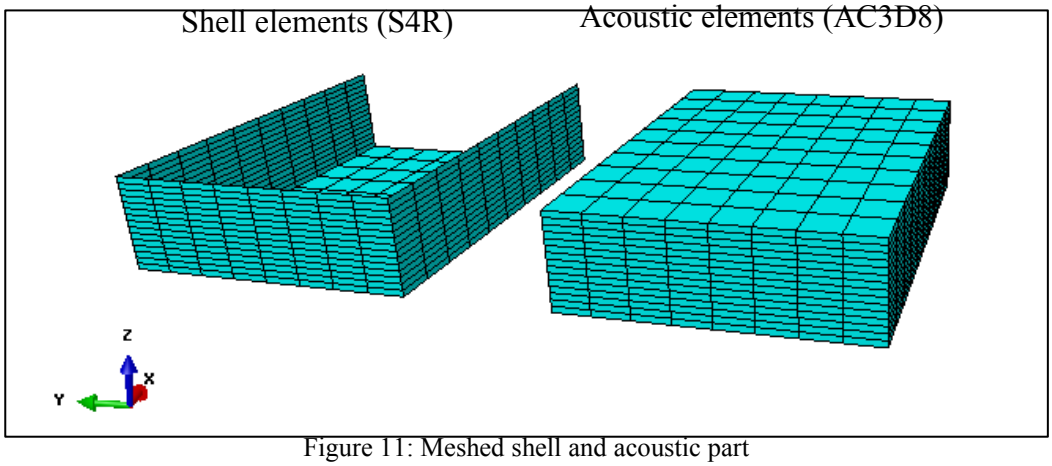

Figure 11: Meshed shell and acoustic part

A 1Hz sinusoidal ground acceleration with peak amplitude of 1.2g was applied to the shell container in the x-direction for a period of 10 seconds. The foundation of the rigid shell was restrained from uplift in the z-direction, and the hydrodynamic pressures on the top surface of the acoustic part were set to zero to agree with the assumption of atmospheric pressure on the top surface. The upstream end of the acoustic part was modelled using a non-reflective surface (Acoustic impedance) which dissipated all pressures tending upstream (only the downstream wall is analysed). The model ran in a dynamic implicit procedure, where the acoustic pressures were set as the output requirements. Finally, the hydrodynamic pressures were extracted at specific time intervals and positions on the downstream surface and compared to the analysis methods.

3.1.2 Comparison of Hydrodynamic Analysis Methods

A comparative study was conducted to investigate the discrepancies between the Westergaard 'added mass' formulation and the assemblage of the finite element fluid structure interaction model. The comparison was considered as the Westergaard analysis formulation was developed for the context of analysing the effect of hydrodynamic pressures existing in seismic conditions. Not much work has been considered in assessing the effect of hydrodynamic loading under ambient state conditions.

This was carried out by comparing the modal parameters obtained from the two methods. A geometric dam wall was created using the Roode Elsberg dam drawings, where the complex geometry was simplified to not include the pulvino (cushion layer) and made symmetric about the centre line of the uncontrolled spillway. The above dam was chosen as a case study would be conducted to verify the formulations.

3.1.2.1 Fluid Structure Interaction (FSI) Model

- Dam Wall

The dam wall section seen in figure 13 was created in a 3 dimensional subspace and defined as a deformable solid part. The geometrical information such as the radii, abutment sub tension angles and datum heights of the cross sectional arches where extracted from the drawings made available by the Department of Water Affairs (*See Appendix C table data*). The radii and sub tension angles of the cross sectional arches were sketched using the wire and datum plane features (See figure 12), where the datum planes were offset using the ground level as the reference plane.

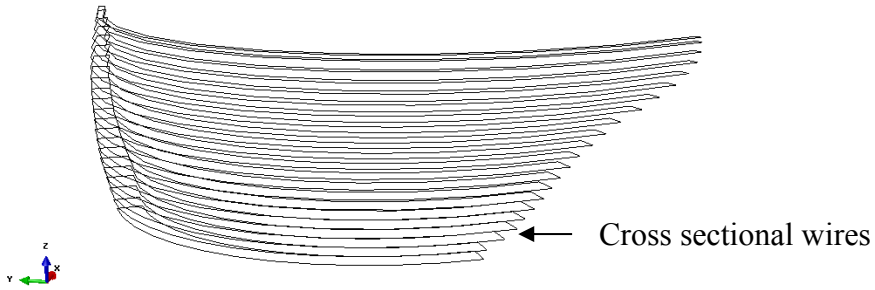

Figure 12: Cross sectional wired arches used to create the dam wall part.

After the cross sectional wires were completed, the lofting method was used to develop the complex three dimensional solid region provided in figure 13. This method was favoured over the extruding, sweeping and revolving techniques, as the cross sectional regions vary with height. The loft feature created a solid segment from the starting wire section to the above wire shape and orientation. Abaqus automatically (default settings) created the path in which the loft solid region would follow, more advance settings can be used to manually control the lofting technique.

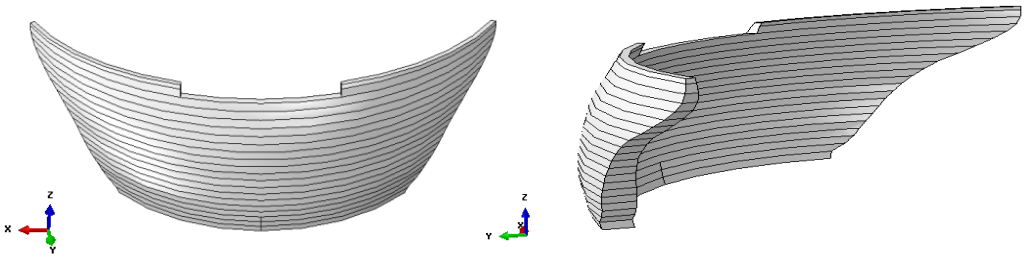

Figure 13: Hypothetical arch dam wall part created using the lofting technique.

- Fluid Medium

A deformable solid part was chosen to create the fluid medium as it would be meshed with compressible three dimensional acoustic elements. The cross sectional wire features were created using the extrados radii's from the dam wall cross section wires, this was achieved by trimming the intrados radii's and subtended abutment edges. The remaining wire features of the extrados were extended upstream three times the height of the dam, to form the wired fluid region recommended by most dynamic analysis studies (U.S. Army Corps of Engineers, 1994). The same lofting procedure used to create the arch dam wall was carried out to create the deformable continuous fluid region. The fluid part was created up until the spillway level i.e. considering a full dam.

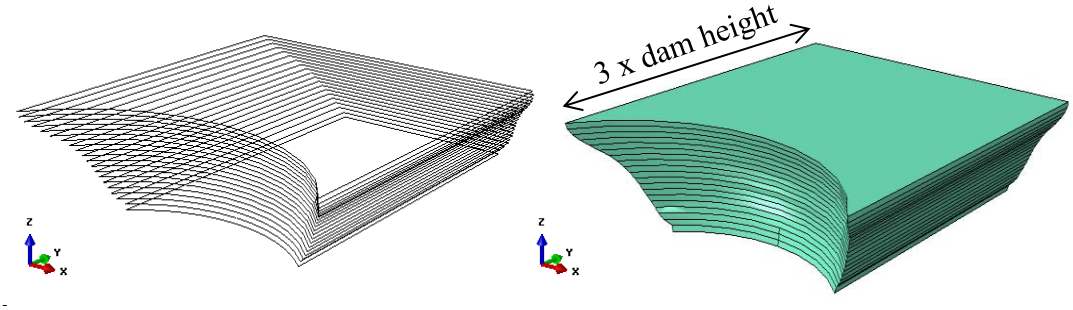

Figure 14: (left) Fluid part created using cross sectional wires and (right) lofted continuous fluid part considered to extend three times the dam wall height.

- Material Properties

Arbitrary dynamic elastic material properties were applied to the dam wall section and typical fluid properties applied to the fluid medium. One must note that when conducting a dynamic analysis, only mechanical properties are considered and the dynamic properties of the materials must be used. Listed in Table 2 below are the dam and fluid material properties used.

Table 2: Material parameters assigned to the dam wall part and fluid medium.

	Dam Wall	Fluid Medium
Dynamic Elastic Modulus (GPa)	40	-
Bulk Modulus (GPa)	-	2,2
Poisson's ratio	0.25	-
Density (kg/m^3)	2400	1000

- Assembly and Meshing

The assembly module was used to create independent instances of the parts. Meshing the dam wall proved to be quite challenging as there are no established rules for creating and optimizing the mesh. An appropriate mesh was selected, by carefully considering the dam geometry and the type of analysis for which the model will be used for. The U.S. Army Corps of Engineers (1994) recommends that several meshes with different element types and seed sizes should be considered, and the user should select the mesh that is computational efficient and provides reasonably accurate results. The main factors to consider in choosing the mesh include: size and geometry of the mesh, and type of elements to be used.

The meshing procedure commenced with a sensitivity study which constituted analysing the behaviour of different element types, shapes and seeds provided in the Abaqus library for use in dynamic modelling. From the validation study conducted above it was found that Acoustic Elements provide a good formulation for modelling fluids undergoing small pressure variations (above static pressures) and coupling with structural interfaces. Thus, the element type presented in figure 15 was considered in the assemblage of the fluid structure interaction model. A description of the 20 node acoustic brick element used to model the impounded water body is provided in figure 15.

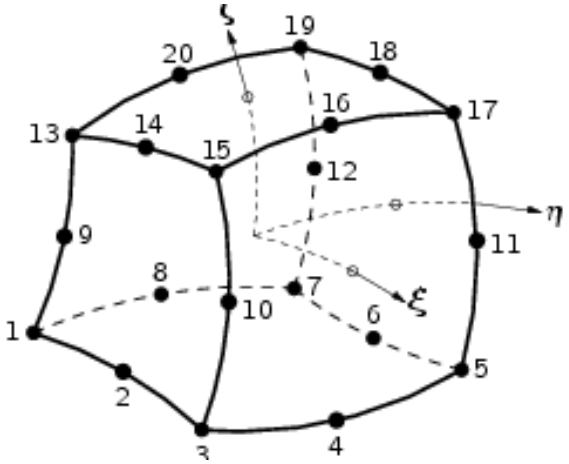

Figure 15: 20 node brick acoustic element (AC3D20) used to capture the dynamic pressures.

A few challenges were encountered during meshing of the water and dam wall region. Firstly, due to the geometry of the parts being complex and irregular in shape, the two parts had to be sufficiently partitioned before meshing, in order to simplify the complex regions into meshable parts. Secondly, C3D20R (Stress) and AC3D20 (Acoustic) quadratic brick elements were used for the dam wall and fluid region respectively, with an initial seeding size (density) of 6. This resulted in timeous computational periods for convergences of the models. The above was later modified by iteratively increasing the global seed size and of the dam wall and fluid to 13 and 15 respectively, but still keeping accurate results (see figure 16). This resulted in the use of fewer elements and improving the computational time, and still obtaining satisfactory output results.

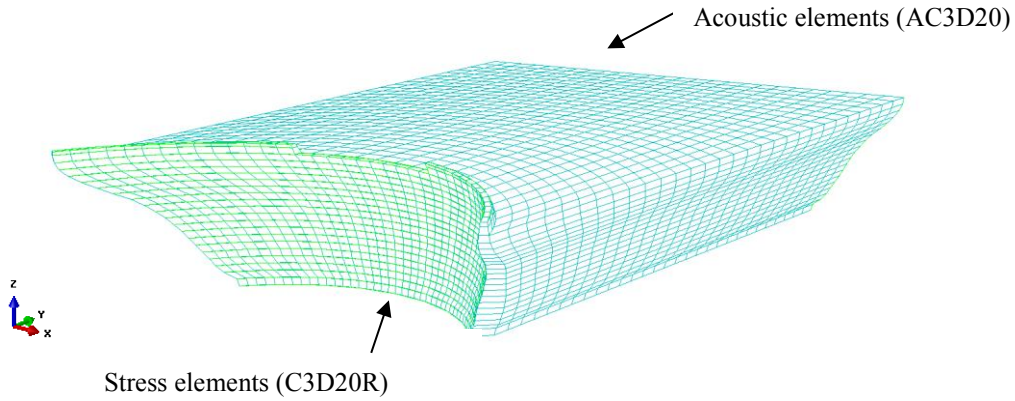

Figure 16: Fluid structure interaction mesh, showing C3D20R dam wall stress brick elements and AC3D20 water-acoustic brick elements

The meshes were analysed by inspecting the displacement behaviour of the elements as a whole, as well as the distortion of the individual elements. The inspection of the mesh behaviour included analysing the first six modes of the arch dam. The behaviour of the

model was contrasted with ambient vibration test results obtained from field testing measurements conducted on the Kouga double curvature arch dam. The quality of the mesh was verified by using the verification feature provided in Abaqus/CAE. The feature uses a failure criterion which checks the following conditions.

i. Face corner angle less than: 10°
ii. Face corner angle greater than: 160°
iii. Aspect ratio greater than: 10

The mesh in figure 16 above, was found to pass the verification test with all the elements fulfilling the criteria check. Failure of the mesh to meet any of the above checks would lead to poor behaviour of the model and inaccurate results.

- Natural Frequency Extraction Procedure

Abaqus/Standard provides a linear perturbation procedure which performs eigenvalue extraction to calculate the natural frequencies and the corresponding mode shapes of the system. Included in Abaqus/Standard are three eigenvalue extraction methods: Lanczos, Automatic multi-level sub-structuring (AMS) and Subspace iteration. In conjunction with the eigen solver an architecture must be selected which has minimal impact on the frequency extraction procedure. For the considered model the Lanczos and the traditional architectural system were used as they account for surface based tie constraint on the structural-acoustic coupled surface.

Table 3: Software architectures available with different eigensolvers in Abaqus/Standard.

Software architecture	Lanczos	Subspace	AMS
SIM	√	×	√
Traditional	√	√	×

Lanczos eigensolver

The Lanczos eigensolver is considered one of the most powerful techniques for extract eigenvalues. In the case of a structural-acoustic (fluid) model, the coupling affects the

natural frequency response of the system. In Abaqus, the Lanczos is the only method that considers the structural-acoustic coupling of the dam wall and fluid surface in the eigenvalue extraction. Abaqus is set to extract these coupled modes by default. The AMS and subspace eigensolvers neglect the coupling when computing the modes and natural frequencies, thus these solvers were deemed to be inappropriate for use in this study. For this method it is necessary to specify the maximum number of eigenvalues required, and Abaqus/Standard determines a default suitable block size. The stepping procedure is terminated once the specified eigen values and vectors are determined. During this analysis a maximum of 18 eigenvalues was specified, as only the lower modes are of interest when working with dam models (Please refer to Appendix A for theory on Lanczo's technique).

- Boundary Conditions, Constraints and Interactions

The boundary condition assigned to the dam wall and the fluid region constituted of the following: (i) The dam-foundation interaction was not considered by applying a completely rigid boundary system, fully restraining the displacement and rotational degrees of freedom on the dam wall perimeter. (ii) The pressure on the fluid surface was considered to be atmospheric and assigned a magnitude of zero. (iii) A surface based tie constraint was used between the upstream dam surface and fluid interacting surface. This type of constraint allows two surfaces to be fused together even when the mesh nodes do not coincide. A master-slave technique was used to keep the two surfaces compatible. The dam wall was chosen as the master surface as it is the primary displacing structure, and the fluid surface being the slave trailing surface (Please refer to Appendix A for theory on Surface based Contact tie technique).

The fluid medium could not be modelled to infinity in the upstream direction, therefore a non-reflective planar Acoustic Impedance boundary was applied on the upstream end surface. It is designed to damp all acoustic hydrodynamic degrees of freedom heading upstream, such that no interferences are inflicted on the solution. The boundary conditions, constraints and interactive surfaces applied to the model are shown in figure 17.

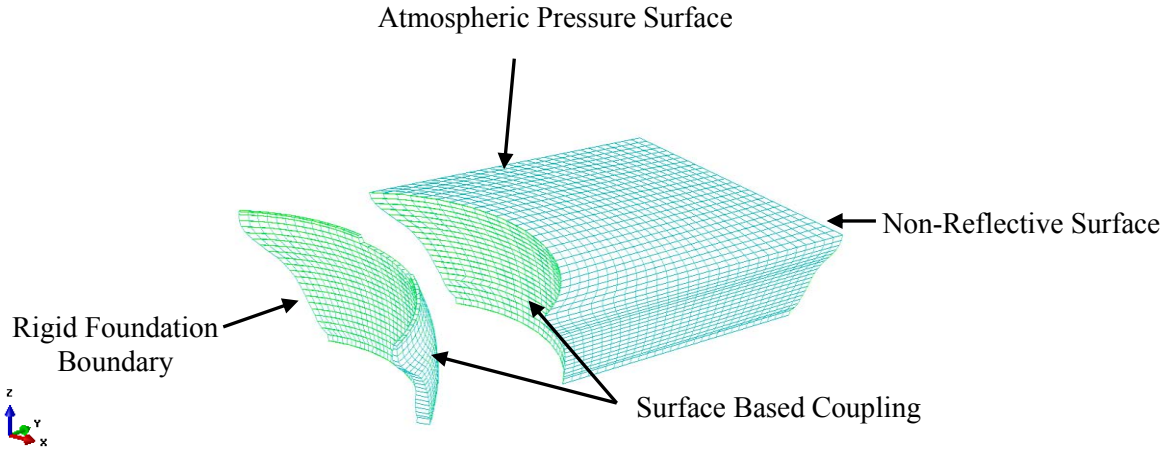

Figure 17: Boundary conditions, constraints and interactions applied to the FSI model

3.1.2.2 Generalised Westergaard Method

The modified Westergaard method developed by Kuo (1982) was the second analysis method to be compared. As discussed in the literature review this is a modification of the Original Westergaard formulation which considers the added masses to be attached in the normal direction to the upstream surface of the dam wall. This method is designed to be more applicable to flexible arch dams because it accounts for the flexibility and curvature of the dam (Kuo, 1982).

The hypothetical arch dam wall used in the parametric study was carried out in the application of the Generalised Westergaard method (From this section onwards this method will be referred to as the Westergaard method). The dam wall properties were kept the same and the mesh properties applied in a similar procedure. The Lanczos eigensolver used in the FSI model was implemented in the extraction of the dynamic characteristics (refer to section 3.1.2.1).

The added mass scalar values were developed using equation (2.6) and applied in conjunction with normal direction cosines (*see equation 2.11*) to the upstream surface of the double curvature arch dam. In plan, the dam is made of varying arched circles where the extrados and intrados centres lie along one reference plane (Y-Z plane). Along the elevated long section the dam is parabolic in nature, and is centred at a height of 15.24m above ground level. In order to find the normal direction cosines of the dam a curvilinear surface created by the intersection of these two geometric shapes had to be considered.

The first step was to define the shapes parametrical in polar co-ordinates using algebraic functions. These parametric equations define any point on the upstream surface of the dam. Provided below are equation (3.1) and (3.2) the parametric equations for the circular arches and the parabolic profiles respectively.

$$P_1(\theta_R) = r \ \mathrm{Cos}\,\theta_R \ \hat{\mathbf{i}} + (b + r \ \mathrm{Sin}\,\theta_R) \ \hat{\mathbf{j}} + h \ \hat{\mathbf{k}} \quad (3.1)$$

Where

r = Radius of the circle of interest

θ_R = Angle measured from positive X – Axis

h = Height above ground level of considered circular arch

$$P_2(\theta_P) = h \ \hat{\mathbf{i}} + (P\,Co\sec^2(\frac{\theta_P}{2}) - 1) \ \hat{\mathbf{j}} + (2P \ \mathrm{Cot} \ (\frac{\theta_P}{2}) + 15.24) \ \hat{\mathbf{k}} \quad (3.2)$$

Where

P = Distance from vertex of parabola to focus and directrix

θ_P = Angle measured from the positive Y-Axis

h = Vertical plane in the X-Axis

In order to determine the normal directional cosine of the arched surface, two vectors lying on the surface had to be determined. Initiallly, the general tangential vector for each curve had to be determined and the cross product applied to obtain the normal direction cosine for any point on this surface. The general tangential vectors for all points on the respective curves are derived below as equation (3.3) and (3.4):

$$\frac{\partial P(\theta_R)}{\partial \theta_R} = \lambda_1 = r\,[-\mathrm{Sin}\,\theta_R, \mathrm{Cos}\,\theta_R, 0] \quad (3.3)$$

$$\frac{\partial P_2(\theta_P)}{\partial \theta_P} = \quad \lambda_2 = \quad \text{P} \quad [0, \quad Co\sec^2(\frac{\theta_P}{2}).\text{Cot} \quad (\frac{\theta_P}{2}), Co\sec^2(\frac{\theta_P}{2})]$$

(3.4)

The unit normal vector at any arbitrary point could be found by applying the cross product to the above vectors λ_1 (vector tangent to r-curve) and λ_2 (vector tangent to p-curve) and normalising the vector by dividing by its length as described below:

$$\vec{n} = \frac{\lambda_1 \times \lambda_2}{|\lambda_1 \times \lambda_2|}$$

The normal to any point on the surface was determined as equation (3.5):

$$\vec{n} = \frac{1}{\sqrt{1 + Sin^2(\theta_R)Cot^2(\frac{\theta_P}{2})}} [\text{Cos}\,\theta_R, \text{Sin}\,\theta_R, \text{-Sin}\,\theta_R . \text{Cot}\,(\frac{\theta_P}{2})] \tag{3.5}$$

This above equation was substituted into equation (3.6).Where M_{Ai} is the added mass matrix derived by Kuo (1982) and is associated with node *i*.

$$M_{Ai} = \alpha_i A_i \vec{n}_I^T \vec{n}_i \tag{3.6}$$

$$M_{Ai} = \frac{\alpha A_i}{1 + Sin^2(\theta_R)Cot^2(\frac{\theta_P}{2})} \begin{bmatrix} Cos^2\theta_R & Cos\theta_R Sin\theta_R & -Sin\theta_R Cos\theta_R \text{Cot}(\frac{\theta_P}{2}) \\ Cos\theta_R Sin\theta_R & Sin^2\theta_R & -Sin^2\theta_R \text{Cot}(\frac{\theta_P}{2}) \\ -Sin\theta_R Cos\theta_R \text{Cot}(\frac{\theta_P}{2}) & -Sin^2\theta_R \text{Cot}(\frac{\theta_P}{2}) & Sin^2\theta_R Cot^2(\frac{\theta_P}{2}) \end{bmatrix}$$

It is to be noted that the added mass components of the 3x3 matrix were coupled with respect to the nodal degrees of freedom but uncoupled with respect to the individual nodes. The consistent mass matrix (non-diagonal) can be inputted into Abaqus using the User Subroutine feature. The above implementation could easily slow down the computational time of the model. An alternative to this was to use the mass lumping technique which only requires the diagonal mass components of the mass matrix, but are scaled by a factor to preserve the added mass at every node. This would make the added masses independent with respect to the degrees of freedom, giving a better physical representation of the mass and improves the computational time for modelling.

The added mass matrices were lumped using the Hinton, Rock and Zienkiewicz (HRZ) lumping technique. The lumping method is only known to preserve the mass but not the moment of inertia. The method was employed by computing the diagonal entries of the mass matrix where the values were scaled by a factor which is a ratio of the total mass at the node and the trace of the matrix (sum of the diagonals). Provided below is the scaling factor from the method (equation (3.7)) and the added mass matrix (equation (3.8) which was employed after mass lumping was conducted using the HRZ method.

$$\beta = \frac{Tot(\sum m_{ab})}{(m_{11} + m_{22} + m_{33})} \tag{3.7}$$

$$M_{Ai} = \frac{\alpha\beta A_i}{1 + Sin^2(\theta_R)Cot^2(\frac{\theta_P}{2})} \begin{bmatrix} Cos^2\theta_R & 0 & 0 \\ 0 & Sin^2\theta_R & 0 \\ 0 & 0 & Sin^2\theta_R Cot^2(\frac{\theta_P}{2}) \end{bmatrix} \tag{3.8}$$

- Partitioning of the Dam Wall

The Westergaard method as detailed in section 2.3.1 requires the added masses to be applied on the upstream side of the dam wall, with a varying parabolic distribution increasing with water depth. The dam wall part was partitioned to allow application of the added masses at specific nodal position as shown in figure 18 below. The dam wall was partitioned horizontally and vertically on the reference planes provided in the design drawings, this was done as the Westergaard masses varied with radial position and height. Further vertical partitioning was required on the abutment sides, as the water depth changes quite significantly as you move towards the outmost edges of the abutment supports. In total 25 vertical and 22 horizontal partitions were created.

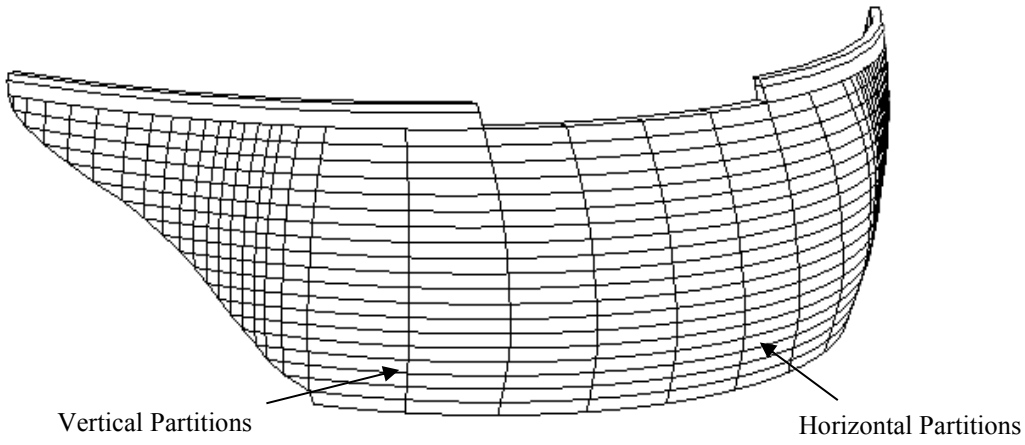

Figure 18: Dam wall partitioned to allow for application of the Westergaard added masses.

- Application of Inertial Mass

In applying the Westergaard formulation the recommended method is to apply the mass as nodal inertial mass on the wetted upstream surface. Each node must be assigned a tributary area, where the hydrodynamic pressures are assumed to be constant over the tributary area and have the same magnitude of 'added mass' as that of the associated node. The allocation of tributary area to a typical node was dependent on the location and positioning of the node. The nodes were grouped into the following classes: internal, abutment edge, top and bottom edge nodes. The internal nodes were assigned a quarter of each of the surrounding surface partitions (See figure 19 below). The abutment edge nodes were allocated 1/3 of the above and below surface areas and a quarter of the internal partition. Finally, the exterior top and bottom edge nodes were assigned a quarter of the adjacent partitioned areas.

The added masses were assigned in Abaqus using the inertia mass engineering feature. The toolkit allowed point masses (m_{11}, m_{22}, m_{33}) associated with the three translational degrees of freedom ($u_1, u_2\ u_3$), to be applied on element nodes located on the upstream surface.

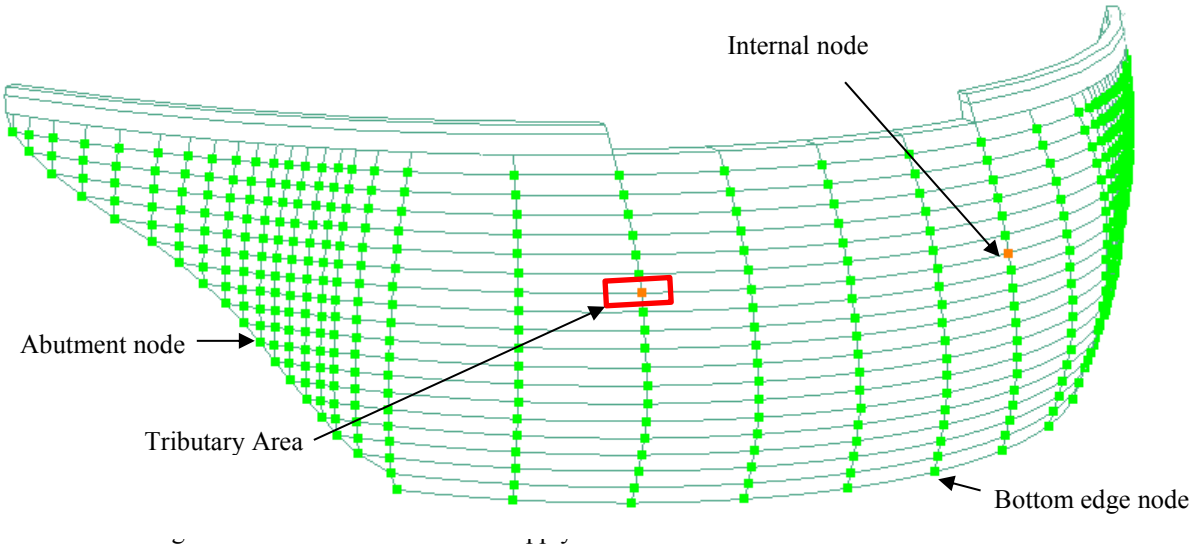

3.1.3 Parametric Study of Reservoir Orientation and Geometry

A parametric study was conducted on the hypothetical double curvature arch dam. This was implemented to consider the effect of the reservoir orientation and geometry on the dynamic characteristics. Work conducted by Kuo (1982) showed that under seismic loading divergence of the reservoir affects the hydrodynamic pressures exerted on the structure near the abutments and crown position. This parametric study would investigate if a similar phenomenon would be experienced in the ambient condition, and whether it would have an influence on the dynamic properties. It also looked at the effect on the hydrodynamic pressures from an asymmetrical orientated reservoir. The latter was considered as a case study and would be conducted on the Roode Elsberg which has an asymmetrically orientated reservoir.

The parametric study was investigated using the FSI model created in the comparison study. The reservoir geometry was considered by analysing the effect of a diverging reservoir on the dynamic characteristics. The fluid medium was opened from the prismatic scenario in incremental angles of $10°$ up until a diverging angle of $40°$ (see figure 20 below). The reservoir orientation was investigated by incrementally skewing the reservoir geometry by $10°$ up until an angle of $40°$ (see figure 20 below).

Diverging and Asymmetric Reservoir

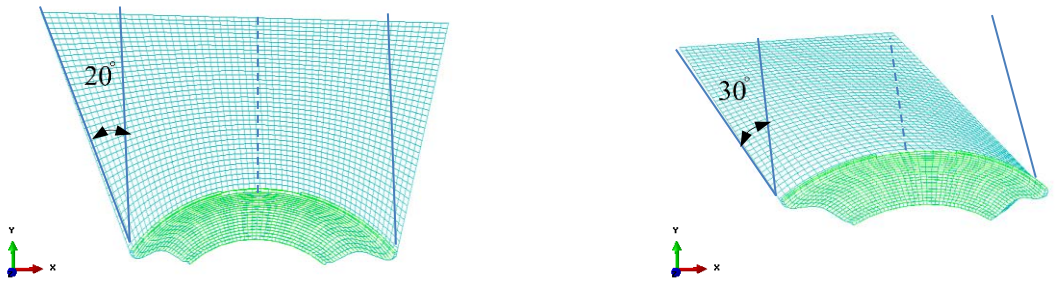

Figure 20: Diverging and asymmetric cases considered in the parametric study.

3.1.4 Modelling of Roode Elsberg Dam

- Description of Roode Elsberg Dam

Roode Elsberg Dam is a double curvature concrete-arch dam that lies in the Sanddrift River and is located at $33°25'\ 39''S$ latitude and $19°34'01''$E longitude which is 30km away from the town of Worcester, in the Western Cape Province of South Africa. The dam is the lower of two storage dams built in the Sanddrift River to provide supplementary water for 2535 ha of land under irrigation. A concrete lined tunnel, 1.98m in diameter and 5.2km long conveys the water from the dam to Hex river valley where distribution is by an enclosed pipe system (Department of Water Affairs, 1971).

The dam was designed to be 72m in height (from lowest foundation level) with a centrally located uncontrolled over spill and reservoir capacity of 8.21 million m^3 (See figure 21). Roode Elsberg is a double curvature arch dam, which has concentric horizontal arches and parabolic vertical arches constructed from different reference points over its height. The dam was built with a pulvino pad which acts as cushion layer, assisting in distributing the load into the abutments and foundation. The Cape Town Department of Water Affairs states that, since the dam began its operation in 1968, there has been continuous sedimentation occurring at a rate of 4.6%, resulting in a reduction in the volume of water stored (Department of Water Affairs, 1971)

Figure 21: Roode Elsberg Dam located in Worcester Western Cape, South Africa

The geometric and material data of Roode Elsberg Dam were sourced from design drawings made available by the Department of Water Affairs (DWA). Table 4 provides some of the main characteristics of the dam.

Table 4: Properties of Roode Elsberg Dam

Main Characteristics	**Value**
Foundation	
Maximum height (m)	72
Foundation altitude (m)	506
Dam body	
Crest altitude (masl)	577
Crest width (m)	2.6
Crest length (m)	274
Spillway length (m)	76
Reservoir	
Normal elevation of water (masl)	573
Minimum elevation of water (masl)	518
Reservoir normal capacity (m^3)	$8.21x10^6$

Reservoir minimum capacity	(m^3)	$2.05x10^6$

- Arch Dam Wall Part

An existing dam wall system used in the static and temperature analysis was employed in this dynamic study. The dam was created with the concept of modelling the cantilevered arch blocks and the pulvino cushion as a monolithic system. Roode Elsberg dam is considered to be a complex arch dam due its asymmetric nature and variation in horizontal and vertical radii. Therefore, the dam wall part was created separately from the foundation using the lofting feature which is described in the parametric study above. Horizontal reference planes, varying sub-tension angles and arch thicknesses defined in the designing drawings were used to construct the reference datum planes and cross sections of the subtended horizontal arches. This allowed for horizontal closed loop arches constituting the pulvino sub-tensions to be sketched and lofted. Figure 22 shows an illustration of the downstream side of the Roode Elsberg dam model.

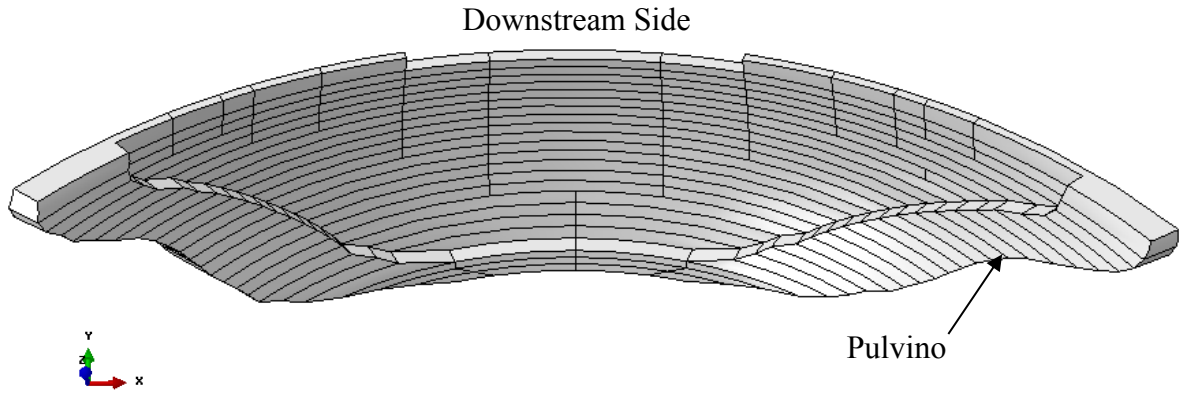

Figure 22: Downstream side of the arch dam (Nzuza, 2013).

In assigning material properties to the dam, the concrete elastic properties were assumed to be isotropic and homogenous throughout the part. According to the US Army Corps of Engineers (1994) a dynamic study only requires three material properties to be assigned to the dam wall part; these include the dynamic modulus, Poisson's ratio and the unit weight of concrete. The dynamic modulus of concrete is estimated by using empirical methods which require the static modulus to be known. For Roode Elsberg dam the working drawings indicated that the dam wall had a 28 day mean strength of 29 MPa with a standard deviation of 4.1MPa. With an understanding that concrete properties change with time, the effects of

creep had to be taken into account. This was done by correlating to a static modulus (inclusive of creep effects) E'_C of GPa using Fulton's concrete technology (2009). The dynamic modulus of concrete was obtained using the empirical formulation (3.9) accepted in the British testing standard BS8110 part 2. The dynamic modulus of concrete for the dam wall was estimated to be 40GPa with an assumed standard deviation of 5 Gpa as suggested by Fultons (2009).

Where

E'_C Sustained static young's modulus including effects of creep.

E_d = Dynamic modulus of concrete

$$E'_C = 1.25E_d - 19 \tag{3.9}$$

- Foundation Part

An idealistic foundation includes all geological features and extends to a distance where boundary effects have no influence on the stresses and dynamic characteristics. This becomes practically impossible as finite element techniques are not yet sufficiently developed, and models would become computationally intensive. The foundation region used in the static analysis was considered to be adequate enough for the dynamic analysis of the dam. The region of the foundation was created using the simplified approach considered in the US Army Corps of Engineers (1994). It specifies that a flexible foundation rock system must be considered, that requires the deformation modulus of the supporting rocks, which accounts for faults and joints in the foundation rock and the Poisson's ratio to be defined for the material properties.

According to jacking field tests conducted on the foundation, it was evident that the left abutment rock had very different elastic properties from the right abutment. It is not clear where the distinguishing boundary lies, an implicit assumption was made for the modulus of deformation of the foundation system: 25 GPa on the left and bottom sections hard rock-grey region (see figure 23), 20 GPa on the bottom right soft rock – blue region (see figure 23) and 23GPa on the top right section soft rock- red (See figure 23). Figure 23 shows the foundation wire region and the completed lofted solid region.

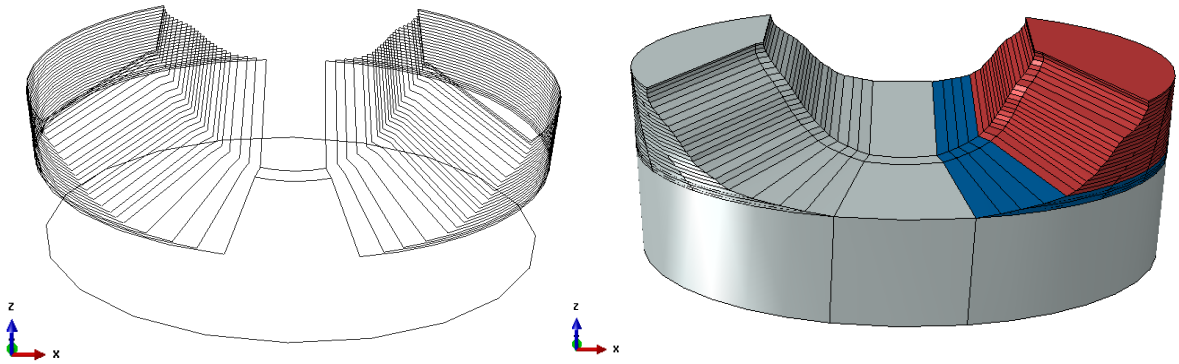

23: (left) Wire developed feature of founda..... ..... (right) completed solid region of foundation.

The foundation walls were created using elliptic planes cut into the supporting canyons, and oriented normally to the dam wall interface. The elliptic planes were created with a major and minor radii of 430m and 280m, respectively. The above is in accordance with a radius of two times the height of the dam for flexible foundation rocks (since $E_f \leq 0.5E_c$), which is recommended by the US Army Corps of Engineers (1994). FERC (1999) recommends that the ratio of the foundation depth to the dam wall depth should be in the range of 1.0 to 1.5. The foundation depth was set to extend to a depth 1.5 times the height of the dam, resulting in a foundation of 90m in depth.

- Material Properties

Summarised in Table 5 are the elastic material properties assigned to the arch dam, and the foundation properties assumed for the supporting foundation rock made of Table Mountain quartzitic sandstone as specified in design drawing no. 43938 (Department of Water Affairs, 1971). Linear properties were assigned to the model, as a linear perturbation solver would be used to compute the eigenvalues.

Table 5: Linear elastic material properties of dam wall and foundation part

Property and Symbol	SI Units	Concrete Wall	Rock Foundation		
			Left	Bedrock	Right
Modulus of elasticity (E_d)	GPa	44	25	25	23/20
Density (ρ)		2400	-	-	-

	kg/m^3				
Poisson's ratio (υ)	-	0.22	0.25	0.25	0.25

- Assembly and Meshing

Two independent native part instances were created for the dam and foundation part in the Assembly module. These were merged into forming a new monolithic part which would allow compatibility of the elements and the mesh at the interface of the concrete wall – foundation rock. The merging still kept the material properties of concrete for the wall and the rock properties for the foundation parts. Figure 24 shows the merging of the dam wall part with the truncated massless foundation part.

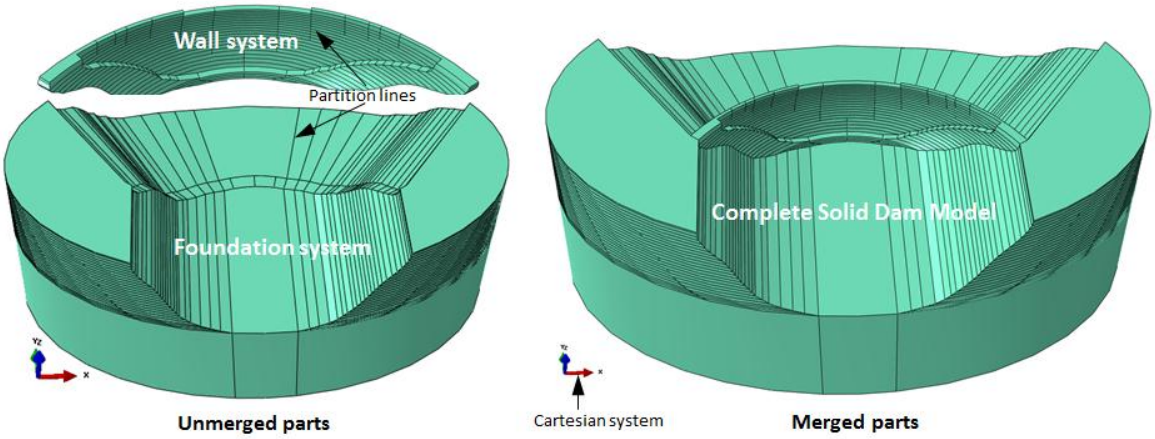

Figure 24: (left) Merging of Dam wall and foundation part. (right) completed merged instance of the two parts (Nzuza, 2013).

As previously determined, there is no rule of thumb for meshing arch dams but guidelines do exist stipulating a few conditions to be considered. Three different meshing techniques were considered after the final mesh was chosen. The main factors governing the ideology behind the selection of the final mesh included the size and geometry of the dam, type of elements to be used, type and location of spillway, foundation profile, and the dynamic characteristics of the dam. A meshing scheme that uses quadratic continuum displacement 10-node tetrahedral elements (C3D10) was selected. The wall system was meshed using

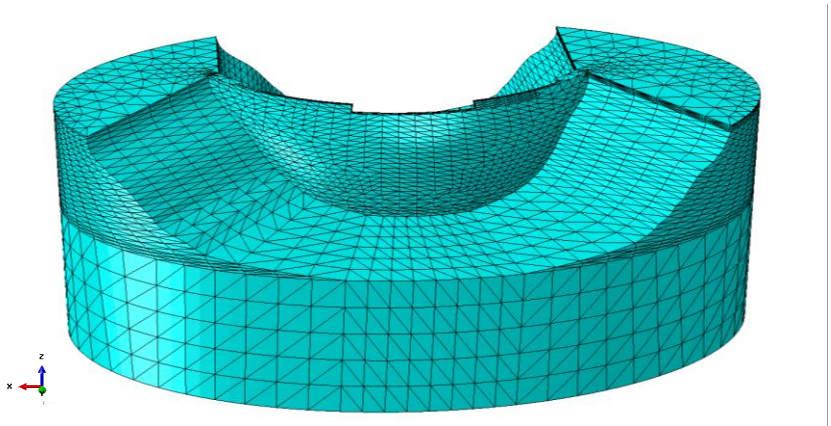

quadratic tetrahedral C3D10 elements with an approximate global seed size of 7. The mesh was refined to 1612 elements and consisted of 9203 nodes. Due to the complexity of the foundation profile, C3D10 elements also had to be used. These elements are ideal in modelling regions with high degrees of curvature. They also helped in reducing computational time as the element consisted of 10 nodes and resulted in only 50421 elements being used, constituting 67742 nodes. Figure 25 shows the completed dam wall-foundation mesh constituting of C3D10 elements.

Figure 25: Completed mesh of dam foundation part using C3D10 tetrahedral elements

3.1.5 Hydrodynamic Analysis of Roode Elsberg Dam

The interaction between the impounded water body and arch dam is an important factor to consider when modelling the dynamic behaviour of arch dam systems during earthquake and ambient responses. In accounting for this effect on the Roode Elsberg dam model, the interaction was represented by the assemblage of acoustic finite elements which is a refined formulation that accounts for water compressibility, orientation and geometry. Secondly, the 'added mass' formulation was considered using the modified Westergaard distribution proposed by Kuo (1982). The two methods would be later on verified by ambient vibration field test measurements.

3.1.5.1 Acoustic Finite Element Model

The use of acoustic finite elements were used to provide a realistic representation of the complicated geometry of the impounded water body. The fluid boundary medium was created using the lofting technique described in *section 3.1.2.* The long sided boundaries were made to coincide geometrically with the foundation profile. This was necessary as the fluid-foundation rock interface would have to be coupled in the later stages. The fluid medium was extended to a length 3 times the height of the Roode Elsberg arch dam, and assigned the water material properties applied in the Comparative study (section 3.1.2).

The fluid medium was instanced as an independent part to the dam-foundation in the assembly module. Hereafter, the part was meshed using 35831 quadratic tetrahedral (AC3D10) elements constituting 54774 nodes at seed size of approximately 8 (See figure 26). The Dam-foundation mesh was kept the same as described above in the Assembly and Meshing sub-section. The behaviour of the mesh was verified using the verification tool pack available in Abaqus and comparative visual inspection with operational mode shapes

of the Kouga arch dam. 313 (0.6%) of the foundation elements were found to have minimum angles less 5 degrees, 4 elements were found to have face corner angles greater than 170 degrees, and 374 (0.7%) had aspect ratios greater than 10. These elements were considered to have an insignificant influence on the results of the model as most of them were foundation elements, which are subjected to very small deformations. The modes were found to be in agreement to the Kouga dam operational modes.

The fluid was coupled to the dam wall and foundation rock side using the surface based contact tie technique used in the *section 3.1.2*. The dam wall and foundation rock interacting surfaces were assigned the master surface, and the fluid as the slave. The river bed material was not modelled as it did not form part of the investigation, resulting in an opening between the foundation bed and fluid bottom of approximately 15 meters. The absorption of energy at the supporting foundation rocks and bedrock was not modelled as no geological information was available. The top and upstream surfaces of the impounded fluid were assigned the same load pressure condition and acoustic impedance surface described in the *section 3.1.2*. The foundation rock region was modelled as being fully fixed by assigning fixed boundary conditions around the surface boundary. Lastly, the Lanczos eigensolver was used to extract the dynamic characteristics of the dam.

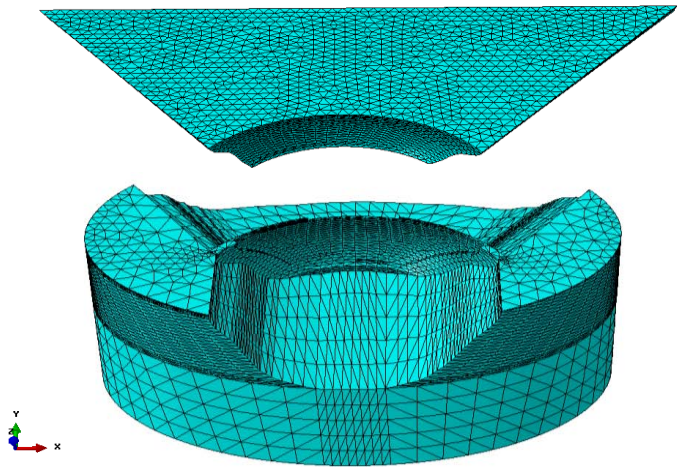

Figure 26: Meshed fluid region using AC3D10 quadratic tetrahedral elements and dam-foundation part meshed using C3D10 quadratic tetrahedral elements.

3.1.5.2 Westergaard Method

Secondly, the modified Westergaard method was used to account for the interaction of hydrodynamic loading. The Westergaard method was employed by partitioning the Roode Elsberg arch dam model horizontally and vertically at the reference plane height. Vertical

and horizontal partitions were created to an approximate depth of 49m, which was considered as the full dam height, measured from the spillway level (see figure 27). The 'added masses' were computed using equation (6) proposed by Kuo (1982) and applied to the model using the inertial mass feature in Abaqus. Only the foundation profile was assigned a boundary condition. The foundation was fully fixed on the boundary surfaces in the same manner as described in the acoustic finite element model.

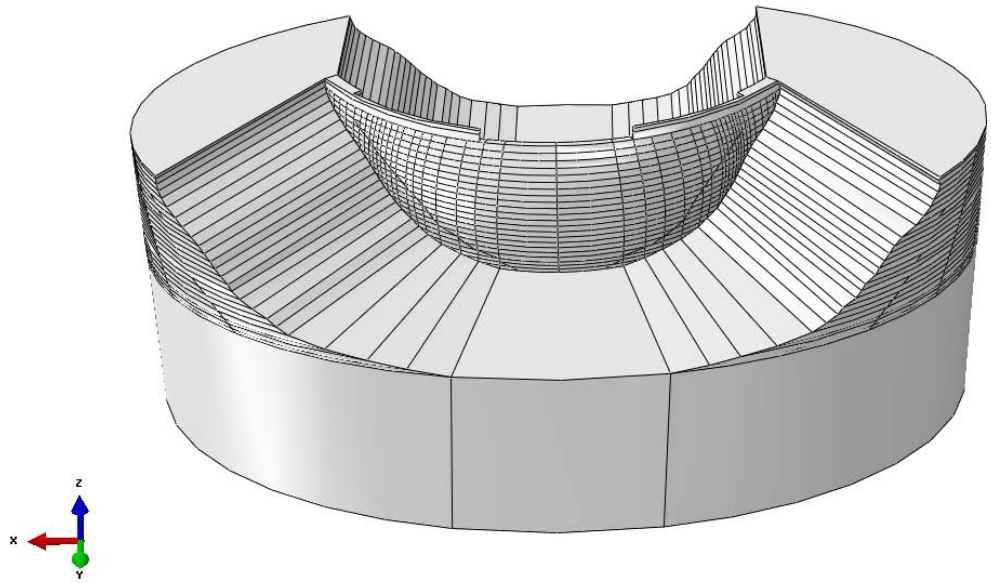

Figure 27 Partitioned dam wall part for application of Westergaard added masses.

The model was meshed using 95730 tetrahedral C3D10 elements, constituting 138529 nodes. An approximate seed size of 12 was used for the dam and abutment supports, and a seed size of 23 for the foundation bed rock. The foundation bedrock profile mesh was made to be coarse as the mesh would not be expected to deform as excessively as the arch dam, and accurate results would still be obtained with a coarser mesh. The mesh was then verified by using the mesh verification tool in Abaqus and visual inspection of the deformed final solution.

The criteria checked for elements which had unacceptable aspect ratios greater than 10, and face corner angles less than 5 and greater than 170. The model was found to have 211 elements (0.21% of elements) with an aspect ratio greater than 10, 230 elements (0.24% of elements) with face corners less than 5, and 15 elements (0.02% of elements) with face corners greater than 170 degrees. This was found to be acceptable as the poor elements only constituted a minor insignificant percentage of the mesh (see figure 28). Further visual

inspection of the deformed mesh showed that the mesh as a whole behaviours in an acceptable manner, producing good results. The Natural frequencies and mode shapes of the model were extracted using the Lanczos eignesolver technique.

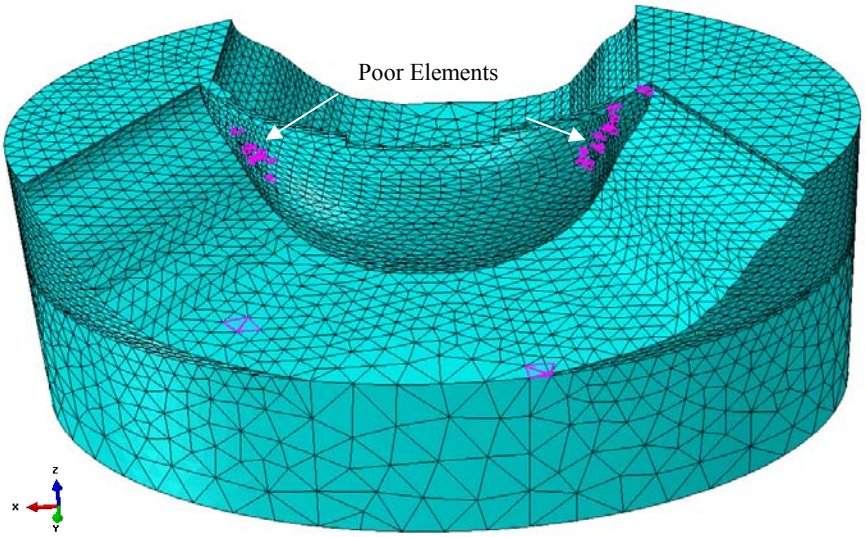

Figure 28: Dam-foundation meshed part illustrating location of the poor elements.

3.2 Ambient Vibration Testing

Ambient vibration testing was conducted on the Roode Elsberg dam as it is a cost effective and reliable field testing technique for analysing and monitoring large civil engineering structures. The testing was carried out to determine the operational dynamic characteristics and secondly, to verify the hydrodynamic analysis methods used in the FE analysis of the Roode Elsberg dam. The excitation on the dam was provided by the wind, temperature and the reservoir flowing over the spillway.

3.2.1 Testing and Analysis Instrumentation

Ambient vibration testing of dams requires instrumentation which can pick up very low vibrations of the stiff structure. The measuring equipment included: 16 roving forced balanced accelerometers (see figure 29). The accelerometers were connected via fibre cables to a NI PCI-4472B device cards mounted into a NI PCI 1045 chassis, connected to a PCI slot of an ordinary PC workstation. The NI PCI 4472B device cards are specialised data acquisition hardware, manufactured to simultaneously acquire each channel with 24-bit high

resolution delta-sigma analog to digital converters. The system is built in with anti-aliasing filters to prevent aliasing and noise from affecting the measurement quality.

The dynamic properties from the ambient vibration measurements were analysed using commercial OMA ARTeMIS Extractor Pro 2010. The analysis of the data was conducted using a Frequency Domain Decomposition (FDD) algorithm, which is a frequency domain

Figure 29 : Field testing of Roode Elsberg dam

based method that identifies the operational modal parameters of the dam.

3.2.2 Test Layout

The measurement instrumentation was setup by placing orthogonal (vertical and horizontal) accelerometers on each of the 8 cantilevered blocks of the dam (one half of the dam was measured). 100m long extension fibre cables were used to allow for the accelerometers to be placed along the length of the crest. Once the instrumentation was setup a sample run of the ambient vibration measurements was conducted to ensure that the accelerometers were working and the data was being acquired correctly. Thereafter, 3 recordings of approximately 20 minutes each were acquired on the test block locations, at a sampling frequency of 1000Hz.

3.3 Chapter Summary

In summary, this chapter begins with the validation of the acoustic finite elements as a viable formulation to model the impounded water body. Followed by the development of

the Abaqus formulation for the acoustic fluid structure interaction method. It defines how the dam wall, fluid part, boundary conditions and constraints were developed and applied in Abaqus Standard. It also describes how the modified Westergaard method was carried out and applied on the dam wall. The selected eigensolver is described to illustrate how the modal parameters were extracted from the governing equations of motion. A parametric study was carried out to investigate the influence of the reservoir geometry and orientation on the dynamic properties, as to carry out the objectives of this study. Thereafter, a formulation of the case study pertaining to the Roode Elsberg dam is carried out to obtain the dynamic characteristics and develop an updateable finite element model. Finally, the steps carried out in the ambient vibration testing on the Roode Elsberg dam to validate the dynamic finite element model are described.

CHAPTER 4

4 RESULTS AND DISCUSSION

4.1 Introduction

This chapter will present and discuss the results relating to the objectives of this study. Firstly, the result obtained from the validation study will be presented and discussed. Secondly, the parametric study results will assess the effects of the reservoir geometry and orientation on the dam's dynamic properties. Thereafter, the Westergaard and Acoustic finite element hydrodynamic analysis methods will be contrasted by scrutinising the dynamic modal parameters. Lastly, the analysis methods used to create an updateable finite element model for Roode Elsberg dam will be evaluated by making comparisons between their results and those of the Ambient Vibration Test results.

4.2 Validation Model

This section presents the results obtained from the modelling procedures carried out for the 3 hydrodynamic modelling techniques under horizontal ground motion. The dynamic pressures are calculated directly for the acoustic elements, and the pressure distribution on the downstream wall is provided in *figure 30*. The hydrodynamic pressure contours show a parabolic increase of pressure as a function of depth acting on the downstream surface.

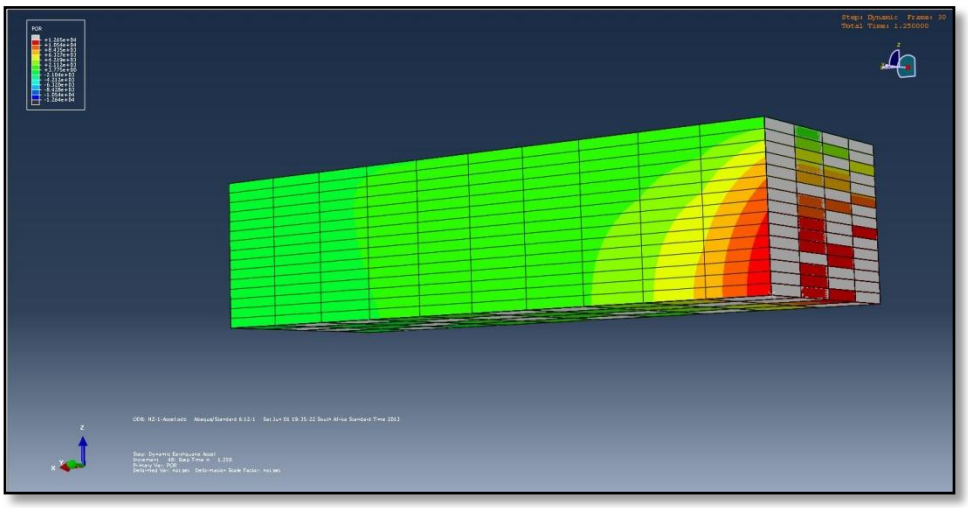

Figure 30: Cross section view of the hydrodynamic pressures acting on the downstream wall.

Figure 31 shows the time history pressure distribution taken at a sample node located mid-point of the downstream surface. The graphical description shows that the 3 formulations produce similar sinusoidal trends with time. In further scrutinizing the results it can be seen that the Houser formulation estimates a greater pressure distribution with change in time when compared with the other two methods, and the Acoustic elements give the smallest approximation. The acoustic element solution is within 1KPa and 2.5KPa of the Original Westergaard and Housner solutions respectively.

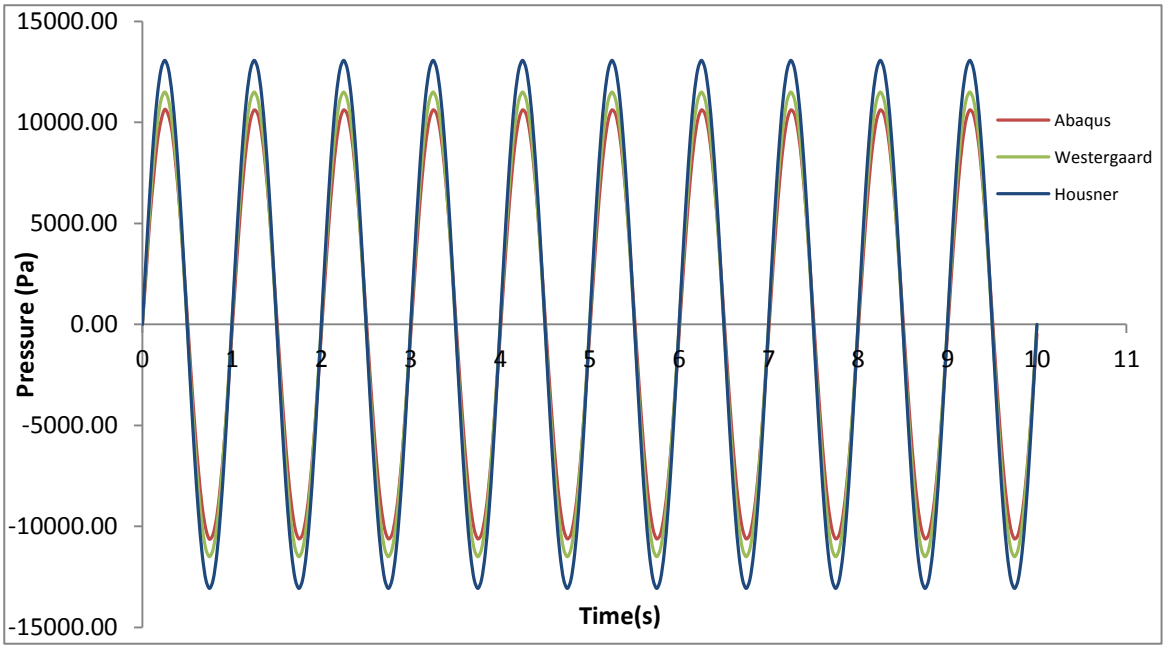

Figure 31: Pressure-time history of a sample point taken mid-section of the downstream surface.

Figure 32 shows the maximum hydrodynamic pressure distribution as a function of depth, the values were recorded at t = 1.25secs. The results show that the acoustic element fields a similar parabolic pressure distribution with a change in depth when compared to the Original Westergaard and Housner distributions. The coefficient of determination of the acoustic element model was computed at R^2 = 0.978 and 0.986 for Housner and Westergaard respectively.

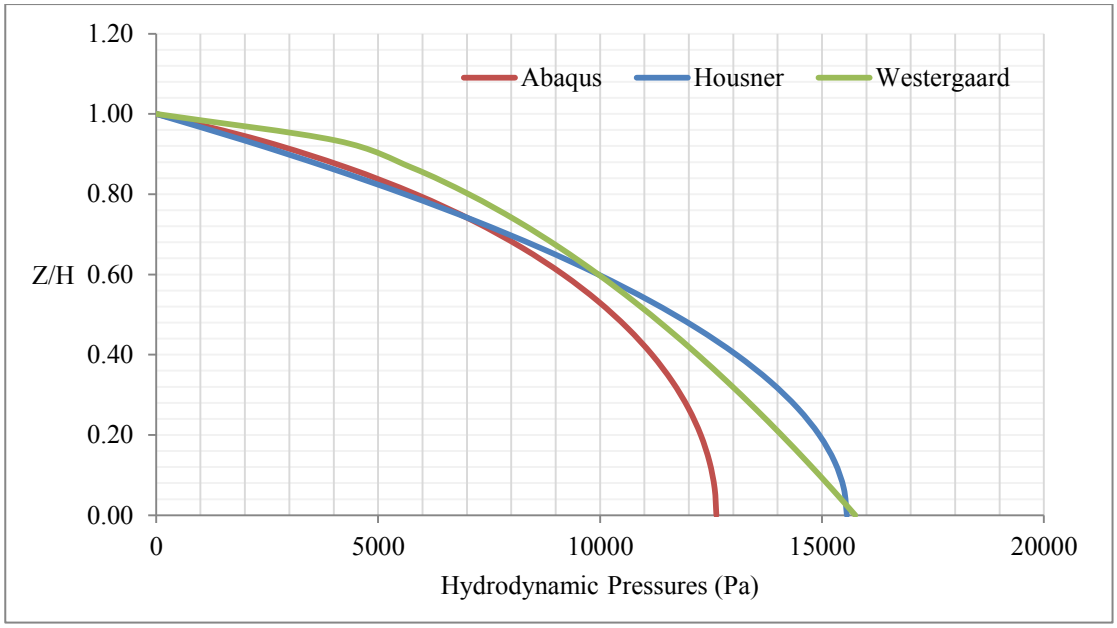

Figure 32: Maximum hydrodynamic pressures with a change in depth acting on the downstream wall surface, recorded at t=1.25secs.

The solutions in figure 32 show that the acoustic element model results in similar approximations as compared to those provided by Westergaard (1933) and Housner (1954) solutions. It's also observed that the Housner and Westergaard solutions produce estimations greater than the acoustic element method. The observed discrepancy could be consequence to the discretization of the mesh model (mesh refinement), and the compressibility effect of the acoustic elements (Rodríguez et al., 2012). Studies using the Original Westergaard formulation have shown that the method is rather conservative in its estimation (Kuo, 1982). This is due to the fact that the formulation does not consider the compressibility of the fluid, the impedance of the surrounding environment and the deformability of the wall. Therefore, the same could be experienced in this validation. The Housner formulation is considered to be analogous to the Raleigh-Ritz method and always overestimate the pressures (Housner, 1954).

In concluding, the assemblage of Acoustic elements provide a reasonably good technique to capture the hydrodynamic pressures and could be considered to be a better representation of the hydrodynamic pressures as the analysis method is capable of capturing the compressibility of the fluid medium, and the impedance with the surrounding environment.

4.3 Comparison of Hydrodynamic Solutions

The results obtained from the comparative study are presented in figure 33, where natural frequencies and mode shapes of the two methods are analysed and contrasted. Comparison between the natural frequencies, show that the Westergaard formulation produces lower frequencies than the FSI model (see figure 33). It's observed that for the first 10 modes an average discrepancy of 23 % exists between the frequencies of the two methods. For the higher modes the difference is greater due to the complexity of modes. When analysing the natural frequencies and mode shapes of dams, the lower modes are of greater importance, as field testing methods can approximately pick up the first six natural frequencies and modes. The constant discrepancy can be used going forward in the modification of the Westergaard method making it applicable to the ambient state.

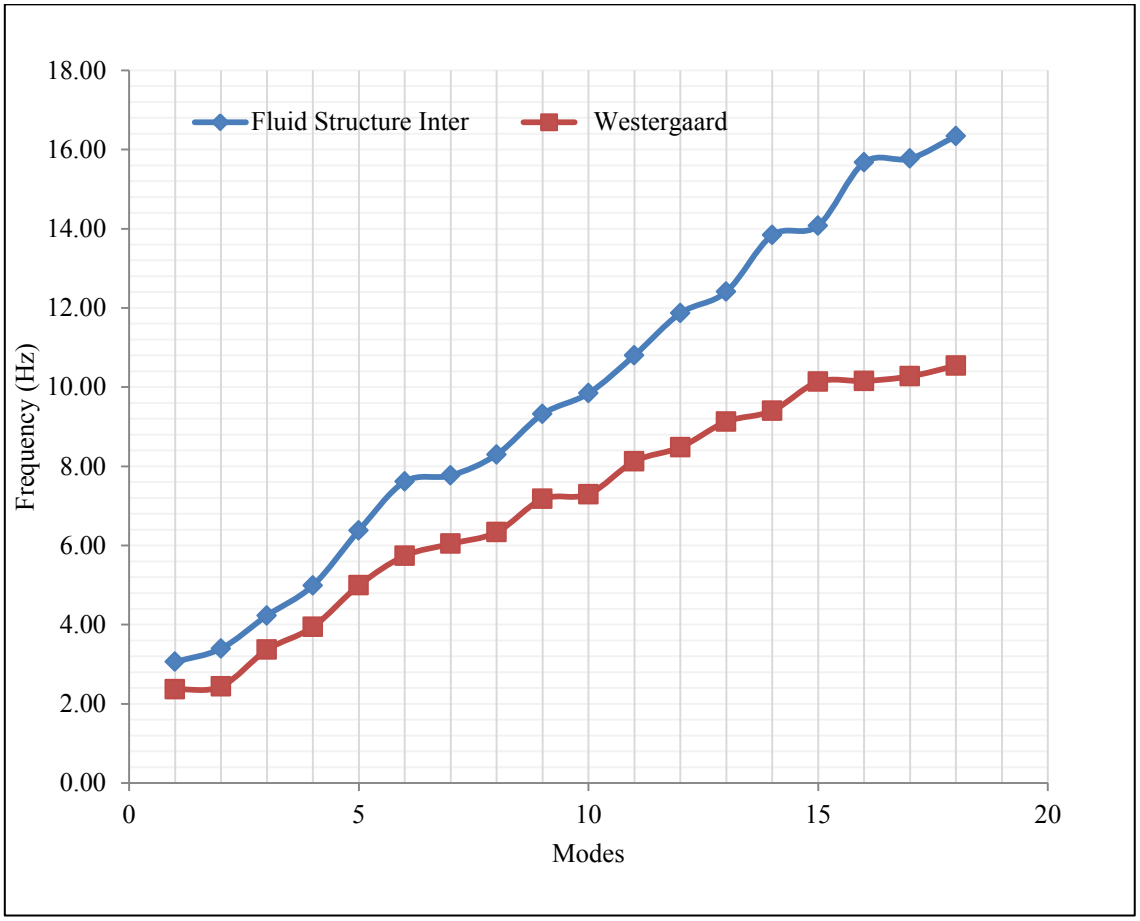

Figure 33: Natural frequency results from the Westergaard and Fluid Structure Interaction model.

Table 6: Natural Frequencies obtained from Westergaard and FSI model.

Modes	FSI	Westergaard	% Diff
1	3.06	2.37	22.61
2	3.40	2.44	28.19
3	4.23	3.37	20.42
4	4.99	3.94	20.99
5	6.38	4.99	21.70
6	7.61	5.74	24.62
7	7.77	6.04	22.23
8	8.29	6.33	23.62
9	9.32	7.17	23.02
10	9.84	7.29	25.89
11	10.80	8.13	24.77
12	11.87	8.48	28.53
13	12.41	9.13	26.44
14	13.84	9.40	32.05
15	14.08	10.13	28.01
16	15.67	10.15	35.20
17	15.77	10.27	34.88
18	16.34	10.54	35.50

The modes obtained in this comparative study were contrasted against the field testing modes of the Kouga dam, which is a dam similar to that created for this comparative study. The results show that the first four modes of vibration from the two analysis methods are in agreement with the field test measurement of the Kouga dam.

The 1st mode of vibration illustrates that thin double curvature arch dams behaviour asymmetrically about the crown position (Y-Axis) and are excited into motion in the upstream - downstream direction (*see figure 26*). The dam is seen to be very flexible at the crest level, where the two halves of the dam move in opposite directions. The 2nd mode of vibration is characterised by symmetric behaviour, in which the crown position vibrates in the upstream-downstream direction. The 3rd mode also illustrates symmetric behaviour about the crown position (Y-Axis). The quarter arc region between the crown and abutment illustrates to be heavily excited in the radial direction, where the mode vibration is characterised by inward - outward radial displacements. The fourth mode is asymmetric about the crown position, and is of a complex nature due to the flexibility of the arch dam. The 5th mode shows similar behaviour as the 4th mode but is symmetric about the crown. The last mode is very distinct as it is not characterised by upstream-downstream movements but by elongation in the z direction.

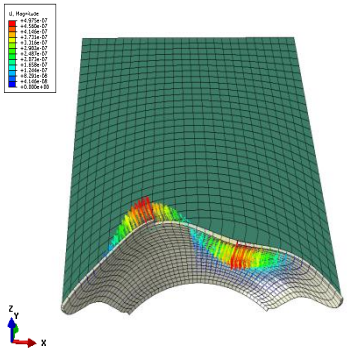

FSI - Mode 1 – 3.06Hz
Asymmetric

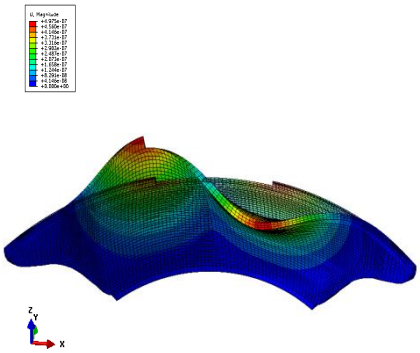

Westergaard - Mode 1 – 2.37Hz
Asymmetric

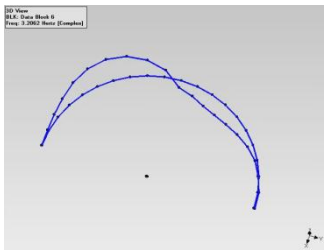

Kouga - Mode 1 –3.20Hz
Asymmetric

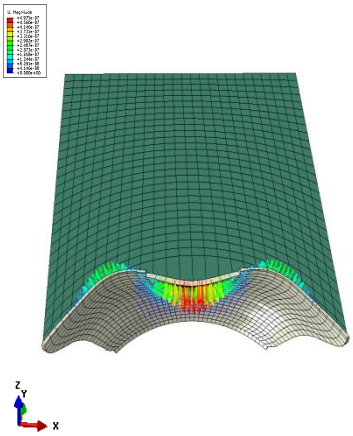

FSI - Mode 2 - 3.40Hz
Symmetric

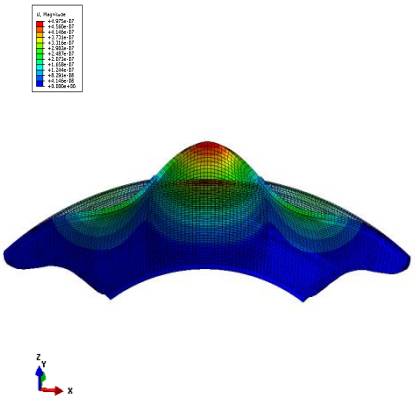

Westergaard - Mode 2 - 2.44Hz
Symmetric

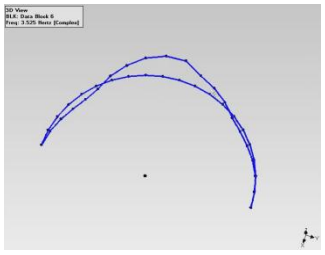

Kouga - Mode 2 - 3.52Hz
Symmetric

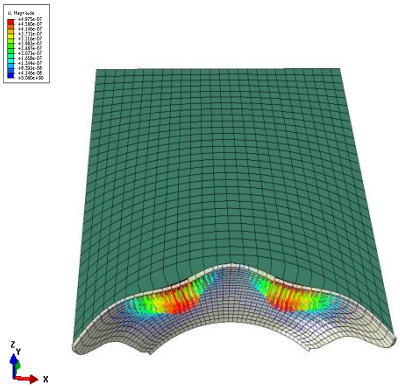

FSI - Mode 3 - 4.23Hz
Symmetric

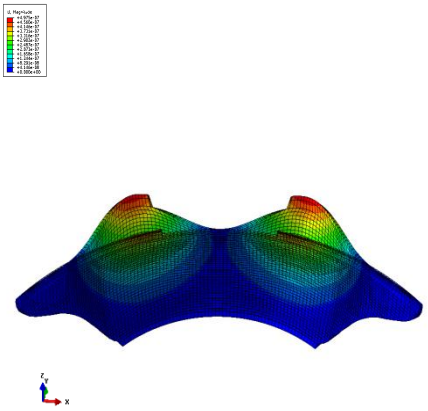

Westergaard - Mode 3 - 3.37Hz
Symmetric

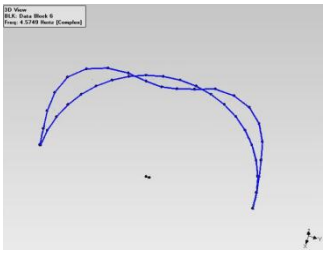

Kouga - Mode 3 - 4.57Hz
Symmetric

Figure 34: Comparison of the first three modes obtained from the models and ambient vibration tests conducted on the Kouga arch dam.

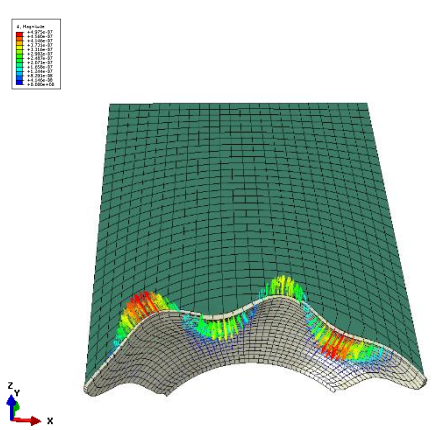

FSI - Mode 4 - 4.99Hz
Asymmetric

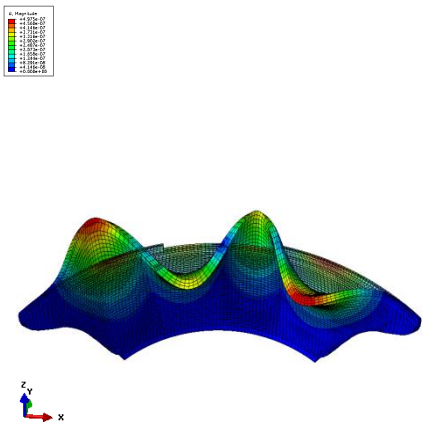

Westergaard - Mode 4 - 3.94Hz
Asymmetric

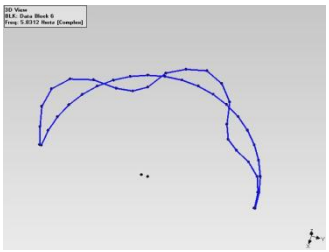

Kouga - Mode 4 – 5.83Hz
Asymmetric

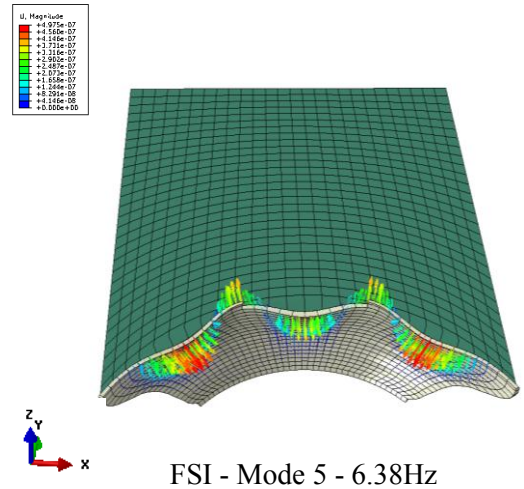

FSI - Mode 5 - 6.38Hz
Symmetric

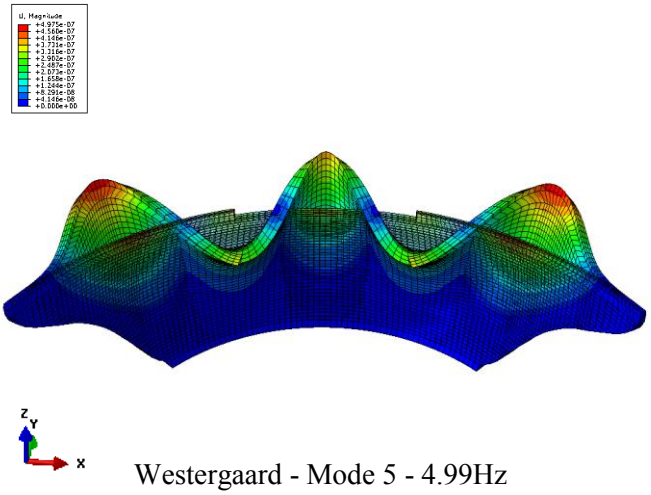

Westergaard - Mode 5 - 4.99Hz
Symmetric

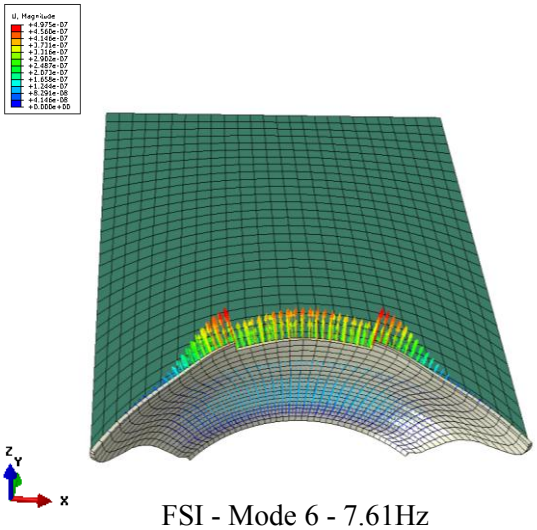

FSI - Mode 6 - 7.61Hz
Symmetric

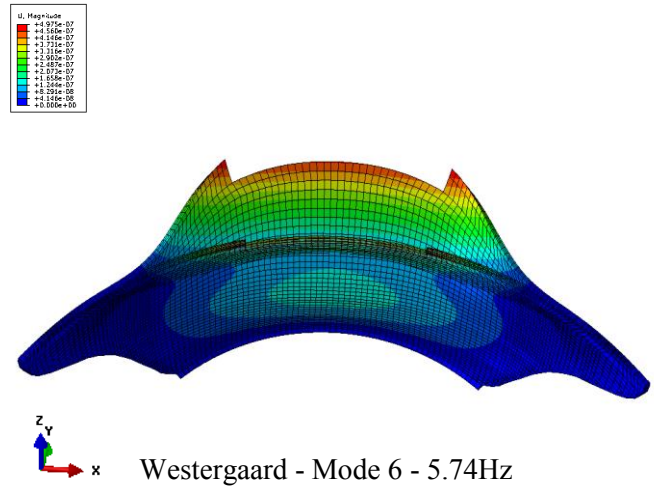

Westergaard - Mode 6 - 5.74Hz
Symmetric

Figure 35: Comparison of mode 4-6 obtained from the Models and Kouga arch dam.

4.4 Parametric Study Results

- Natural frequencies

The study was conducted to assess whether the modal parameters and hydrodynamic pressures acting on the arch dam wall would be influenced by the geometry and orientation of the reservoir in the ambient state. A parametric study conducted by Kuo (1982) showed that under seismic loading the hydrodynamic pressures decrease as the reservoir geometry diverged. This would have to be clarified before a case study would be conducted on the Roode Elsberg dam, where the reservoir is diverging and asymmetric.

Figure 36 and table 7 show the natural frequencies obtained in the diverging reservoir parametric study. The results obtained show that the natural frequencies do not change significantly as the impounded water body geometry is opened in incremental angles of 10°. The general trend is that the natural frequencies increase marginally as the reservoir geometry diverges. The maximum increase in frequency was experienced at Mode 14, where after an accumulated increment of 40° the frequency had increased by 0.11Hz (0.8%).

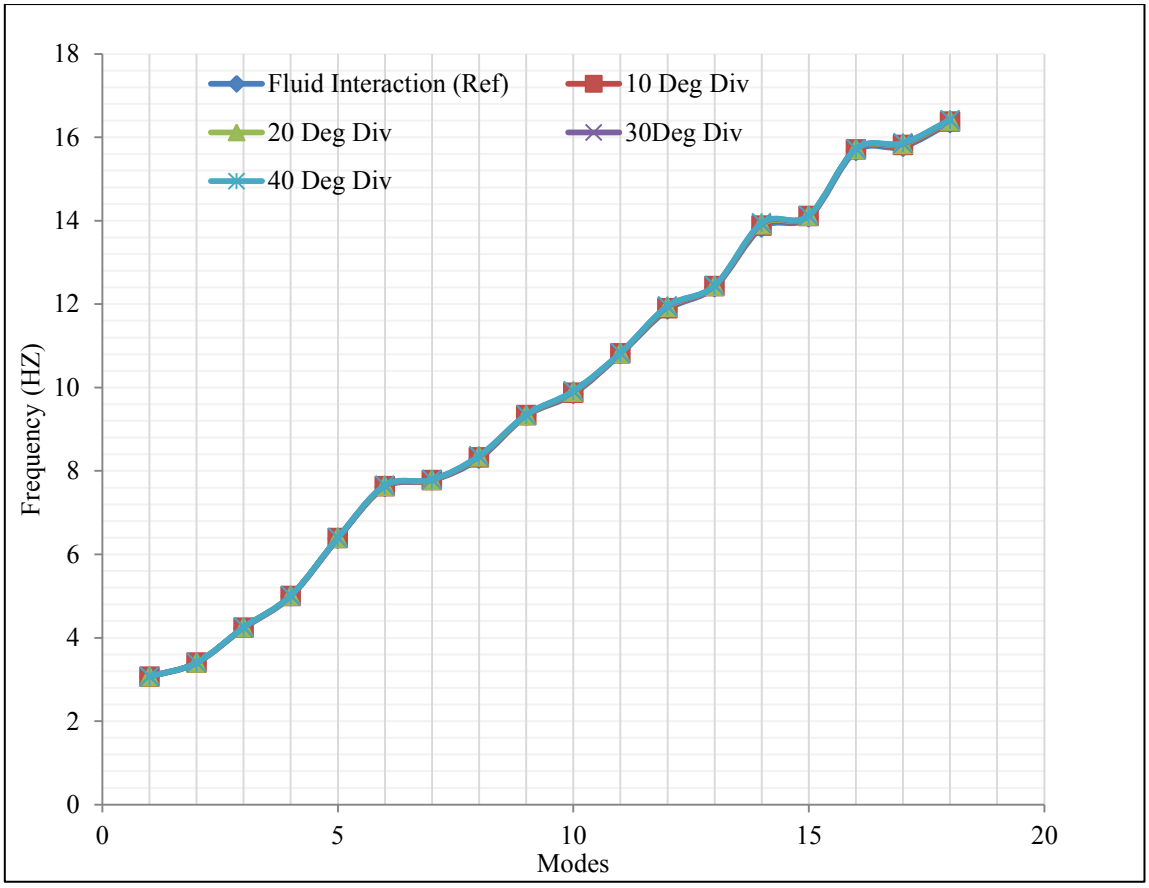

Figure 36: Results from parametric study of diverging reservoir

Table 7 : Natural Frequency (Hz) from diverging parametric study

Mode	Ref	10 Deg Div	20 Deg Div	30Deg Div	40 Deg Div
1	3.06	3.06	3.07	3.07	3.07
2	3.40	3.40	3.40	3.40	3.40
3	4.23	4.24	4.24	4.25	4.25
4	4.99	5.00	5.01	5.01	5.01
5	6.38	6.39	6.39	6.40	6.40
6	7.61	7.63	7.64	7.65	7.65
7	7.77	7.78	7.78	7.79	7.79
8	8.29	8.32	8.34	8.35	8.36
9	9.32	9.33	9.34	9.34	9.34
10	9.84	9.87	9.89	9.91	9.92
11	10.80	10.82	10.82	10.83	10.83

12	11.87	11.90	11.93	11.94	11.95
13	12.41	12.43	12.44	12.44	12.44
14	13.84	13.88	13.91	13.93	13.95
15	14.08	14.11	14.12	14.12	14.12
16	15.67	15.70	15.72	15.72	15.72
17	15.77	15.81	15.83	15.85	15.86
18	16.34	16.37	16.40	16.41	16.42

Similar results are observed when orientating the reservoir asymmetrically behind the dam. The first 3 angles produced insignificant change in the properties (see figure 37 and table 8). The reservoir skewed at an orientation of 40° produced technical difficulties in the modelling phase as regions of the foundation canyons would intersect with the geometry of the dam, this being unacceptable. It may be concluded that this is an excessive skew, which is physically not practical, as portions of the fluid at that specific orientation could not be modelled. Please note, the results of the 40° skew are provided for completeness of the study. In analysing the influence of the orientation, it is observed that skewing the reservoir decreases the natural frequencies. The maximum decrease was observed on the 18^{th} mode, where after an asymmetric shift of 40° the frequency had decreased by 0.41Hz (2.5%).

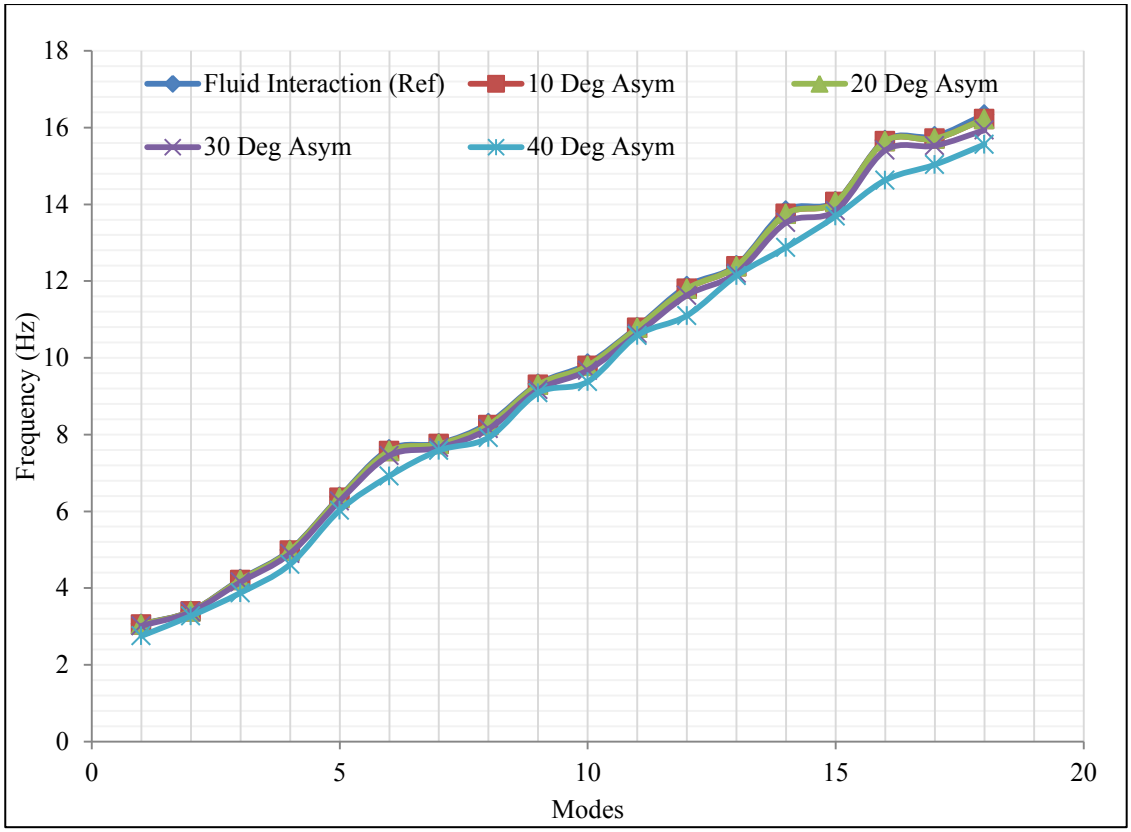

Figure 37: Natural frequencies from the asymmetric parametric study

Table 8: Natural Frequency (Hz) from asymmetric parametric study

Mode	Ref	10 Deg Asym	20 Deg Asym	30 Deg Asym	40 Deg Asym
1	3.06	3.06	3.05	3.02	2.75
2	3.40	3.40	3.39	3.38	3.27
3	4.23	4.23	4.21	4.16	3.88
4	4.99	4.99	4.97	4.90	4.62
5	6.38	6.37	6.35	6.27	6.03
6	7.61	7.60	7.57	7.45	6.92
7	7.77	7.77	7.75	7.66	7.59
8	8.29	8.28	8.25	8.15	7.92
9	9.32	9.32	9.30	9.17	9.09
10	9.84	9.83	9.79	9.67	9.38
11	10.80	10.80	10.78	10.63	10.58

12	11.87	11.85	11.80	11.63	11.10
13	12.41	12.41	12.39	12.20	12.14
14	13.84	13.82	13.75	13.52	12.88
15	14.08	14.09	14.06	13.84	13.69
16	15.67	15.68	15.65	15.41	14.63
17	15.77	15.76	15.71	15.53	15.03
18	16.34	16.32	16.22	15.93	15.56

The results obtained in the parametric study show that the orientation and geometry of the reservoir have an insignificant effect on the natural frequencies. This is supported by the first 18 natural frequencies of the diverging and asymmetric study (see table 7 & 8). The hydrodynamic pressure distribution acting on the dam wall were analysed to explain the observed behaviour of the dynamic properties. The distribution of pressure was extracted at the crown, quarter arc and abutment edges on the upstream side of the wall. The first 3 modes of the reference, diverging and asymmetric models were analysed.

- Hydrodynamic Pressure Distribution

The 1st Mode was analysed at the quarter arc position due to it being characterised by an asymmetric motion at this location in the upstream-downstream direction. Presented in *figure 38, 39 & 40* is the pressure distribution as a function of depth plotted for all diverging and asymmetric reservoir walls respectively. For both parametric cases the dynamic pressures acting at the quarter arc position have a complex distribution which is not a parabolic shape as that proposed by Westergaard (1933) for gravity dam walls under seismic loading. The maximum pressure is approximately 1 Pa at a height of 18m below the water surface level. The distribution of pressure at this location indicates that small changes in pressure are experienced with an increase of diverging angle (see figure 38). The dynamic pressures decrease slightly with a maximum drop of 0.038 Pa. For the diverging case the pressure distribution was only measured on the left half of the arch wall, due to the reservoir being symmetric about the crown position. The pressure was found to be equal in magnitude at either side of the crown, but acting in the opposite direction due to the asymmetry of the mode.

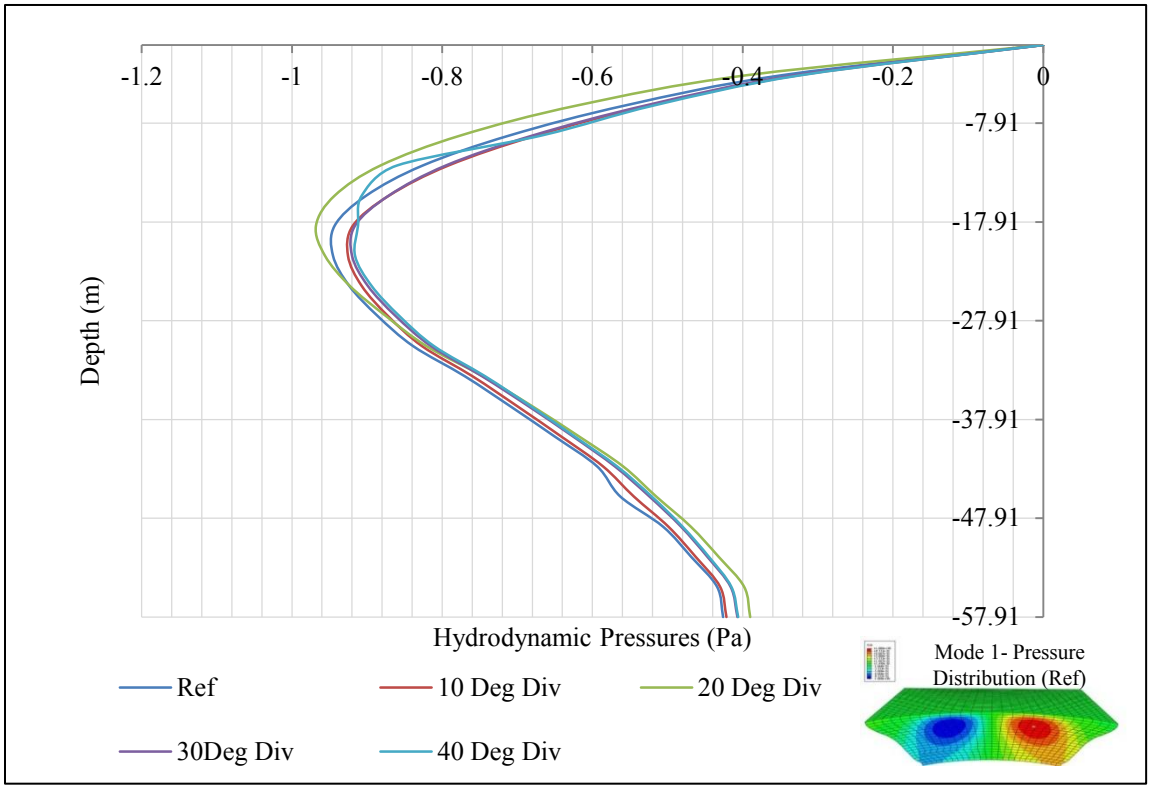

Figure 38: Pressure distribution at quarter arc location for Mode 1 (Diverging Reservoir Walls)

The asymmetric pressure distribution on the arched wall is dependent on the side of the arch which is being analysed, as a result of opening the left flank and closing the right flank of the reservoir,. The graphical representation provided in *figure 39 & 40* illustrates the pressure distribution on the left and right quarter arc positions respectively. In *figure 39,* the pressure distribution on the left arch of the dam wall illustrates an increase pressure, with an increase in asymmetry. The increase in pressure can be attributed to the confinement of the water, by the canyon wall. As the dam wall vibrates in its modal fashion it applies traction forces against the impounded water body. The fluid is impeded from displacing in the transverse lateral direction as a result of the skewed reservoir wall (closing), resulting in intensified pressures acting on the dam wall as a result of the impedance. Figure 40 shows the opposite phenomenon as the rock supporting wall opens, the pressure distribution decreases on the upstream surface of the wall. This can be explained by the opening of the supporting rock which allows bilateral movement for the impounded water as the dam wall displaces in the downstream direction. This results in a decrease in the participating acoustic fluid in motion and hence a decrease in hydrodynamic pressure acting on the upstream

surface of the dam. Opening up the left flank by 30° decreases the dynamic pressures by a maximum of 0.245 Pa (26%).

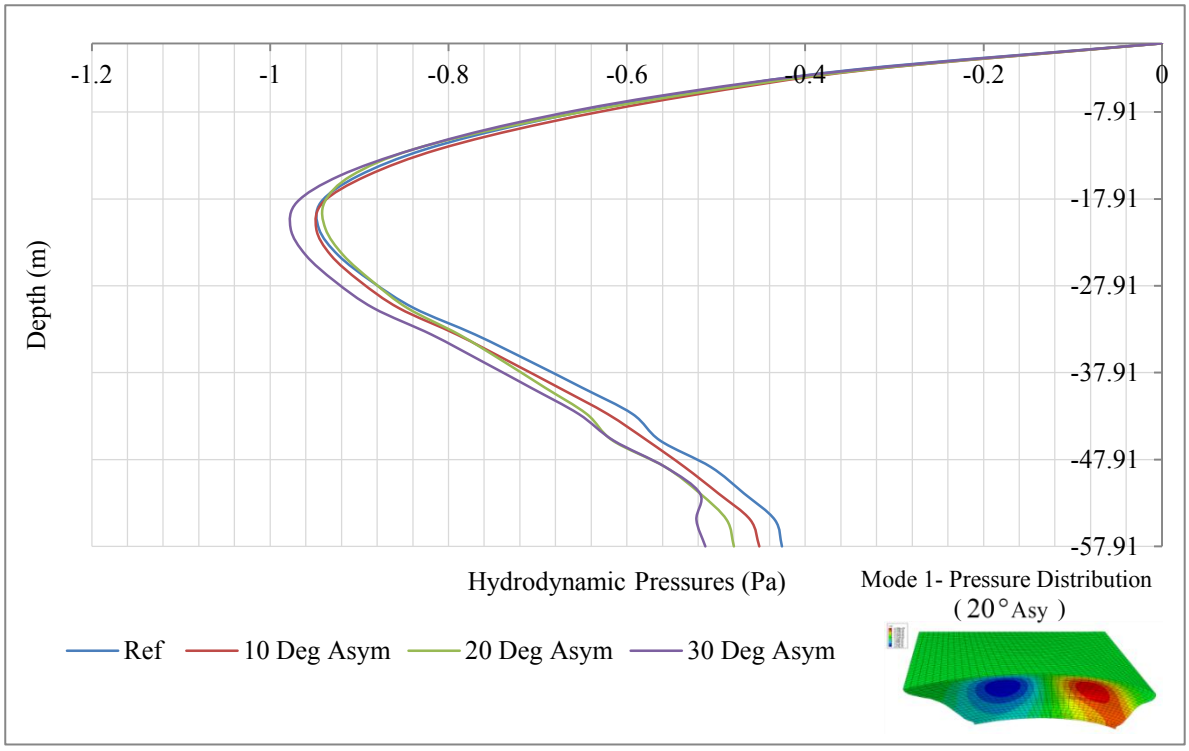

Figure 39: Pressure distribution at left quarter arc location for Mode 1 (Asymmetric Reservoir Walls)

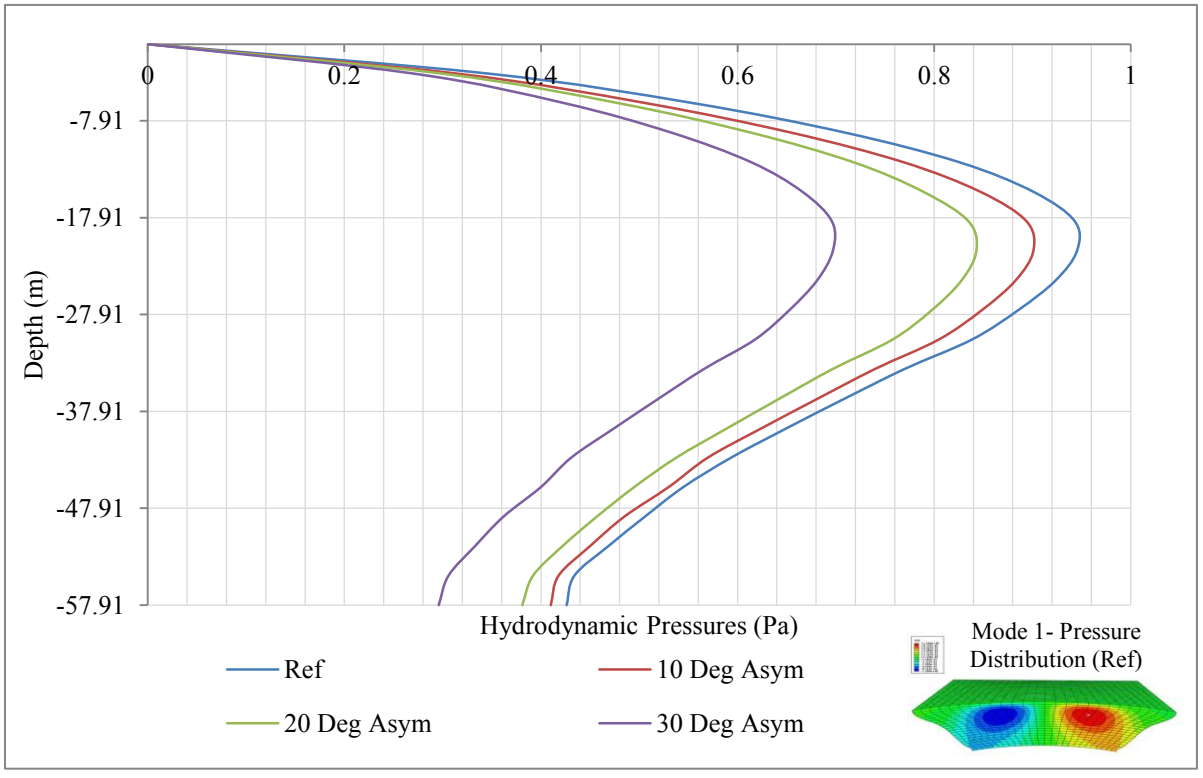

Figure 40: Pressure distribution at right quarter arc location for Mode 1 (Asymmetric Reservoir Walls)

The 2nd Mode was analysed at the crown and abutment edge positions. Presented in *figure 41, 42, 43 & 44* is the pressure distribution as a function of depth plotted for all diverging and asymmetric reservoir walls respectively. For both parametric cases the dynamic pressures acting at the crown and abutment support differ and have a complex distribution of pressure. The crown pressure distribution and magnitudes are similar to that observed for the first mode acting on the quarter arc position. The abutment pressure distribution is similar for both parametric cases but differs from that existing at the crown position. The abutment pressure distribution is unique and peaks at a height of 36m below surface level (*see figure 42 & 44*).

During the diverging parametric case, the pressure distribution at the crown level showed no change in pressure as the reservoir walls are set to diverge (*See figure 41*). This could be as a result of insufficient transverse motion (liberation) in the fluid to decrease the pressure distribution at this mode. *Figure 42* shows contrasting behaviour at the abutment edges, as significant changes in pressure are experienced as the reservoir diverges in geometry. Since the divergence occurs at the abutment regions the impounded fluid is allowed to diverge with the reservoir as it opens up, resulting in a reduction in pressures acting on the arch at the abutment edges with divergence. After a divergence of 40 degrees of the reservoir, a maximum pressure drop of 0.07 Pa (34%) is experienced at the edges.

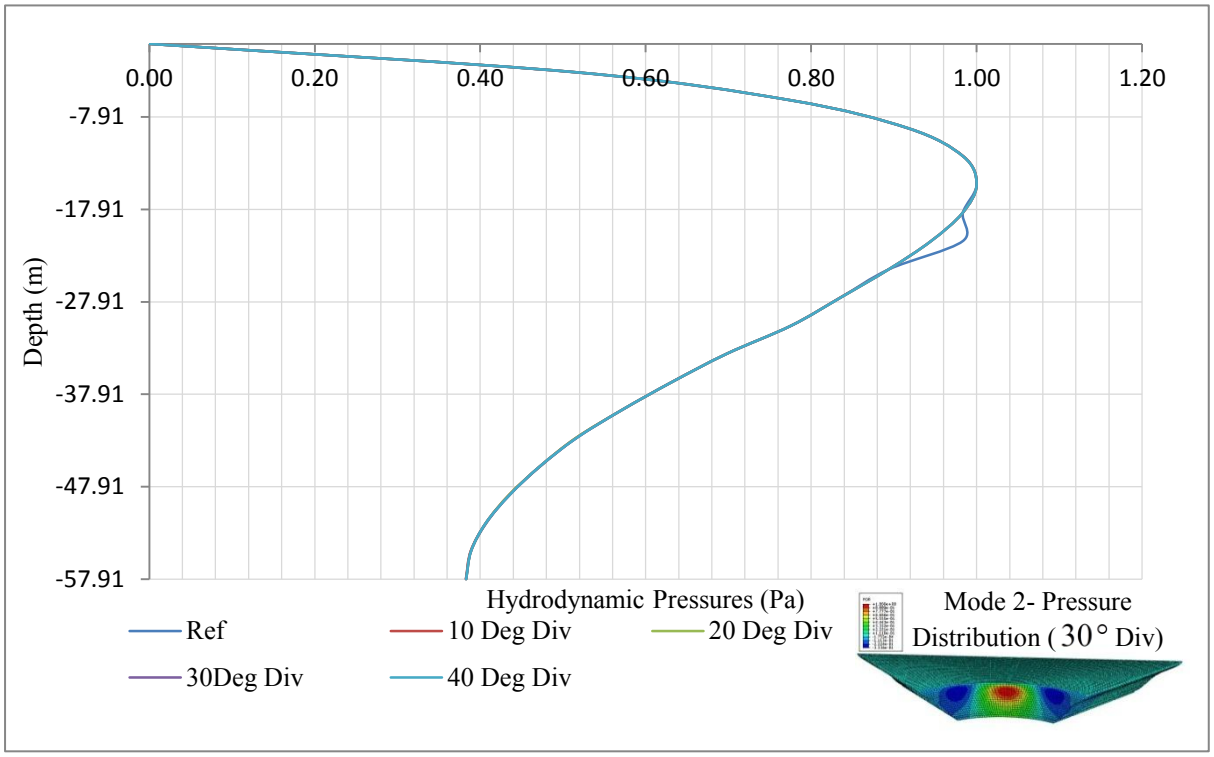

Figure 41: Pressure distribution at crown level for diverging parametric case.

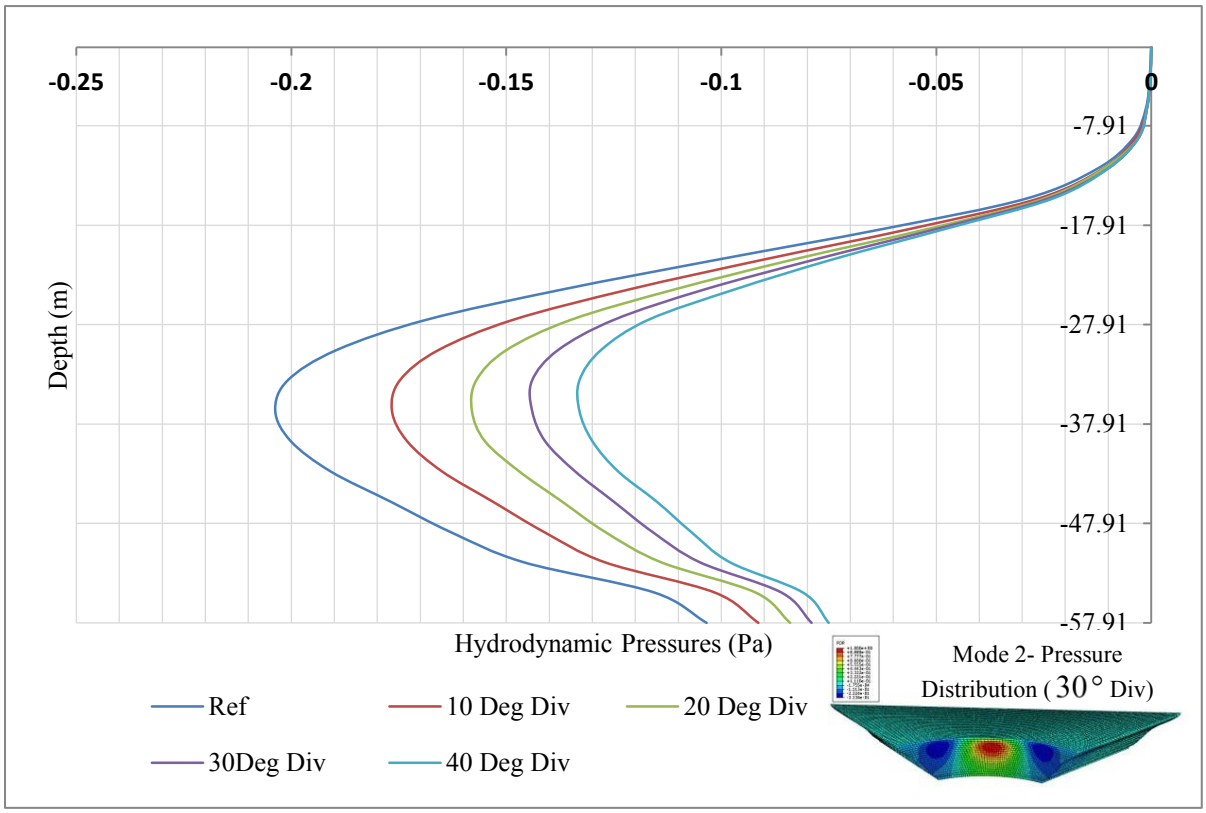

Figure 42: Pressure distribution at abutment region for diverging reservoir.

In the asymmetric case the pressure distribution profile at the crown level is synonymous to the diverging case, with an insignificant change in pressure distribution as the reservoir orientation becomes asymmetric in standing (*see figure 43*). The orientation change at the abutment region can be seen to not have much of an impact on the pressures acting at the crown level. In contrast, the pressures acting at the abutment edges show significant variation with a change in orientation of the reservoir. The pressure distribution at the right abutment edge increases, while at the left abutment edge the pressure distribution decreases with asymmetry of the reservoir (*see figure 44*). The change in pressure values can be attributed to the closing and opening of the flanked reservoir wall which was discussed above for the 1st mode. *Figure 44* shows the change in pressure on the left and right abutment as the reservoir becomes asymmetrical. On the left abutment it can be seen that the pressures decreases as the supporting wall opens up. The drop in pressure is very small with a maximum drop of 0.05Pa (24.5%). While at the right abutment region a significant increase is experienced. The maximum pressure at the height of 33.5m increases by 0.4 Pa (200%).

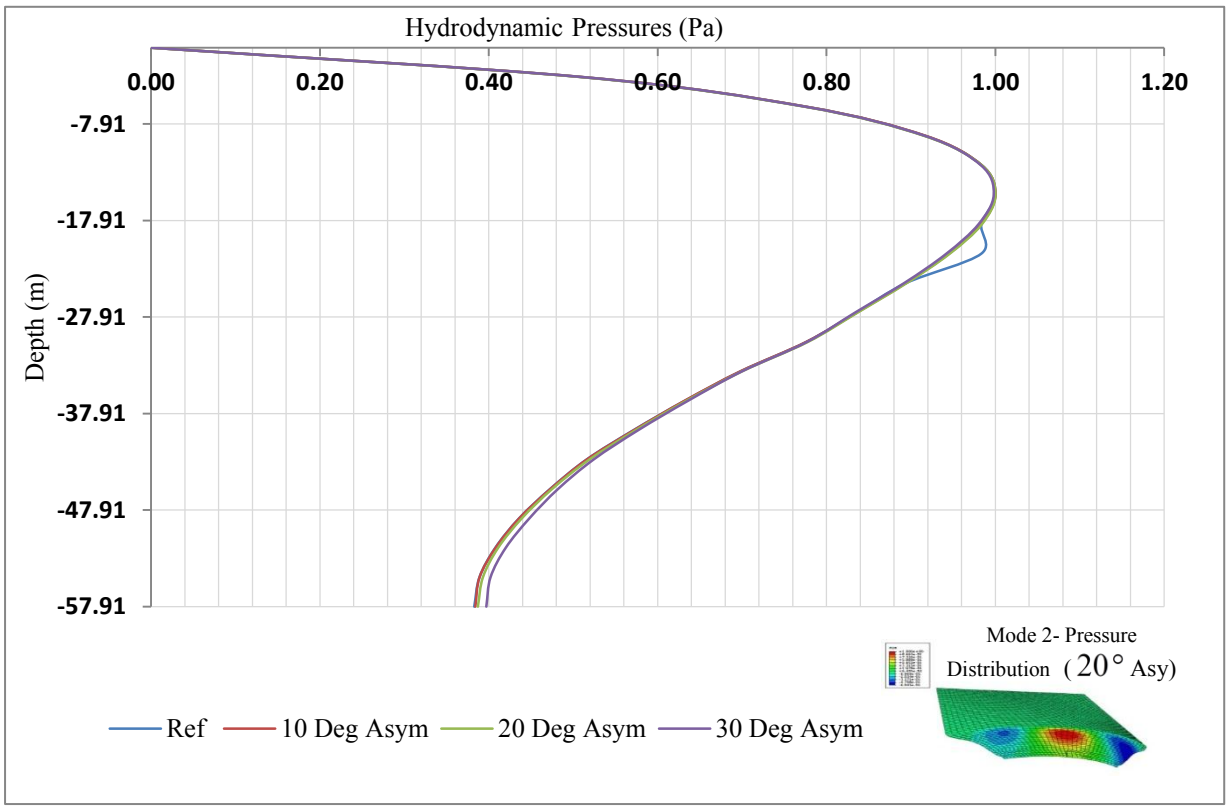

Figure 43: Pressure distribution at crown level for asymmetric scenario of mode 2.

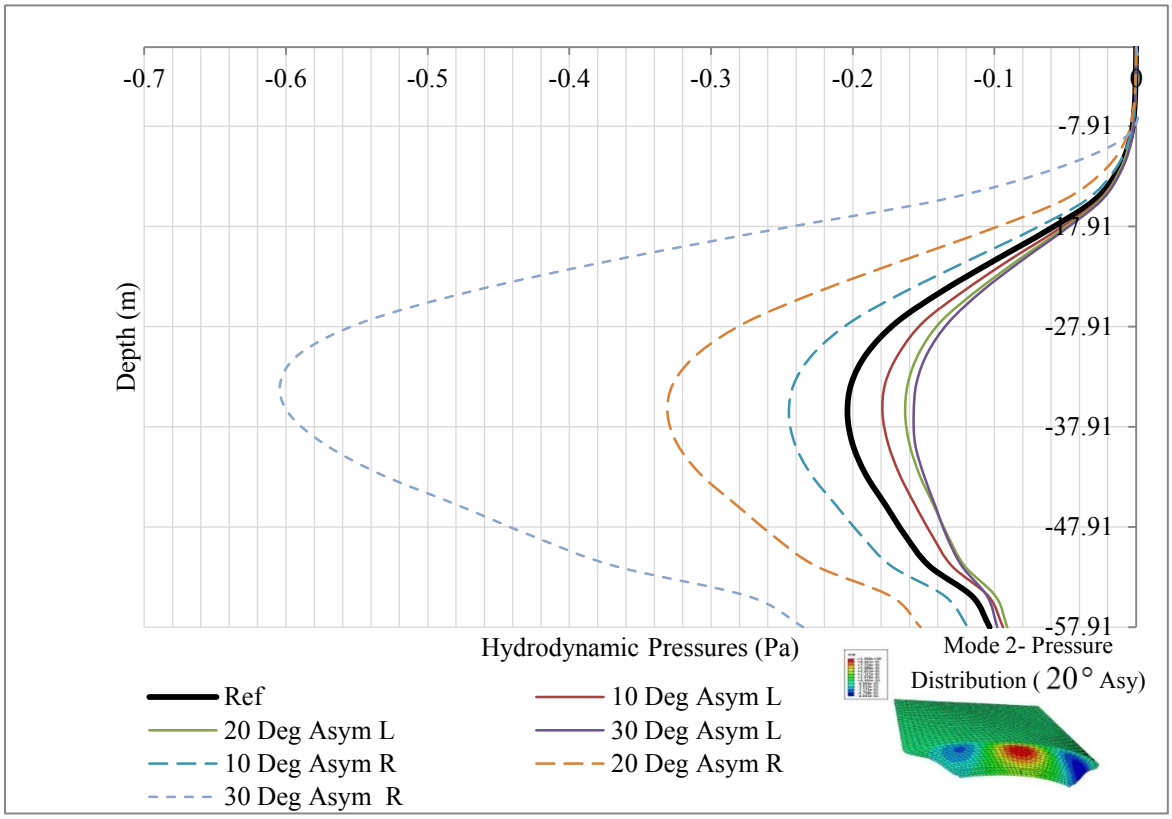

Figure 44: Pressure distribution at left & right abutment for asymmetric scenario of mode 2.

Finally, the 3rd Mode was analysed at the crown position and abutment edges. Presented in figure 45, 46, 47 & 48 is the pressure distribution as a function of depth plotted for all diverging and asymmetric reservoir walls respectively. The pressure distribution profile at the crown position for both parametric cases seems to be similar and consistent as that of the 1st and 2nd mode. At the abutment regions the pressure distribution profile is almost parabolic and can be considered to follow the parabolic profile shape that was proposed by Westergaard (1933). The maximum pressures are experienced at the bottom of the reservoir at the abutment positions, while at the crown position, at a height of approximately 28m.

Small changes in pressure distribution are experienced with an increase in diverging angle at the crown position (see figure 45). The dynamic pressures decrease slightly with a maximum drop of 0.02 Pa (4%).The same explanation considered in the analysis of the first two modes can be used to explain the absence of influence at the crown position. At the abutment region the change in pressure distribution is more prominent than that at the crown position *(*see figure 46). Although when scrutinised closely the change in pressure distribution at the abutments isn't significant with a maximum decrease of 0.16 Pa (29%).

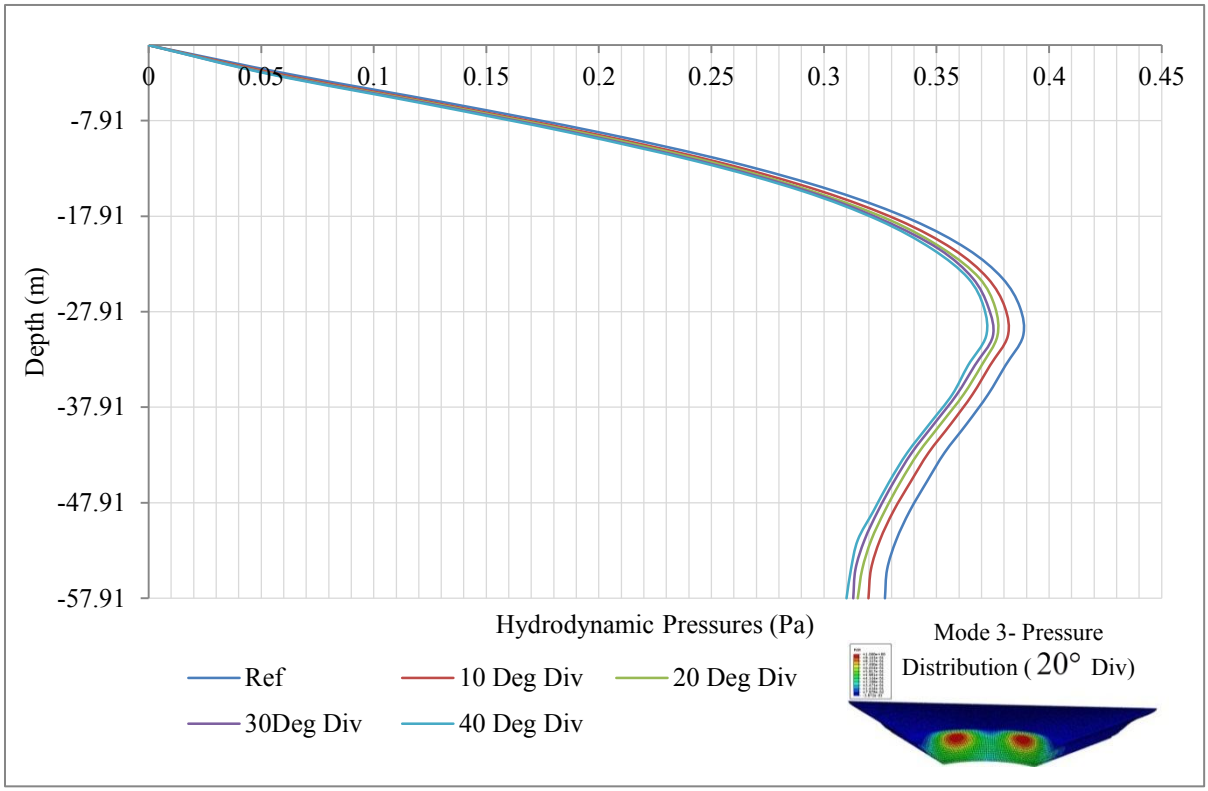

Figure 45: Pressure distribution at crown position for diverging scenario of mode 3

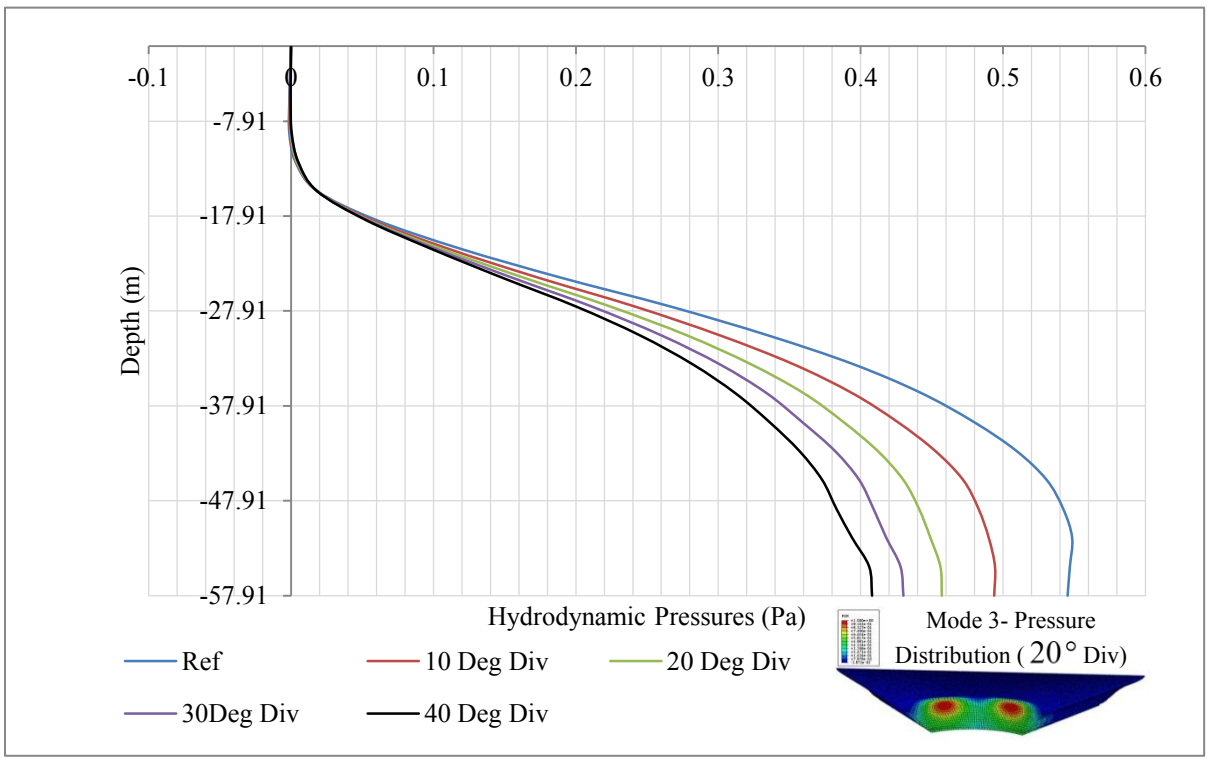

Figure 46: Pressure distribution at the abutment position for the diverging scenario of mode 3.

The asymmetric scenario illustrated a rather inconsistent change in pressure at the crown position. After an asymmetry of 10° the pressure distribution increases by 0.01 Pa (3%) which can be considered to be an insignificant change. With a further increase in skewness (20°) the profile drops back to the original distribution of pressure, and after 30° the pressure distribution drops by a maximum of 0.04 Pa (9%). The drop in pressure could be caused by the shift in water body towards the left flank wall (opening flank relative to the crown position). Resulting in the dynamic pressures acting at the crown position being heavily influenced by the behaviour of the opening reservoir wall, more than the closing, hence the minor drop in pressure experienced at the crown level.

The asymmetric pressure distribution at the abutment is dependent on the side of the arch which is being analysed. The graphical representation provided in figure 48 illustrates the change in pressure distribution on the left and right abutment edge positions. On the left abutment the pressures decrease while on the right an increase is experienced. It is interesting to notify that the increase in pressure on right abutment is not proportional to the decrease experienced on the left abutment, but is slightly greater by 32.7 %. Once again this is attributed to the opening and confining of the flanks at the left and right abutments. Resulting in more impounded water being excited into motion on the confined side (right) and less on the open side (left).

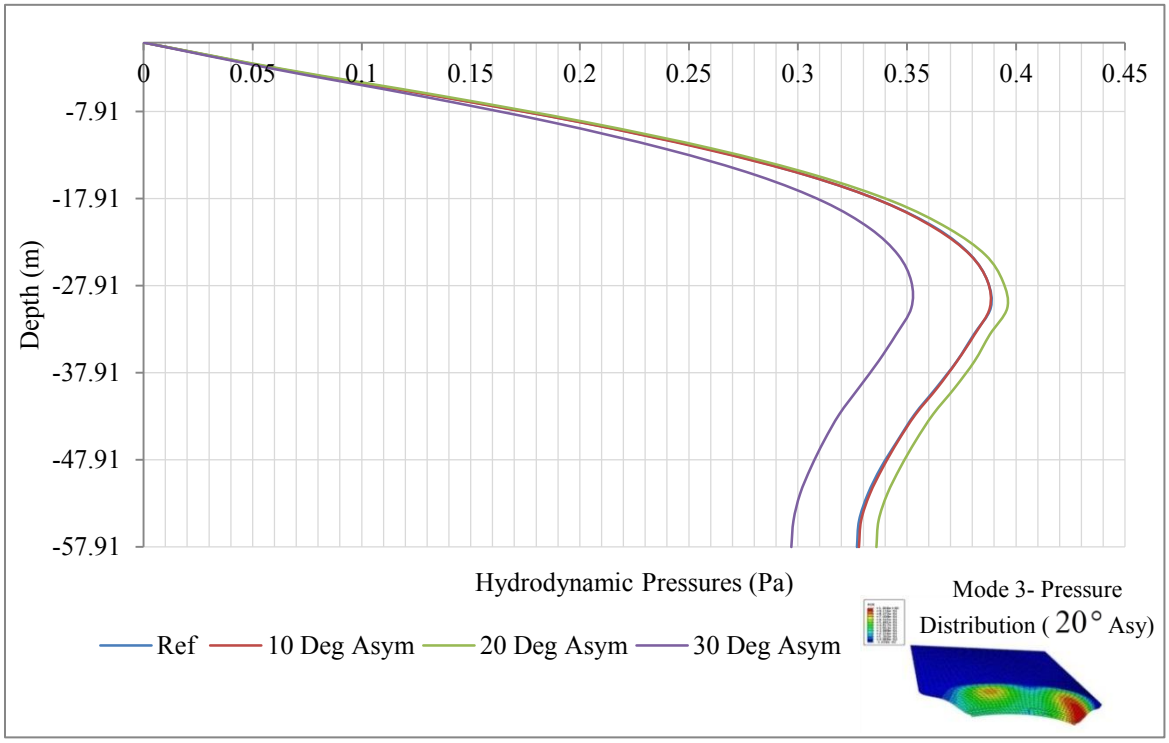

Figure 47: Pressure distribution at crown position for the asymmetric scenario of mode 3

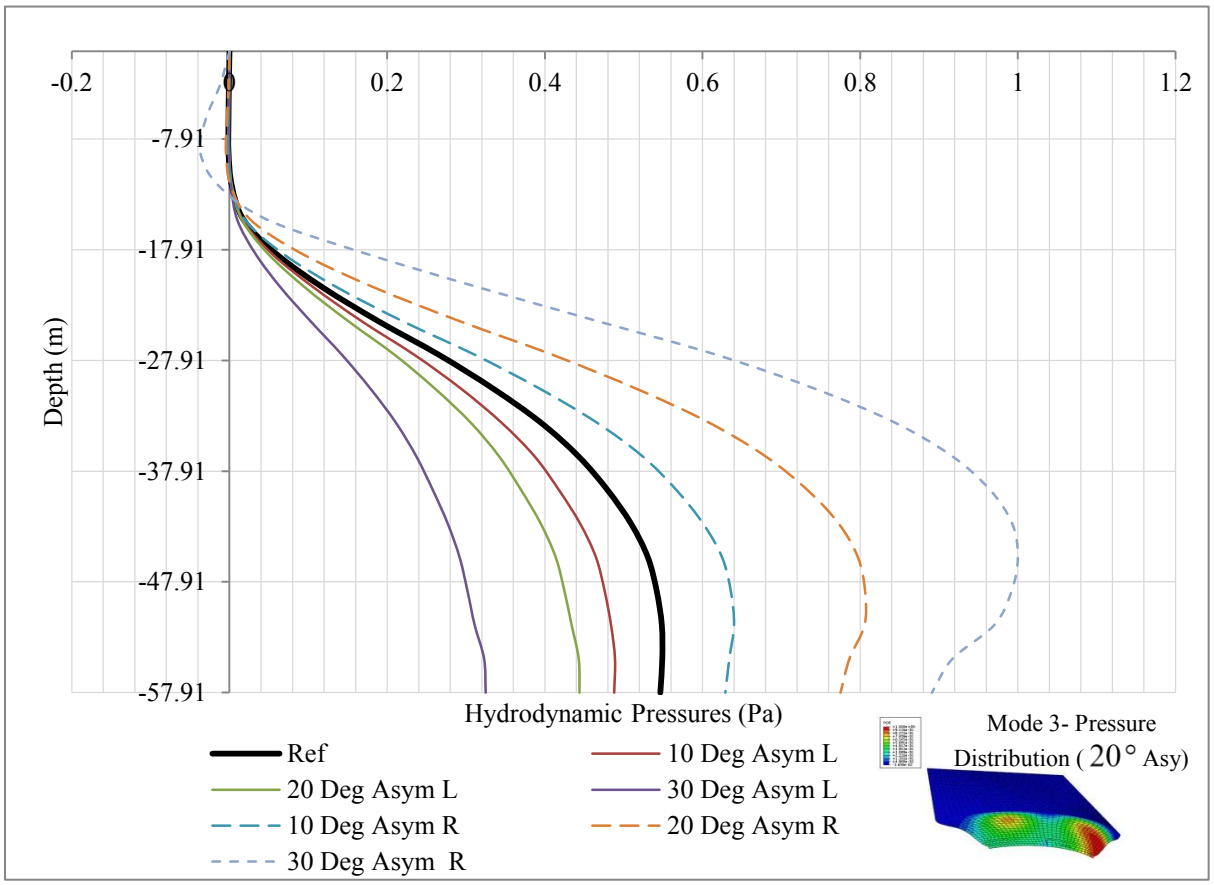

Figure 48: Pressure distribution at left and right abutment for the asymmetric scenario of mode 3.

The results obtained from the analysis of the hydrodynamic pressures of the parametric study indicate that the geometry and orientation of the impounded reservoir have an influence on the hydrodynamic pressures acting on the upstream side of the arch dam wall. From the above results, we can conclude that a diverging geometry results in a decline of the hydrodynamic pressures acting at the abutment regions and not much change at the crown region. The results obtained above partially agreed with those found by Kuo (1982) in a diverging parametric study of a cylindrical upstream face arch dam subjected to horizontal ground motion. At the abutment regions the pressures were found to decrease quite significantly, but at the crown and quarter arc positions the decrease in hydrodynamic pressure was not as significant. This could be due to that dynamic pressures are heavily sensitive to the geometry of the impounded water body under seismic loading, as when compared to the ambient case.

The reservoir orientation was also found to have an influence on the pressures acting on both sides of the arch, where the pressures on the confined flank of the reservoir were find to increase and those at the opening abutment side were found to decrease with the asymmetry.

It was also noted that the rate of increase was found to be greater than the decrease experienced found at the opening abutment.

The above can be seen to influence the small change in natural frequencies observed with change in geometry and orientation of the reservoir. The minor increase in natural frequency with the diverging reservoir is as a result of the reservoir flanks opening which allows bilateral motion of the fluid at the abutment regions (see table 7). This results in less volume of the impounded water being excited into motion as the dam wall vibrates in its modal fashion, hence resulting in an increase in the natural frequency at every mode. The decline in natural frequencies with an increase asymmetry is attributed to the overall increase in pressures acting on the dam wall. As noted above, the confined wall experiences an increase in pressure distribution which is greater than the decrease at the opposite abutment edge. The difference results in more water being excited with each mode, and moving back and forth with the dam, hence a drop in the natural frequencies which is associated with each mode (see table 8).

- Acoustic Participation Factors

In addition to the hydrodynamic pressures, the acoustic participation factors were analysed to try and support the behaviour of the natural frequencies. The acoustic participation factors represent how strongly acoustic motion is associated with the specific mode. The factor is strongly related to the mass and the hydrodynamic pressure of the fluid which is associated with that mode and is defined below as equation (4.1):

$$\Gamma_{\alpha}^{ac} = \sqrt{\Gamma_{\alpha}^{L}\Gamma_{\alpha}^{R}/m_{ac}} \tag{4.1}$$

Where: Γ_{α}^{L} and Γ_{α}^{R} represent the left and right acoustic participation factors provided below as equation (4.2) and (4.3). m_{ac} is the total acoustic mass which is defined by $m_{ac} = T_a^T M_f T_a$.

$$\Gamma_{\alpha}^{L} = \frac{1}{m_{\alpha}} \psi^{Q} M_F T_a \tag{4.2}$$

$$\Gamma_{\alpha}^{R} = \frac{1}{m_{\alpha}} (-T_a S_{FS} u^{M} + T_a M_F p^{Q}) \tag{4.3}$$

Figure 49 shows the participation factors obtained for the diverging parametric study. It can be seen that the acoustic participation factors rise as the modes increase. This means that fluid motion is strongly associated with the higher modes and is not so much with the small modes (less than 6). Thus, we can relate that any change in the impounded water body upstream will greatly affect the behaviour of the higher modes rather than the lower. The acoustic participation factor profile shows that not much change is associated with the divergence of the reservoir (see figure 49). Only minor changes are experienced in the higher modes where a decrease in the participation factor is associated with an increase in divergence. The decrease in the participation factor can be interpreted in this context as a reduction of fluid mass which is set into motion, and a decrease of the hydrodynamic pressures acting on the dam. Hence, resulting in the minor increase (maximum of 0.58%) observed in the natural frequencies (see table 7).

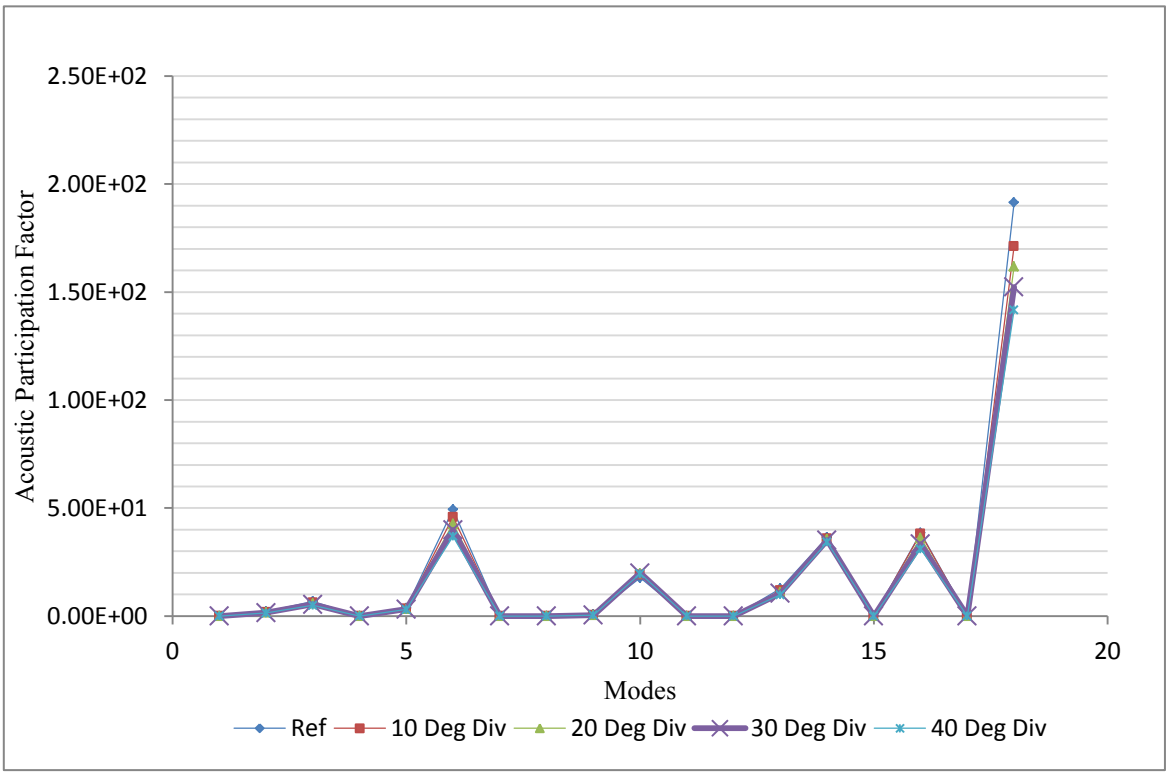

Figure 49: Acoustic Participation Factor distribution with diverging reservoir

Figure 50 shows the participation factors associated with the asymmetric parametric study. The distribution is similar to that of the diverging parametric study profile. In comparison the participation factors are influenced a considerable amount by the asymmetry when compared to the diverging parametric case, after an asymmetric shift of $30°$ a maximum increase of 1.7 is observed in the profile at mode 16 (*see figure 50*). The rise in the

participation factors is associated with an increase in acoustic motion for each mode; this is attributed to the increase in hydrodynamic pressures observed in the analysis of pressure distribution. The following results in the minor increase (maximum of 2.48%) in natural frequencies observed after a reservoir orientation shift of 30° .

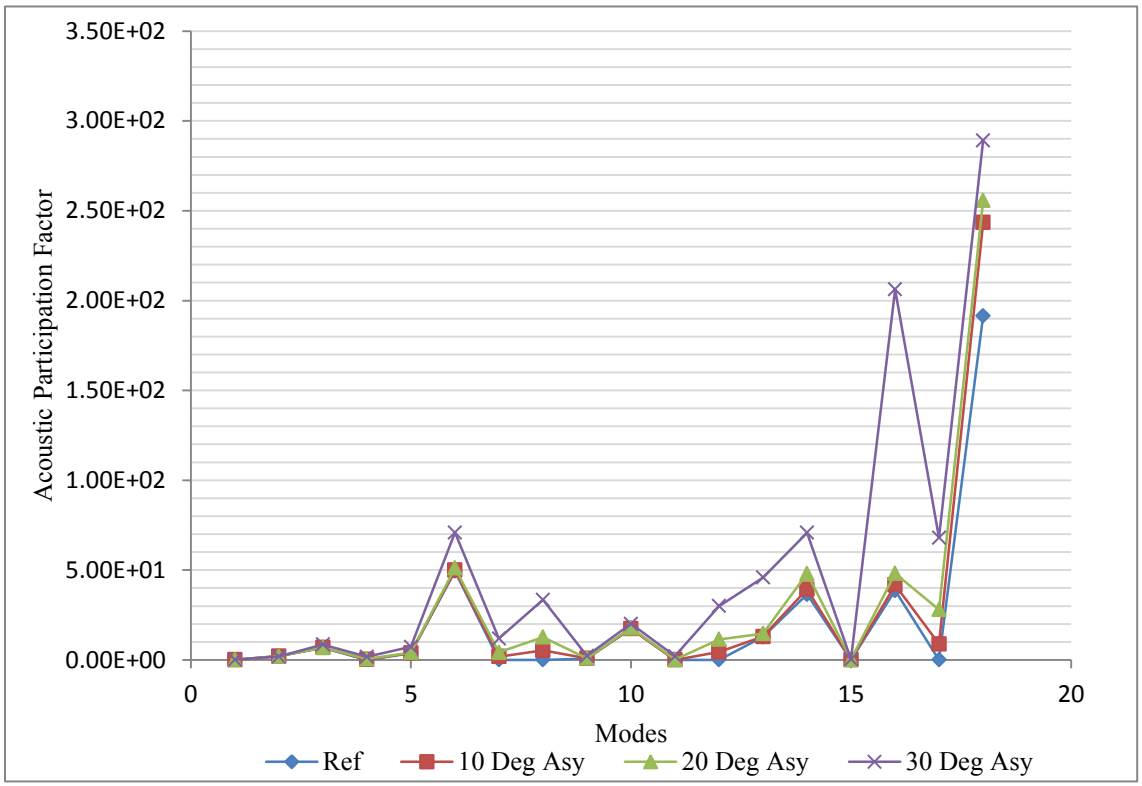

Figure 50: Acoustic Participation Factor associated with asymmetric reservoirs

The results obtained from this parametric study clarify that the hydrodynamic behaviour experienced in seismic conditions differs from that in the ambient state. Firstly, the distribution of pressure is not of a parabolic nature that was proposed by Westergaard (1933) and described by Kuo (1982). The distribution of pressure in the ambient state is dependent on the location of the arch and the behaviour of the mode. The diverging and asymmetry of the reservoir have an insignificant effect on the natural frequencies of the dam with a maximum increase of 0.58% and decrease of 2.48% respectively.

4.5 Roode Elsberg Model Results

The two analysis methods compared in *Section 4.3* were further assessed in a case study conducted on the Roode Elsberg Dam. The results obtained from the finite element analysis methods illustrated a similar discrepancy to that previously exhibited in *section 4.3*. Once again, the natural frequencies obtained from the Westergaard method compared to be lower

than that of the FSI model. When analysing the first six natural frequencies an average discrepancy of 20% was observed between the two methods (*see table 9*). The results obtained appear to be consistent with the comparative process conducted previously.

Table 9: Comparison of natural frequencies (Hz) obtained from the FSI model and Westergaard method of the Roode Elsberg model.

Modes	FSI Model	Westergaard	% Difference
1	2.96	2.34	21.06
2	3.23	2.50	22.55
3	4.49	3.60	19.87
4	5.54	4.62	16.53
5	6.67	5.56	16.58
6	7.20	5.77	19.84

The first six modes obtained from the finite element models of the Roode Elsberg dam were scrutinised to verify the modal behaviour of the dam. Both 1st modes of vibration illustrate that the Roode Elsberg arch dam behaviours asymmetrically about the crown position (Y-Axis) and is excited into motion in the upstream - downstream direction (See Figure 51). The dam is seen to be very flexible at the crest level, where the two halves of the dam move in the opposite direction relative to the crown. The 2nd mode of vibration of the FSI model is characterised by symmetric behaviour, in which the crown position vibrates in the upstream-downstream direction. The Westergaard mode produces a similar shape in profile, but is slightly skewed to the left. The 3rd mode also illustrates symmetric behaviour about the crown position (Y-Axis). The quarter arc region between the crown and abutment illustrates to be heavily excited in the radial direction, where the mode vibration is characterised by inward - outward radial displacements. The fourth mode is asymmetric about the crown position, and is of a complex nature due to the flexibility of the thin arch. The 5th and 6th mode are interchanged for the two analysis methods. The 5th mode of the FSI model illustrates that dam undergoes a tensile elongation mode of vibration in the z direction, which coincides with the 6th mode of the Westergaard model. Finally, the last mode of the FSI model shows similar flexibility of the arch as the 4th mode but is symmetric

about the crown, this coincides with the 5th mode from the Westergaard method. The modes of vibration correlate to those obtained from the comparative study in *Section 4.3* and those obtained by Kuo (1982) and Mohammed (2011) in the analysis of Techi and Karun arch dam.

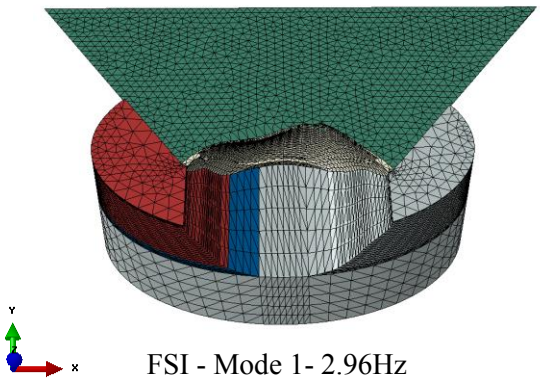

FSI - Mode 1- 2.96Hz
Asymmetric

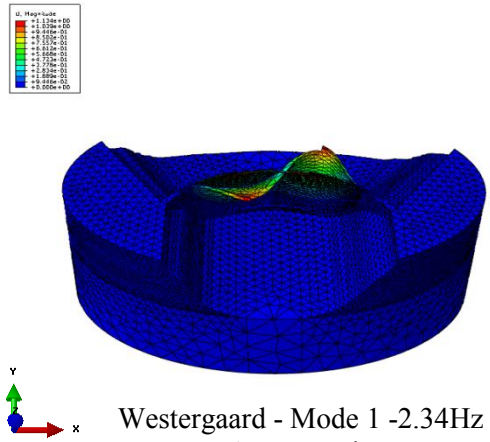

Westergaard - Mode 1 -2.34Hz
Asymmetric

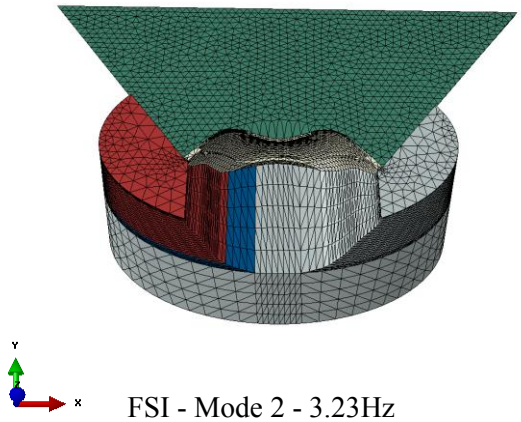

FSI - Mode 2 - 3.23Hz
Symmetric

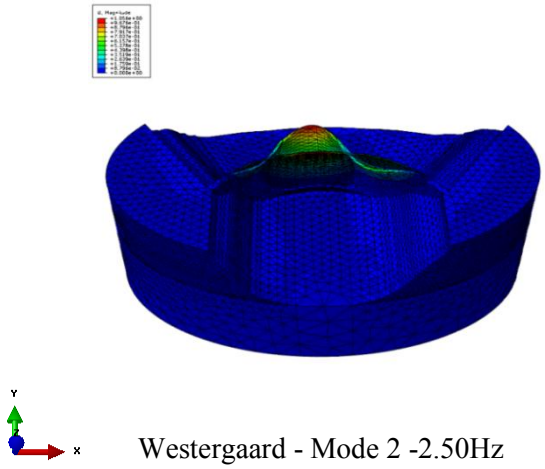

Westergaard - Mode 2 -2.50Hz
Asymmetric

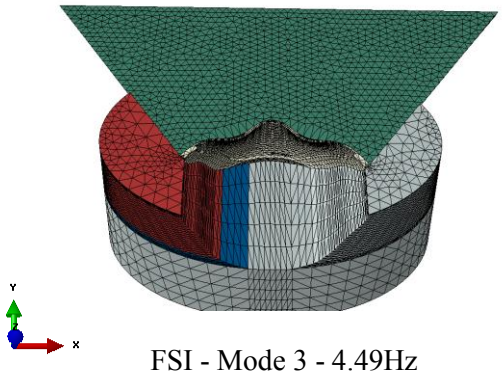

FSI - Mode 3 - 4.49Hz
Symmetric

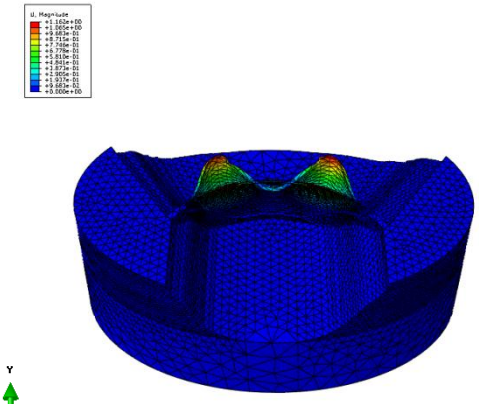

Westergaard - Mode 3 - 3.60Hz
Symmetric

Figure 51: Mode 1-3 of Roode Elsberg dam obtained from the FSI and Westergaard model.

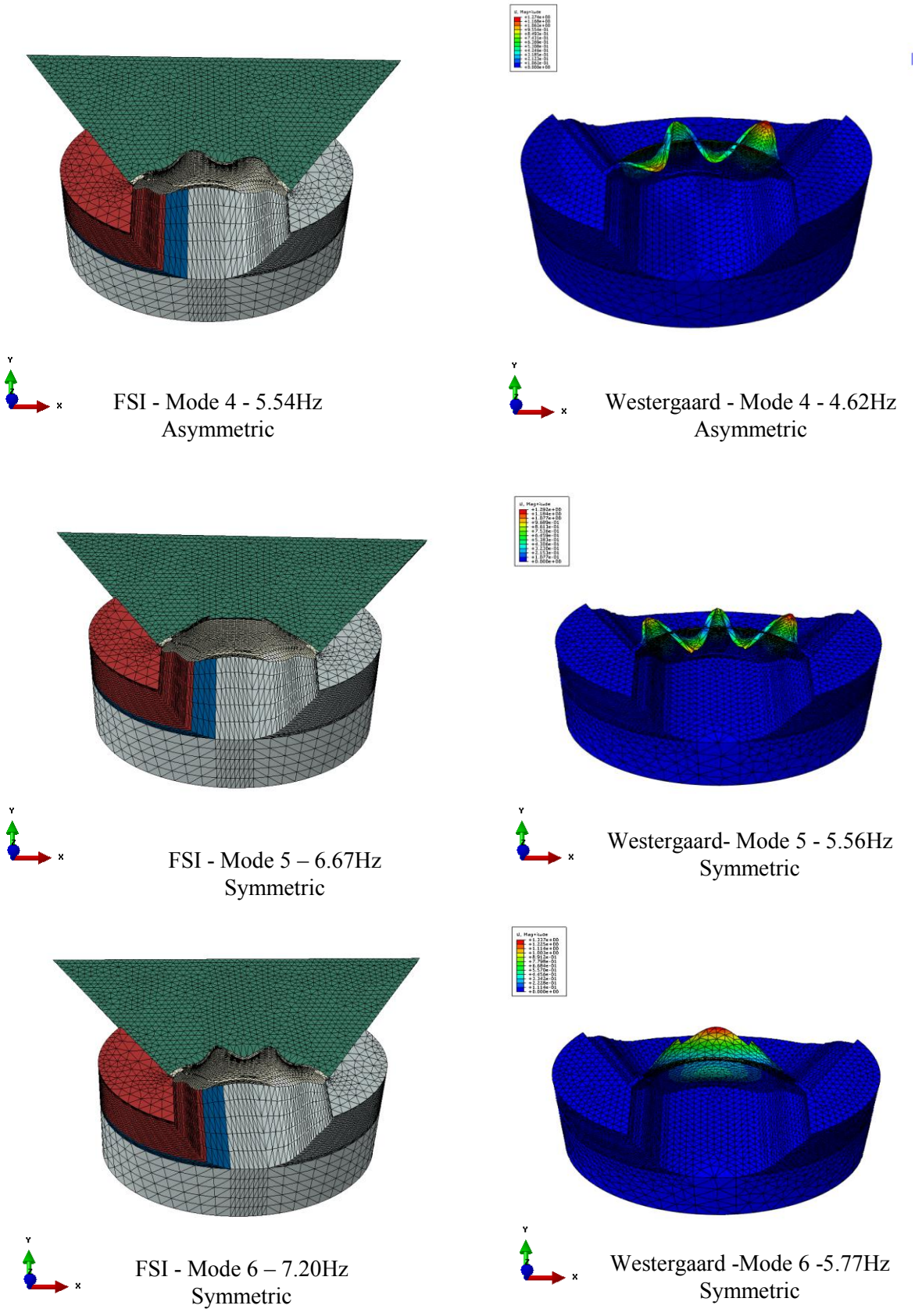

Figure 52: Mode 4-6 Roode Elsberg dam obtained from the FSI and Westergaard model.

4.6 Ambient Vibration Test Results

The results obtained from the ambient vibration testing were quite prominent, as a result of high wind speeds and an over flowing water level. Data pre-processing such as Detrending, Resampling and Low pass filtering to reduce noise was carried out in order to obtain accurate results. During the determination of the as built modal parameters the natural frequencies were extracted and not the mode shapes, due to that the spillway of Roode Elsberg dam could not be accessed. The modal analysis of the data recorded using the Frequency Domain Decomposition (FDD) yielded the singular values of the spectral density shown in *figure 53*.The first six modes were identified in the data acquired from the recording, this is supported by the peak picking of the natural frequency seen in the spectrum below.

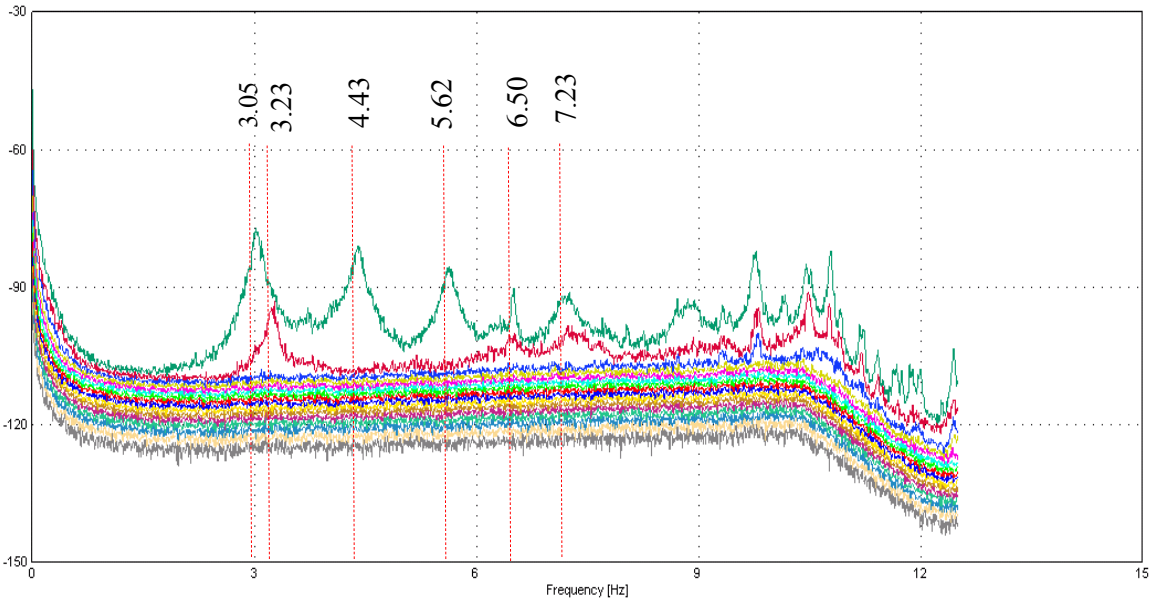

Figure 53: Singular values of spectral matrices (Natural Frequencies Hz) of Roode Elsberg dam, extracted using the FDD algorithm.

4.7 Verification of Roode Elsberg Model

The results obtained from the field measurements were then used to verify the two analysis methods. The FSI model was successfully updated as the results compared well to the field test measurements (see table 10). The results were within an average error of 1.45%. On the contrary, the Westergaard method resulted in lower natural frequencies which do not correlate with the filed test measurement results. The results show to be erroneous by an

average of 20%. The results obtained in this case study using the Westergaard method correlate to that obtained by Kuo (1982) in the analysis of the Techi arch dam.

Table 10: Comparison of natural frequencies (Hz) obtained from AVT test in Sep-2013 with the FSI model and Westergaard method.

Modes	AVT 10-09-2013	FSI Model	Westergaard	FSI % Error	Westergaard % Error
1	3.05	2.96	2.34	2.81	23.28
2	3.23	3.23	2.50	0.05	22.52
3	4.43	4.49	3.60	1.44	18.71
4	5.62	5.54	4.62	1.41	17.71
5	6.50	6.67	5.56	2.61	14.40
6	7.23	7.20	5.77	0.43	20.18

One can conclude that this is a result of the assumptions and context considered in the derivation of the Westergaard method. The parabolic pressure distribution proposed by Westergaard (1933) is not the distribution found in the ambient state. Hence, resulting in an overestimation of the added mass region being applied in the ambient state.

Findings made by Mircevska (2012) conclude that the Westergaard added mass method only provides acceptable results in the context it was developed. The method neglects the dam flexibility and water compressibility, wherever these features have an impact on the magnitude of hydrodynamic effects it will result in discrepancy in the obtained results. It is evidence that the Roode Elsberg arch dam is quite flexible in between its first six modes (see figure 51 &52). This can be seen to have an influence in the discrepancy of the results obtained.

4.8 Chapter Summary

In summary, this chapter contains the results and discussion that carry out the objectives of this work. Initially we assessed the behaviour of the acoustic finite elements as a suitable option of representing the impounded water body. Thereafter the objectives of this work were carried out, these included; (i) Comparison of the hydrodynamic methods, (ii) evaluating the effect of a reservoir orientation and geometry on the dynamic characteristics

of an arch dam, (iii) Development of the dynamic finite element models of the Roode Elsberg arch dam (iv) Validation of the Roode Elsberg finite element models using as built operational modal parameters obtained from ambient vibration testing.

CHAPTER 5

5 CONCLUSION AND RECOMMENDATIONS

5.1 Summary

Operational concrete arch dams are permanently subjected to hydrodynamic loading by the impounded water body. Previous studies have shown that the impounded water body has a significant effect on the dynamic properties of the dam. This influence can be analysed using computational analysis methods and field testing techniques, such as the finite element method and ambient vibration testing, respectively. Finite element methods have been used to assess the influence of external loading on the structural properties of the dam. Ambient vibration testing has been used to effectively obtain the as built operational dynamic properties of arch dams.

The objective of the study aims at developing an updatable dynamic finite element model of the Roode Elsberg dam. The Roode Elsberg dam was considered as a case study as it has been continuously monitored since it began operating in the 960' s. The dam has an asymmetrically located and diverging reservoir at an approximate angle of 26°. It has also developed a horizontal crack from the horizontal pulvino, along the central spillway blocks. The crack acts as a bondless joint with 3mm opening and closing cycle between winter and summer in the central position of the dam wall (Moyo & Oosthuizen, 2011).

Firstly, acoustic finite elements were validated as a possible formulation to represent the impounded water body. Thereafter, a parametric study was conducted, in order to ensure that all potential influences on the dynamic properties were taken into consideration. The parametric study assessed whether the divergence and the asymmetrical located reservoir had an influence on the dynamic properties. Finally, the Westergaard method of analysis and the acoustic fluid structure interaction method were carried out to develop computational models of the Roode Elsberg dam.

The challenges in creating the finite element model were experienced in the seeding and meshing of the dam wall and the fluid region. This was due to the complex nature of the geometries, and the computational time taken for each model. This was overcome by an

iterative partitioning procedure that was carried out to simplify the geometric regions, and a sensitive study carried out to minimize the computational time of convergence.

The acoustic finite elements were validated as a good approach to represent the impounded water body and gave a good approximation of the hydrodynamic pressures. From the parametric study it was found that the dynamic properties were insensitive to the divergence and asymmetry of the reservoir under ambient conditions. The fluid structure interaction method gave a better representation of the impounded water body when compared to the added mass technique proposed by Westergaard. This was considered to be normal as the Westergaard method is proven to provide a crude estimation of the hydrodynamic pressures. The good representation of the FSI method was verified by the as-built operational natural frequencies obtained by ambient vibration testing conducted on the Roode Elsberg dam.

The objectives pertaining to this study are concluded below and future aspects to be considered going forward are provided in the recommendation section.

5.2 Conclusion

The Finite Element Analysis technique provides a good computational method to analyse the dynamic behaviour of an arch dam. It provides an economical solution as compared to other analytical models. A major challenge was in developing a formulation that can provide a good representation of the impounded water body. Various techniques have been developed but do not perform well in representing the impounded water body and its influence on the dynamic properties. From this study it was proven that acoustic elements provide a realistic and effective formulation to model the impounded water body. Upon comparing it against the two analytical solutions, it was found to provide reasonably accurate results, comparing quite well with the analytical methods being within 1KPa and 2.5 KPa of the hydrodynamic pressures. The acoustic element method can be considered to be more realistic as it includes important effects such as compressibility and the geometry of the water, which were not considered by the two analytical solutions. Despite the fact that the two closed form formulations were considered to overestimate the pressure distribution, they still serve as sound checks to validate the use of the acoustic elements.

Based on the modelling procedure and results and discussion of this work, the following conclusions were drawn:

(i) A 23% discrepancy was observed in the comparative study of the natural frequencies produced by the Westergaard method and FSI Model. The first four modes of both methods compared quite well to the operational modes of the Kouga arch dam obtained using ambient vibration testing (AVT). The Kouga arch dam was considered to be a good comparative benchmark, as it was similar to the hypothetical arch dam developed.

(ii) The parametric study confirmed that the orientation and geometry of the reservoir have an insignificant effect on the modal parameters in the ambient state. This was attributed to the small influence the change in reservoir had on the hydrodynamic pressures exerted on the upstream surface of the dam wall. Diverging reservoir walls were found to decrease the amount of fluid excited in each mode, resulting in an increase in the natural frequencies (maximum increase of .0.8%.) An asymmetrically orientated reservoir caused an increase in the water body associated with each mode, leading to a decrease in the natural frequencies (maximum decrease of 2.5%)

(iii) The case study conducted on the Roode Elsberg dam reaffirmed the discrepancies between the hydrodynamic analyses methods, by producing an average difference of 20%. The modes were found to be similar to those of the parametric study. The first six natural frequencies of the Roode Elsberg dam were obtained using ambient vibration testing, and then used to verify the dynamic finite element models of the Roode Elsberg dam.

(iv) The FSI model of the Roode Elsberg dam was validated successfully using the ambient vibration measurement data, however the Westergaard method underestimated the natural frequencies by a factor of approximately 20%. With the above results, it is evident that the Westergaard method does not lead to an accurate estimation of the dynamic pressures in the ambient state. Thus, it should be only considered in preliminary studies to obtain crude estimations of the dam's dynamic properties. The acoustic fluid structure interaction method is the preferred method to be used for a more accurate idealisations of the impounded water body in the ambient state. As it provides a more realistic approach that includes the compressibility, geometry, refraction and absorption of upstream waves and orientation of the fluid.

5.3 Recommendations

The following recommendations are suggested for future works related to this topic:

(i) Future analyses pertaining to Roode Elsberg dam should utilize a non-linear model to model the vertical contraction joints due to the large influence they have on the seismic evaluation of arch dams. Also, such a model should be used to model the horizontal crack located in the lower region of the dam as it is considered to have hindered the dam's stiffness.

(ii) An accurate approximation of the foundation and dam material properties on-site must be established. This would entail conducting field investigations on the foundation and dam materials. Rough estimates were used for the foundation in this study. Hence, only a rough study into the effects of the differential foundation properties could be used due to a lack of field testing conducted on this site.

(iii) Future modelling of the Roode Elsberg dam should include modelling the sedimentation on the upstream bedrock. Modelling of the sedimentation which has developed on the upstream bedrock of the dam will have an influence on the static and possibly the dynamic behaviour of the dam.

CHAPTER 6

6 BIBLIOGRAPHY

Bathe, K. J., & Wilson, E.L. (1976). Numerical Methods in Finite Element Analysis. PrenticeHall, Englewood Cliffs, N.J., 1-582

Brincker R, & Andersen P. (2006). Understanding Stochastic Subspace Identification. *In Proceedings of the 24 International Modal Analysis Conference (IMAC)*, St. Louis, Missouri USA, 2006.

Alexander, M. G., & Beushausen H.., (2009). Fulton's concrete technology 9th edition. *Cement & Concrete Institute*, Midrand, South Africa,1-465

Chopra, K. A. (1967). Hydrodynamic pressure on dams during earthquakes. *ASCE Journal of Mechanical Engineering Division*, 205-223.

Chuhan, Z., Jianwen, P., & Jinting, W. (2009). Influence of seismic input mechanisms and radiation damping on arch dam response. *Soil Dynamics and Earthquake Engineering*, 1282-1293.

Clough, R. W. (1980) Nonlinear Mechanism in seismic response of Arch Dams. *International Conference on Earthquake Engineering*, Skopje, Yugoslavia.

Clough, P. W., & Tocher, J. L. (1964). Analysis of Thin Arch Dams by the Finite Element Method. *International Symposium*. Southampton: Pergamon Press, 107-122.

Bayraktar, A., Sevim, B., & Altunisik, C. A. (2011). Finite element model updating effects onnonlinear seismic response of arch dam-reservoir-foundation systems. *Finite elements in analysis and design*, 85-97.

Daniell, W. E., & Taylor, C. A. (1999). Effective ambient vibration testing for validating numerical models of concrete dams. *Earthquake engineering and structural dynamics*, 1327-1344.

Darbre, G. R., & Proulx, J. (2002). Continuous ambient-vibration monitoring of the arch dam of Mauvoisin. *Earthquake Engineering & Structural Dynamics*, *31*(2), 475–480.

Dassault Systems Simulia Corp. (2010). *Abaqus/CAE User's Manual.* Providence: Dassault Systems.

Du, X., Zhang, Y., & Zhang, B. (2006). Nonlinear seismic response analysis of arch dam foundation systems- part I dam-foundation rock interaction. *Bulletin of Earthquake Engineering*, *5*(1), 105–119.

Fenves, G. L., Mojtahedi, S., & Reimer, R. B. (1992). Effect of Contraction Joints on Earthquake Response of an Arch Dam. *Journal of Structural Engineering*, *118*(4), 1039.

Fok, K. A., & Chopra, A. (1987). Water compressibility in earthquake response of arch dams. *Journal of Structural Engineering*, 958-975.

Fok, K. L., & Chopra, A. (1986). Earthquake analysis of arch dams including dam-waater interaction, reservoir boundary absorption and foundation flexibility. *Earthquake Engineering and Structural Dynamics*, 155-184.

Gersdorff, N. Von. (2009). Numerical Model Validation For large Concrete Gravity Dams, 233–248.

Ghaemian, M., & Ghobarah, A. (1999). Nonlinear seismic response of concrete gravity dams with dam – reservoir interaction, *21*, 306–315.

Ghanaat, Y. (1993). *Theoretical Manual for Analysis of Arch Dams.* Washington DC: U.S. Army Corps of Engineers.

Goldgruber, M., Shahriari, S., & Zenz, G. (2013). Influence of damping and different interaction modelling on a high arch dam, *2013*(559), 28–30.

Housner, G. (1954). Earthquake Pressures on Fluid Containers.

Kuo, J. S.-H. (1982). Fluid Structure Interactions: Added Mass Computations for Incompressible Fluid. National Science Foundation.

Leung, A., Fok, A., Dai, H., & Su, R. (2008). The fractal finite element method for added mass type problems. *International Journal for Numerical Methods in Engineering*, 1194-1213.

Makha, R., & Moyo, P., (2012) Observations from the calibration of an arch dam model using ambient modal properties. *Concrete Repair, Rehabilitation and Retrofitting III: 3rd International Conference on Concrete Repair, Rehabilitation and Retrofitting.*

Mivehchi, M. R., Ahmadi, M. T., & Hajmomeni, A. (2003). E ffective Techniques for Arch Dam Ambient Vibration Test : Application on Two Iranian Dams, *5*(2), 23–34.

Moyo, P., & Oosthuizen, C. (2013). *Structural Health Monitoring of Arch Dams Using Dynamic and Static Measurements*.

Moyo, P., & Oosthuizen, C. (2010). Ambient Vibration Survey Trials of two arch dams in South Africa. *8th ICOLD EUROPEAN CLUB SYMPOSIUM* (pp. 589-594). Innsbruck: Grez University of Technology.

Nzuza, M., & Moyo, P. (2013). Thermo-Mechanical Modelling of Arch Dams for Performance Assessment. *University of Cape Town*, 1-136.

Poursartip, B., & Lotfi, V. (2008). Modal Analysis of Concrete Arch Dams In Time Domain Including Dam-Reservoir Interaction.

Proulx, J., Darbre, G. R., & Kamileris, N. (2004). Analytical and Experimental Investigation of Damping in Arch Dams based on Recorded Earthquakes, *13 th World Conference on Earthquake Engineering*, (68).

Rodríguez, J., Crespo, M. J., Lacoma, L. M., & Martínez, F. (2012). Fluid-Structure Interaction in Civil Engineering Structures, 1–14.

Samii, A., & Lofti, V. (2007). Comparison of coupled and decoupled modal approaches in seismic analysis of concrete gravity dams in time domain. *Finite Elements in Analysis and Design*, 1003-1012.

Sani, A. A., & Lofti, V. (2007). Linear dynamic analysis of arch dams utilizing modified efficient fluid hyper-element. *Engineering Structures*, 2654-2661.

Sevim, B., Bayraktar, A., & Altunisik, A. C. (2011). Journal of, (October 2010).

Sooch, G. S., & Bagchi, A. (2007). Effect of Seismic wave scattering on the Response of Dam-Reservoir-Foundation Systems, (1972).

Tiliouine, B., & Seghir, A. (1998). Fluid-structure models for dynamic studies of dam-water systems. *Elenth European Conference on Earthquake Engineering.* Paris.

U.S. Army Corps of Engineers. (1994). Engineering and Design: Arch dam design. *Washingtom DC: Department of the Army*, 1-300.

United States Bureau of Reclamation. (1977). *Design of Arch Dams.* Colorado: Water Resource Technical.

Westergaard, H. (1933). Water Pressures on Dams During Earthquakes. *American Society of Civil Engineers*, *1*(1835), 419–433.

Zienkiewicz, C., & Taylor, R. (2000). *The finite element method.* London: McCGraw-Hill.

Zienkiewicz, O. C., Clough, R., & Seed, H. B. (1984). *Earthquake Analysis procedures for concrete and earth dams: State of the art.* I..C.O.L.D.

CHAPTER 7

APPENDICES

Appendix A: Abaqus Modelling Theory

- **Acoustic Element Formulation**

The impounded water body was modelled using linear acoustic elements, which are predefined elements in the program. The acoustic equilibrium equation is represented by equation (7.1), and one can note that displacements are not calculated.

$$\frac{\partial p}{\partial x} + \gamma(x,\theta_i)\dot{u}^f + \rho_f(x,\theta_i)\ddot{u}^f = 0 \tag{7.1}$$

Where:

p hydrodynamic pressure in the fluid (in excess of any static pressure)

$\dot{u}^f$ fluid particle velocity

$\ddot{u}^f$ fluid particle acceleration

$\theta_i =$ Independant variables such as temperature, salinity of water on which

ρ_f and may depend on.

The constitutive equation assumes the fluid to be in-viscid, linear, and compressible.

$$p = K(x,\theta_i)\frac{\partial}{\partial x}\dot{u}^f \tag{7.2}$$

The fluid system is discretised using a Galerkin-Petrov approach where the dynamic pressures are the arguments. The structural system is discretised using a Galerkin method and refers to the displacement degrees of freedoms (Simulia, 2010).

The following constraints and physical boundaries conditions were applied:

S_{fs} -Where the motion of the acoustic medium is directly coupled to the motion of a solid. On the acoustic-structural boundary the acoustic and structural media have the same displacement normal to the boundary, but with tangential motions which are uncoupled.

S_{fi} - A "radiating" acoustic boundary. Where the acoustic media extend sufficiently far from the dam wall of interest, the acoustic medium must be modelled as being infinite in extent. In such cases it was convenient to truncate the computational region and apply an impedance boundary condition to simulate waves passing exclusively outward from the computational region.

In Abaqus, the formulations are slightly different in direct integration transient and modal analyses or steady state, primarily with regard to the handling of the volumetric drag loss parameter and spatial variations of the constitutive parameters. In this research the steady state formulation was employed as the all degrees of freedom and loads are assumed to vary harmonically at an angular frequency. This formulation uses the nodal degrees of freedom in the solid and acoustic regions to form a large linear system of equations defining the coupled structural-acoustic mechanics at a single frequency.

To derive the differential equation used in the fluid structure interaction method equation (7.1) is divide by ρ_f, taking its gradient with respect to *x* and neglecting the gradient of γ/p_f, and combine the result with the time derivative of equation (7.2) to obtain the equation of motion for the fluid in terms of the pressures:

$$\frac{1}{K_f}\ddot{p} + \frac{\gamma}{p_f K_f}\dot{p} - \frac{\partial}{\partial x}\cdot\left(\frac{1}{\rho_f}\frac{\partial p}{\partial x}\right) = 0 \tag{7.3}$$

An equivalent weak form for the equation of motion (7.3) is obtained by introducing an arbitrary variational field, δp, and integrating over the fluid:

$$\int_{V_f} \delta p\left(\frac{1}{K_f}\ddot{p} + \frac{\gamma}{p_f K_f}\dot{p} - \frac{\partial}{\partial x}\cdot\left(\frac{1}{\rho_f}\frac{\partial p}{\partial x}\right)\right)dV$$

(7.4)

Applying Greens theorem to the above equation (7.4)

$$\int_{V_f}\left[\delta p\left(\frac{1}{K_f}\ddot{p}+\frac{\gamma}{p_f K_f}\dot{p}\right)+\frac{\partial}{\partial x}\cdot\frac{1}{\rho_f}\frac{\partial\delta p}{\partial x}\cdot\frac{\partial p}{\partial x}\right]dV+\int_S \delta p\left(\frac{1}{\rho n_f}\bar{n}.\frac{\partial p}{\partial x}\right)dS=0$$

(7.5)

Assuming that ***p*** is prescribed on S_{fp}, the equilibrium equation (7.1) is used on the boundary to relate the pressure gradient to the motion of the boundary:

$$\bar{n}\cdot\left(\frac{\partial p}{\partial x}+\frac{\gamma}{\rho_f}\dot{u}^f+\ddot{u}^f\right)=0 \qquad \text{on} \qquad S-S_{fp}$$

(7.6)

Using

$$\int_{V_f}\left[\delta p\left(\frac{1}{K_f}\ddot{p}+\frac{\gamma}{p_f K_f}\dot{p}\right)+\frac{\partial}{\partial x}\cdot\frac{1}{\rho_f}\frac{\partial\delta p}{\partial x}\cdot\frac{\partial p}{\partial x}\right]dV-\int_{S-S_{fp}}\delta p(T(x))dS=0$$

the above substitution the last term of equation (7.5) is eliminated to produce

Where the traction terms represents

$$T(x)=\bar{n}\cdot\left(+\frac{\gamma}{\rho_f}\dot{u}^f+\ddot{u}^f\right)=\bar{n}\frac{1}{\rho_f}\frac{\partial p}{\partial x} \text{ on} \qquad S-S_{fp}$$

(7.7)

All other boundary terms can be formulated with respect to T(x) this includes boundary terms S_{fi} and S_{fs}. The defined boundary values are introduced to produce the finalised weak form equation (7.8):

$$\int_{V_f}\left[\delta p\left(\frac{1}{K_f}\ddot{p}+\frac{\gamma}{p_f K_f}\dot{p}\right)+\frac{\partial}{\partial x}\cdot\frac{1}{\rho_f}\frac{\partial\delta p}{\partial x}\cdot\frac{\partial p}{\partial x}\right]dV$$
$$-\int_{S_{fp}}\delta p\left(\frac{1}{c_1}\dot{p}+\frac{1}{a_1}p\right)dS-\int_{S_{fs}}\delta p\bar{n}\cdot\ddot{u}^m dS=0 \qquad (7.8)$$

The structural behaviour of the system is defined by the virtual work equation (7.9)

$$\int_V \delta\varepsilon : \sigma dV + \int_V \alpha_c \rho \delta u^m \cdot \dot{u}^m dV + \int_V \rho \delta u^m \cdot \ddot{u}^m dV + \int_{S_{fs}} \delta p u^m \cdot \bar{n} dS - \int_{S_t} \delta p u^m \cdot t dS = 0 \qquad (7.9)$$

Where σ is the stress at a point on the structure, ***p*** is the pressure acting on the fluid-structural interface, *n* is the outward normal to the structure, ρ is the density of the material, α_c is the mass proportional damping factor , $\ddot{u}^m$ is the acceleration of a point on the solid structure, and δu^m is a variational displacement field, and $\delta\varepsilon$ is the strain variation that is compatible with δu^m .

Discretized finite element equation

The vibrational problem is defined by equation (7.8) and (7.9), the coupled fields u^m and ***p*** define the structural and the fluid arguments respectively**.** The problem is discretized by introducing interpolation functions in the fluid $p = H^p p^p$ *p=1, 2...* which goes up to the number of pressure nodes. In the structure $u^m = N^N u^N$ N , 2… up to the number of displacement degrees of freedom. In these equations we perform a summation over the degrees of freedom of the discretized model. Where the superscripts P and Q refer to the pressure degrees of freedom in the fluid and N, M refer to the displacement degrees of freedom in the structure, The Galerkin method is employed on the structure where the variation field has the same form as the displacement $\delta u^m = N^N \delta u^N$ and for the fluid the Petrov-Galerkin variational form has the form $\delta p = H^p \delta p^p$.

The finite element linearization of the equation used in the acoustic formulation is defined by:

$$\begin{aligned} &-\delta p^p \left\{ (M_f^{PQ} \ddot{p}^Q + C_f^{PQ} \dot{p}^Q + (K_f^{PQ} + K_{fi}^{PQ}) p^Q - S_{fs}^{PM} \ddot{u}^M - P_f^P \right\} dp^Q + \\ &\delta u^N \left\{ M^{NM} \ddot{u}^M + C_m^{NM} \dot{u}^M + \left[S_{fs}^{QN} \right]^T P^Q - P^N \right\} du^M = 0 \end{aligned} \qquad (7.10)$$

Where *dp* and *du* are the corrections from the new iteration method, K^{NM} is the structural stiffness matrix, C^{NM} is the structural damping matrix, M^{NM} is the structural mass matrix and S_{fs} is the coupling of the solid and acoustic motion at the interface.

Eigenvalue extraction and mode-based procedures

From the discretised equation the linear system equation can be written in the frequency domain as

$$\begin{bmatrix} K_s & S_{fs}^T \\ 0 & K_f \end{bmatrix} \begin{Bmatrix} u \\ p \end{Bmatrix} + i\omega \begin{bmatrix} C_{(m)} & 0 \\ 0 & C_f \end{bmatrix} \begin{Bmatrix} u \\ p \end{Bmatrix} - \omega^2 \begin{bmatrix} M_s & 0 \\ -S_{fs} & M_f \end{bmatrix} \begin{Bmatrix} u \\ p \end{Bmatrix} = \begin{Bmatrix} P_s \\ P_s \end{Bmatrix} \tag{7.11}$$

Where ω is the natural frequency of the structure, and the superscripts have been omitted for brevity. Damping and any forcing terms are considered to be negligible in the ambient condition, they can be suppressed, and resulting in the following linear eigenvalue equation (7.12). The equation cannot be solved directly in Abaqus due to the asymmetric stiffness and mass matrices.

$$\begin{bmatrix} K_s & S_{fs}^T \\ 0 & K_f \end{bmatrix} \begin{Bmatrix} u \\ p \end{Bmatrix} - \omega^2 \begin{bmatrix} M_s & 0 \\ -S_{fs} & M_f \end{bmatrix} \begin{Bmatrix} u \\ p \end{Bmatrix} = 0$$

(7.12)

The above equation (7.12) can be shown to yield real-valued natural frequencies and modes and hence can be rewritten in a symmetric form. In this problem this done by using Lanczos formulation by introducing an auxiliary variable $\psi = \rho / \omega^2$, augmenting the system of equations with $K_f p = \omega^2 K_f \psi$ and manipulating the equations yields to the following symmetric equation:

$$\left(\begin{bmatrix} K_s & S_{fs}^T & 0 \\ S_{fs} & -M_f & K_f \\ 0 & K_f^T & 0 \end{bmatrix} - \omega^2 \begin{bmatrix} M_s & 0 & 0 \\ 0 & 0 & 0 \\ 0 & 0 & K_f \end{bmatrix} \right) \begin{Bmatrix} u \\ p \\ \psi \end{Bmatrix} = 0$$

(7.13)

The auxiliary variable is internal to Abaqus and is not made available for output. The left and right eigenvectors for the original system of equation can be constructed from the Lanczos solution and used to obtain the modal quantities.

- **The Lanczos eigensolver**

The Lanczos eigensolver is a powerful tool for extraction of eigenvalues and corresponding eigenvectors of a sparse symmetric generalise eigenproblem. It consists of a set of runs, in

which a set of iterations called steps is performed. For each Lanczos run the following spectral transformation is applied:

$$[M]([K]-\sigma[M])^{-1}[M]\{\phi\} = \theta[M]\{\phi\} \quad (7.13)$$

Where σ is the shift, θ is the eigenvalue, and ϕ is the eigenvector. This transformation allows rapid convergence to the desired eigenvalues. The eigenvectors of the symmetrized problem equation (7.13) and the transformed problem equation (7.14) are identical, while the eigenvalues of the original problem and the transformed problem are related in the following way:

$$\omega^2 = \frac{1}{\theta} + \sigma \quad (7.14)$$

A Lanczos run will be terminated when it does not converge towards the required eigenvectors. In general, only tens of eigenvalues are computed in a single Lanczos run. The Lanczos eigensolver provides the capability of computing many eigenmodes by carrying out several runs with different shift values.

Within each run a sequence of Krylov subspaces is created, and the best possible approximation of the eigenvectors on each subspace is computed in a series of steps. In each step the dimension of the subspace is allowed to grow, allowing for a better approximation of the required eigenvectors. This is in contrast to the subspace iteration method, in which the dimension of the subspace is fixed and is not allowed to grow.

In theory, the basic Lanczos process is designed only to determine simple eigenvalues. The shifting strategy detects missing modes and enforces computation of all the modes during the subsequent runs. However, this strategy is expensive if the required number of certain eigenvalues is high. Therefore, a blocked version of the Lanczos algorithm is implemented in Abaqus/Standard. The idea is to start with a block of orthogonal vectors and to increase the dimension of the Krylov subspaces by the block size at each Lanczos step.

This approach allows automatic computation of all multiple eigenvalues if the largest required eigenvalue does not exceed the block size. Also, another important advantage of the blocked Lanczos method is that it allows efficient implementation of expensive

computational kernels such as matrix-blocked vector multiplications, blocked back substitutions, and blocked vector products.

As discussed above, the Lanczos process consists of several runs. Each Lanczos run is associated with a shift value that remains constant during the run. The initial shift value, is determined by a heuristic approach which uses the geometric mean of the centres of the Gershgorin circles, known as problem scale. At the beginning of each Lanczos run a factorization of the shifted matrix (where p is the run number) is carried out, after which a sequence of Lanczos steps is performed.

Please refer to Simulia (2010) Theory manual for a more detailed comprehensive outline of the Lanczos steps implemented to obtain the eigenvectors and values.

- **Surface Based Acoustic –Structural Interaction modelling**

Abaqus provides two techniques for modelling interaction between acoustic and structural media. These include surface based interaction and acoustic interface elements. The surface based approach can be used to model interacting structural and acoustic meshes which constitute different node numbering and whose surface meshes may not be spatially coincident (Simulia, 2010). Whereas, the special purpose interface elements are restricted to meshes whose node numbers coincide. Hence, the above comparison led to the surface based approach being picked as it is easier to use and computationally cost effect.

In the surface based coupling the interaction surface $S_{fS} \cup S_{fTS}$ is formed by the boundary between possibly nonconforming structural and acoustic meshes. To derive the coupling matrices on the surface based procedure, a variation of the master slave procedure is employed. In the master-slave procedure the two interface mediums were distinguished by assigning the structural system as the master surface, and the acoustic fluid as the slave surface.

At the start of the analysis, projections x_N of the slave nodes are made onto the master surface. The areas A_N and normal $\overline{n}(x_N)$ of the acoustic fluid slave nodes are computed. Projections P (x_N) are made onto the master surface, and master nodes within the vicinity are identified. The structural master nodes in the vicinity of the slave nodes are used to interpolate an averaged value for the displacement of the projected P (x_N) fluid node. Since

the structural surface has the displacements and the acoustic has pressures as its arguments a fluid solid coupling condition must be employed.

Solid Master and Fluid slave

In the case where the fluid is designated as the slave, the fluid node values must be constrained to be an average of the values at nearby master surface nodes (*see figure 54*). The following point wise fluid-solid coupling condition equation (7.15) is enforced at the slave nodes, which results in displacement degrees of freedom added to the fluid slave surface.

$$\frac{1}{\rho_f}\frac{\partial p}{\partial x}.\bar{n} + \ddot{u}^m.\bar{n} = 0 \qquad (7.15)$$

These slave displacements are constrained by the master displacement and thereby eliminated; the slave pressures are not constrained directly. Hence, the fluid equation coupling term is:

$$\int_{S_{fs}\cup S_{fTS}} \delta p\bar{n}\cdot\frac{\partial p}{\partial x}dS = -\int_{S_{fs}\cup S_{fTS}} \delta p\bar{n}\cdot\ddot{u}^m dS \qquad (7.16)$$

The term will now be interpolated by values of structural displacements at the nearby nodes times the area of the slave node (*see equation 7.17*).

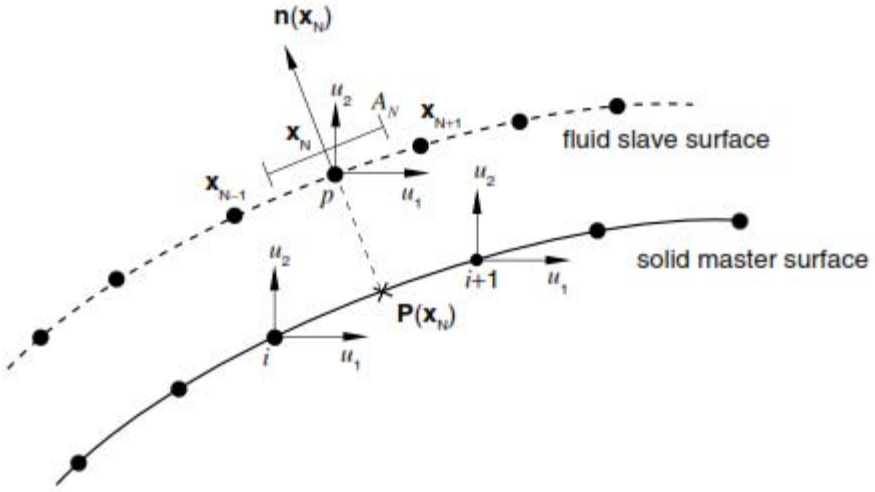

Figure 54: fluid slave and solid master surface

$$\int_{S_{fS} \cup S_{fTS}} \delta p \bar{n} \cdot \ddot{u}^m dS \approx P_N A_N \left[\sum_i \bar{n}(x_N) \cdot N^i(p(x_N)) \right]$$

(7.17)

Where $N^i(p(x_N)$ is the master surface interpolant calculated at the projection of the slave node, $\ddot{u}^m$ are the structural accelerations at the master nodes, and $\bar{n}(x_N)$ is the normal vector, pointing into the fluid, evaluated at the slave node. The above summation is repeated for all master nodes in the vicinity of the slave node projection P (x_N). The calculation is repeated for each slave node x_N on the coupled face of the fluid and solid $S_{fS} \cup S_{fTS}$ and assembled to form the coupling matrix.

Similarly the contribution to the pressure coupling term in the structural equation due to slave node x_N is approximated by equation (7.18):

$$\int_{S_{fS} \cup S_{fTS}} \delta \ddot{u}^m \cdot \bar{n} p dS \approx P_N A_N \left[\sum_i \bar{n}(x_N) \cdot N^i(p(x_N)) \right]$$

(7.18)

Where P_N is the acoustic pressure at slave node x_N, and the sum is again over the master nodes *i* in the vicinity of the slave node projection.

Appendix B: Finite Element Results

Table 10: Natural frequencies of Roode Elsberg dam obtained using Fluid Structure Interaction model with varying dam Elastic modulus (35-45GPA).

	AVT	Fluid Structure Interaction									
Mode No.	AVT 10-09-2013	35 GPA	% Error	36 GPA	% Error	37 GPA	% Error	38 GPA	% Error	39 GPA	% Error
1	3,05	2,68	11,99	2,72	10,89	2,75	9,82	2,78	8,76	2,81	7,73
2	3,23	2,92	9,57	2,96	8,43	2,99	7,30	3,03	6,20	3,06	5,12
3	4,43	4,06	8,34	4,11	7,17	4,16	6,02	4,21	4,90	4,26	3,80
4	5,62	5,02	10,59	5,09	9,49	5,18	8,42	5,21	7,36	5,26	6,32
5	6,5	6,13	5,73	6,19	4,70	6,26	3,70	6,32	2,72	6,38	1,77
6	7,23	6,52	9,82	6,60	8,70	6,68	7,60	6,76	6,52	6,84	5,46
Ave Error %			9,34		8,23		7,14		6,08		5,03

Mode No.	40 GPA	% Error	41 GPA	% Error	42 GPA	% Error	43GPA	% Error	44 GPA	% Error	45 GPA	% Error
1	2,81	7,75	2,88	5,71	2,91	4,73	2,94	3,76	2,96	2,81	2,99	1,87
2	3,08	4,75	3,13	3,00	3,17	1,97	3,20	0,95	3,23	-0,05	3,26	-1,03
3	4,26	3,92	4,36	1,65	4,40	0,60	4,45	-0,43	4,49	-1,44	4,54	-2,44
4	5,29	5,83	5,38	4,30	5,43	3,32	5,49	2,36	5,54	1,41	5,59	0,48
5	6,09	6,29	6,50	-0,06	6,56	-0,93	6,62	-1,78	6,67	-2,61	6,72	-3,42
6	6,88	4,82	6,98	3,39	7,06	2,39	7,13	1,40	7,20	0,43	7,27	-0,53
Ave Error %		5,56		3,00		2,01		1,04		0,09		-0,84

Table 11: Natural frequencies of Roode Elsberg dam obtained using Modified Westergaard model with varying dam Elastic modulus (35-45GPA).

Mode No.	AVT 10-09-2013	35GPA	% Error	36 GPA	% Error	37 GPA	% Error	38 GPA	% Error	39 GPA	% Error
1	3,05	2,11	30,70	2,14	29,82	2,17	28,95	2,19	28,10	2,22	27,26
2	3,23	2,26	30,04	2,29	29,15	2,32	28,27	2,34	27,41	2,37	26,56
3	4,43	3,24	26,90	3,28	25,93	3,32	24,98	3,36	24,04	3,41	23,12
4	5,62	4,19	25,47	4,24	24,54	4,29	23,63	4,34	22,74	4,39	21,87
5	6,5	5,02	22,78	5,08	21,78	5,15	20,81	5,21	19,85	5,27	18,90
6	7,23	5,21	27,94	5,28	27,02	5,34	26,12	5,41	25,23	5,47	24,35
Ave Error %			27,30		26,37		25,46		24,56		23,68

40 GPA	% Error	41 GPA	% Error	42 GPA	% Error	43 GPA	% Error	44 GPA	% Error	45GPA	% Error
2,24	26,44	2,27	25,63	2,29	24,83	2,32	24,05	2,34	23,28	2,36	22,52
2,40	25,73	2,43	24,90	2,45	24,10	2,48	23,30	2,50	22,52	2,53	21,74
3,45	22,21	3,49	21,32	3,52	20,44	3,56	19,57	3,60	18,71	3,64	17,87
4,44	21,00	4,49	20,16	4,53	19,33	4,58	18,51	4,62	17,71	4,67	16,91
5,33	17,97	5,39	17,06	5,45	16,16	5,51	15,28	5,56	14,40	5,62	13,55
5,53	23,49	5,59	22,65	5,65	21,81	5,71	20,99	5,77	20,18	5,83	19,38
	22,81		21,95		21,11		20,28		19,47		18,66

Appendix C : Modelling Data

Table 12: hypothetical arch dam data

Elevation	Position of Centres			Radii			Subtended angles		Delta sub-ten			Co-ordinates	ext co-ordinate		int co-ordinate	
z (m)	y-ext	y-mid	y-int	R-ext	r-mid	r-int	θ-Right	Θ-left	Delta θR=Θl			Slope	x	y	x	y
62,48	0,00	0,00	0,00	144,48	143,26	142,04	47,50	47,50	9,70	57,20	32,80	0,64	121,44	78,26	119,39	76,94
60,96	2,12	2,12	2,12	143,48	142,05	140,63	48,00	48,00	10,00	58,00	32,00	0,62	121,67	76,03	119,26	74,52
57,91	6,36	6,36	6,36	141,45	139,64	137,83	49,00	49,00	10,30	59,30	30,70	0,59	121,63	72,22	118,51	70,37
54,86	10,60	10,60	10,60	139,39	137,23	135,07	50,00	50,00	10,20	60,20	29,80	0,57	120,96	69,27	117,21	67,13
51,82	14,84	14,84	14,84	137,29	134,82	132,35	50,20	50,20	10,10	60,30	29,70	0,57	119,26	68,02	114,96	65,57
48,77	19,00	19,00	19,00	135,16	132,41	129,67	49,00	49,00	10,70	59,70	30,30	0,58	116,69	68,19	111,95	65,42
45,72	23,01	23,01	23,01	132,98	130,03	127,02	47,00	47,00	11,50	58,50	31,50	0,61	113,39	69,48	108,30	66,37
42,67	26,87	26,87	26,87	130,78	127,59	124,40	46,00	46,00	11,10	57,10	32,90	0,65	109,81	71,04	104,45	67,57
39,62	30,57	30,57	30,57	128,53	125,18	121,83	44,60	44,60	10,60	55,20	34,80	0,70	105,55	73,36	100,04	69,53
36,58	34,13	34,13	34,13	126,26	122,77	119,28	43,30	43,30	10,80	54,10	35,90	0,72	102,27	74,03	96,63	69,94
33,53	37,53	37,53	37,53	123,94	120,36	116,78	41,90	41,90	11,40	53,30	36,70	0,75	99,37	74,07	93,63	69,79
30,48	40,77	40,77	40,77	121,61	117,95	114,29	40,50	40,50	12,10	52,60	37,40	0,76	96,61	73,86	90,80	69,42
27,43	43,60	43,60	43,60	119,48	115,54	111,60	39,10	39,10	13,00	52,10	37,90	0,78	94,28	73,39	88,06	68,56
24,38	46,79	46,79	46,79	117,35	113,13	108,91	37,80	37,80	14,00	51,80	38,20	0,79	92,22	72,57	85,59	67,35
21,34	49,60	49,60	49,60	115,22	110,72	106,22	36,60	36,60	15,00	51,60	38,40	0,79	90,30	71,57	83,25	65,98
18,29	52,24	52,24	52,24	113,09	108,31	103,53	35,80	35,80	15,50	51,30	38,70	0,80	88,26	70,71	80,80	64,73
15,24	54,73	54,73	54,73	110,96	105,90	100,84	35,00	35,00	15,80	50,80	39,20	0,82	85,99	70,13	78,15	63,74
12,19	56,70	56,70	56,70	108,79	103,86	98,92	34,20	34,20	16,00	50,20	39,80	0,83	83,58	69,64	76,00	63,32
9,14	58,08	58,08	58,08	107,07	102,25	97,42	33,40	33,40	16,10	49,50	40,50	0,85	81,42	69,54	74,08	63,27
6,10	59,07	59,07	59,07	105,60	100,87	96,14	31,90	31,90	16,00	47,90	42,10	0,90	78,35	70,80	71,34	64,46
3,05	59,75	59,75	59,75	104,30	99,66	95,01	29,00	29,00	16,10	45,10	44,90	1,00	73,88	73,62	67,30	67,07
0,00	60,17	60,17	60,17	103,13	98,55	93,98	26,30	26,30	18,50	44,80	45,20	1,01	72,67	73,17	66,22	66,69